Title:

Lipid Peroxidation and Type I Interferon Coupling Fuels Pathogenic Macrophage Activation Causing Tuberculosis Susceptibility

Authors: Shivraj M. Yabaji,[1] Vadim Zhernovkov,[2] Prasanna Babu Araveti,[1] Suruchi Lata[1] Oleksii S. Rukhlenko[2] Salam Al Abdullatif,[3] Arthur Vanvalkenburg,[6,7] Yuriy Alekseev,[5] Qicheng Ma,[14] Gargi Dayama,[14] Nelson C. Lau,[1,14] W. Evan Johnson,[6,7] William R. Bishai,[4] Nicholas A. Crossland,[1,5] Joshua D. Campbell,[3] Boris N. Kholodenko,[2,8,9] Alexander A. Gimelbrant,[10] Lester Kobzik,[11] Igor Kramnik,[1,12,13,15*]

Affiliations:

1. The National Emerging Infectious Diseases Laboratory, Boston University, Boston, MA
2. Systems Biology Ireland, School of Medicine, University College Dublin, Dublin 4, Ireland
3. Department of Medicine, Boston University Chobanian & Avedisian School of Medicine, Boston, MA
4. Center for TB Research, Johns Hopkins School of Medicine, Baltimore, Maryland
5. The Department of Pathology and Laboratory Medicine, Boston University Chobanian & Avedisian School of Medicine, Boston, MA 02118.
6. Rutgers University, New Jersey Medical School, Division of Infectious Disease, Department of Medicine.
7. Rutgers University, New Jersey Medical School, Center for Data Science.
8. Conway Institute of Biomolecular & Biomedical Research, University College Dublin, Dublin 4, Ireland
9. Department of Pharmacology, Yale University School of Medicine, New Haven CT, USA
10. Altius Institute for Biomedical Sciences, Seattle, WA, USA
11. Cellecta, Inc., Mountain View, CA
12. Pulmonary Center, The Department of Medicine, Boston University Chobanian & Avedisian School of Medicine.
13. Dept. of Microbiology, Boston University Chobanian & Avedisian School of Medicine
14. Department of Biochemistry, and Cell Biology and Genome Science Institute, Boston University Chobanian & Avedisian School of Medicine
15. Lead Contact

[*]Corresponding author (ikramnik@bu.edu)
Igor Kramnik, MD, PhD Boston University School of Medicine, NEIDL
620 Albany St., Boston, MA 02118, phone: (617) 358-9187, e-mail: ikramnik@bu.edu

Abstract
A quarter of human population is infected with Mycobacterium tuberculosis, but less than 10% of those infected develop pulmonary TB. We developed a genetically defined sst1-susceptible mouse model that uniquely reproduces a defining feature of human TB: the development of necrotic lung granulomas and determined that the sst1-susceptible phenotype was driven by the aberrant macrophage activation. This study demonstrates that the aberrant response of the sst1-susceptible macrophages to prolonged stimulation with TNF is primarily driven by conflicting Myc and antioxidant response pathways leading to a coordinated failure 1) to properly sequester intracellular iron and 2) to activate ferroptosis inhibitor enzymes. Consequently, iron-mediated lipid peroxidation fueled *Ifnβ* superinduction and sustained the Type I Interferon (IFN-I) pathway hyperactivity that locked the sst1-susceptible macrophages in a state of unresolving stress and compromised their resistance to Mtb. The accumulation of the aberrantly activated, stressed, macrophages within granuloma microenvironment led to the local failure of anti-tuberculosis immunity and tissue necrosis. The upregulation of Myc pathway in peripheral blood cells of human TB patients was significantly associated with poor outcomes of TB treatment. Thus, Myc dysregulation in activated macrophages results in an aberrant macrophage activation and represents a novel target for host-directed TB therapies.

Keywords: macrophage, inflammation, lipid peroxidation, type I interferon, antioxidant defense, Myc, tuberculosis

INTRODUCTION

Thousands of years of co-evolution with modern humans has made *Mycobacterium tuberculosis* (Mtb) arguably the most successful human pathogen(Orgeur & Brosch, 2018). It currently colonizes approximately a quarter of the global population(WHO, 2022). Most Mtb-infected people develop latent TB, in which the host responses either eliminate or sequester the bacteria inside a granuloma structure (Pagan & Ramakrishnan, 2018; Pai *et al*, 2016). However, about 5-10% of Mtb-infected individuals will eventually develop active TB either within a year after the primary infection, or later in their life after re-activation of persistent bacteria or re-infection(Behr *et al*, 2021; Drain *et al*, 2018; Horsburgh & Rubin, 2011; Reichler *et al*, 2018). A plethora of genetic, developmental and environmental factors contribute to TB progression in individuals that initially resisted the pathogen(Cohen *et al*, 2022; Simmons *et al*, 2018).

Infection of the lung is central to Mtb's evolutionary success because it allows the pathogen to spread among human hosts via aerosols. After systemic dissemination from primary lesions, Mtb can be found in many human organs(Bussi & Gutierrez, 2019; Ulrichs *et al*, 2005). However, approximately 85% of the disease develops in the lungs(Pai *et al.*, 2016). Necrotic lesions are the major pathologic manifestation of pulmonary TB ranging from central necrosis in organized granulomas during primary TB to massive necrotizing pneumonia and the formation of cavities in post-primary pulmonary TB(Hunter, 2011; Pai *et al.*, 2016). The necrotic lung lesions develop in immunocompetent hosts despite the presence of active T cell mediated immune response(Cohen *et al.*, 2022).

Existing mechanistic concepts explaining the lesion necrosis fall into two main categories: i) *inadequate* local immunity that allows exuberant bacterial replication and production of virulence factors that drive tissue necrosis, vs. ii) *excessive* effector immunity that results in immune-mediated tissue damage (Ernst, 2018; O'Garra *et al*, 2013; Ogongo & Ernst, 2023). Although both scenarios are credible, they are mechanistically distinct and would require different therapeutic strategies. Therefore, in-depth understanding of mechanisms of pulmonary TB progression in immunocompetent hosts is necessary for accurate patient stratification and for the development of personalized approaches to immune modulation(DiNardo *et al*, 2021).

Mouse models have been successfully used for mechanistic studies of Mtb infection, although classical inbred mouse strains routinely used in TB research, such as C57BL/6 (B6) and BALB/c, do not develop human-like necrotic TB lesions(Apt & Kramnik, 2009). Nevertheless, even in these models, Mtb predominantly replicates in the lungs irrespective of the route of infection(North & Jung, 2004). Mouse models that recapitulate the necrotization of pulmonary TB lesions have also been developed (reviewed in (Kramnik & Beamer, 2016). We have previously found that C3HeB/FeJ mice develop necrotizing granulomas after infection with virulent Mtb and mapped several genetic loci of TB susceptibility using a cross of the C3HeB/FeJ with the resistant B6 mice (Kramnik *et al*, 1998; Kramnik *et al*, 2000; Yan *et al*, 2006). A single locus on chromosome 1, *sst1* (***s***uper***s***usceptibility to ***t***uberculosis 1), was specifically responsible for the control of the necrotization of TB lesions (Sissons *et al*, 2009). The *sst1*-susceptible mice develop necrotic lung lesions irrespective of the route of infection – aerosol, intravenous or intradermal(Kramnik *et al.*, 1998; Kramnik *et al.*, 2000; Pan *et al*, 2005; Pichugin *et al*, 2009; Yabaji *et al*, 2023) – thus demonstrating a common underlying mechanism.

We further found that the *sst1* locus primarily controls innate resistance to intracellular pathogens (Boyartchuk *et al*, 2004; He *et al*, 2013; Pan *et al.*, 2005; Yan *et al*, 2007), and the *sst1*-mediated susceptibility was associated with the hyperactivity of the type I interferon (IFN-I) pathway in activated macrophages in vitro and in vivo (Bhattacharya *et al*, 2021; He *et al.*, 2013;

Ji *et al*, 2019). Of note, the hyperactivity of IFN-I pathway has been associated with TB susceptibility and the disease progression both in human patients and experimental models (Donovan *et al*, 2017; Moreira-Teixeira *et al*, 2018; O'Garra *et al.*, 2013; Stanley *et al*, 2007). However, mechanisms that underlie the IFN-I hyperactivity and their roles in susceptibility to TB were insufficiently elucidated. Thus, the *sst1*-mediated susceptibility recapitulates the morphologic and mechanistic hallmarks of human TB disease and provides a genetically defined mouse model to study both the upstream mechanisms responsible for the IFN-I pathway hyperactivity(Bhattacharya *et al.*, 2021) and its downstream consequences(Kotov *et al*, 2023).

The *sst1* locus encodes the Sp110 (Pan *et al.*, 2005) and Sp140 (Ji *et al*, 2021) proteins – known as interferon inducible chromatin binding proteins(Fraschilla & Jeffrey, 2020a). The expression of mRNAs encoding both proteins is greatly diminished in mice that carry the *sst1* susceptibility allele and protein expression is undetectable for both(Bhattacharya *et al.*, 2021; Ji *et al.*, 2021). Both proteins were shown to be involved in regulation of type I interferon pathway(Ji *et al.*, 2021; Lee *et al*, 2012). The overexpression of Sp110b in macrophages increased their resistance to intracellular bacteria in vitro(Pan *et al.*, 2005), while the *Sp140* gene knockout dramatically increased the mouse susceptibility to several intracellular bacteria including virulent Mtb(Ji *et al.*, 2021). It was suggested that Sp140 plays a dominant role in TB susceptibility, via direct regulation of the interferon beta gene (*Ifnb1*) mRNA stability(Witt *et al*, 2024). In humans, the *Sp140* hypomorphic alleles were associated with susceptibility to multiple sclerosis and Crohn's disease(Matesanz *et al*, 2015; Mehta *et al*, 2017). Moreover, the *Sp140* mutations predicted the responsiveness of Crohn's disease patients to anti-TNF therapy, suggesting its role in regulating TNF response. Mechanistically, Sp140 was implicated in silencing "lineage-inappropriate" and developmental genes, maintenance of heterochromatin in activated macrophages (Mehta *et al.*, 2017) and downregulating transcriptional activity by inhibiting topoisomerases(Amatullah *et al*, 2022).

Previously, we found that prolonged TNF stimulation of the *sst1*-susceptible B6.Sst1S macrophages in vitro uniquely induced an aberrant response that was characterized by the *Ifnb1* superinduction, and a coordinated upregulation of interferon-stimulated genes (ISGs), markers of proteotoxic stress (PS) and the integrated stress response (ISR). The upregulation of all these pathways was prevented by a reactive oxygen scavenger (BHA) (Bhattacharya *et al.*, 2021) suggesting that oxidative stress was driving the aberrant activation of the *sst1*-susceptible macrophages. Current literature provides ample evidence of the crosstalk between the above pathways: 1) stress kinase activation by oxidative stress(Blaser *et al*, 2016; Kamata *et al*, 2005); 2) promotion of type I interferon (IFN-I) responses by stress kinases(Boccuni *et al*, 2022; Buskiewicz *et al*, 2016; Karin & Gallagher, 2005); 3) suppression of AOD by IFN-I (Lei *et al*, 2021; Riedelberger *et al*, 2020); 4) suppression of IFN responses and AOD by Myc (Levy & Forman, 2010; Torti & Torti, 2002; Zimmerli *et al*, 2022) (F**ig.1A**). However, the dynamic interactions and regulatory dependencies of these pathways in homeostasis and disease-specific contexts remain poorly understood.

In this study, we specifically addressed connectivity of the AOD and IFN-I pathways in *sst1*-susceptible macrophages persistently activated by TNF, a cell state relevant to TB granuloma microenvironment(Flynn & Chan, 2022). We determined that their aberrant response to prolonged TNF stimulation was primarily fueled by conflicting Myc and anti-oxidant responses leading to *Ifnb1* superinduction and the IFN-I pathway hyperactivity that locked the *sst1*-susceptible macrophages in a state of persistent oxidative stress. This unresolving stress compromised the macrophage resistance to virulent Mtb in vitro, and the accumulation of stressed macrophages

within TB lesions was associated with the failure of Mtb control within pulmonary TB lesions and their necrotization in vivo.

RESULTS

1. The *sst1* locus controls diverse trajectories of macrophage activation by TNF

To explore the spectrum of TNF responses in the B6 and B6.Sst1S BMDMs, we compared gene expression in the BMDM populations either naïve, or after 24 h of stimulation with TNF (10 ng/ml) using single-cell RNA sequencing (scRNA-seq)(**Fig.1B**). The naïve macrophage populations of both backgrounds were similar. All BMDMs responded to TNF stimulation, as evidenced by the de novo formation of clusters 1- 6, where cluster 3 appeared exclusively in the resistant (B6) and clusters 4 and 5 in the susceptible (B6.Sst1S) macrophage populations (**Fig.1C** and **Suppl.Fig.1A**). After TNF stimulation, the expression of the *sst1*-encoded *Sp110* and *Sp140* genes coordinately increased only in the B6 macrophages (**Fig.1D** and **Suppl.Fig.1B**). The IFN pathway was dramatically upregulated in TNF stimulated B6.Sst1S cells that lacked the *Sp110* and *Sp140* expression, but it was upregulated to a lesser degree in cluster 3 exclusive for TNF-stimulated *Sp110/140*-positive B6 macrophages (**Fig.1E** and **Suppl.Fig.1C**).

To determine the relatedness of the diverse macrophage subpopulations, as they emerge during TNF stimulation, we performed trajectory analysis that clearly demonstrated partial overlap and the divergence between the trajectories of TNF-stimulated resistant (RT) and susceptible (ST) subpopulations (**Fig.1F**). Subpopulations sp1 and sp2 of the B6 and B6.Sst1S macrophages were closely related and were characterized by the upregulation of cell division pathways in both backgrounds (**Fig.1G**). Cell cycle analysis demonstrated that TNF stimulation increased the fraction of macrophages in S phase (**Suppl.Table 1**).

The susceptible (ST) and resistant (RT) activation trajectories diverged as the RT transitioned from sp2 to sp3, but the ST transitioned from sp2 to sp4 and 5. The transition from sp2 to sp3 in the resistant B6 BMDMs, was characterized by an increase of the G1/S ratio, the downregulation of anabolic pathways involved in cell growth and replication (E2F and Myc), and the upregulation of anti-oxidant genes (**Fig.1G and 1H).** In contrast, in the susceptible B6.Sst1S macrophages, the sp2 transitioned to subpopulations sp4 and sp5 that were characterized by the decreased G1/S ratios as compared to sp3, signifying an increased G1 – S transition (**Suppl. Table 2**). The sp4 represented an intermediate state between sp2 and sp5 and was primarily characterized by the upregulation of the IFN pathway (**Fig.1G**), as evidenced by the upregulation of known IFN-I pathway activation markers (*Rsad2, IL1rn, Cxcl10*) (**Suppl.Fig.1C and D**).

The ST macrophages in sp5 uniquely demonstrated a coordinated upregulation of the IFN, TGFβ, Myc, E2F, and stress response (p53 and UPR) pathways (**Fig.1G**). They upregulated the Integrated Stress Response (ISR) genes (*Ddit3/Chop10*, *Atf3, Ddit4, Trib1, Trib3, Chac1*) in parallel with markers of immune suppression and apoptosis (*Cd274/PD-L1, Fas, Trail/Tnfsf10, Id2*, and a pro-apoptotic ligand – receptor pair *Tnfsf12/Tweak* and *Tnfrsf12a/Tweak* receptor) (**Suppl.Fig.1D**). Of note, IFN-I pathway genes were upregulated in all TNF-stimulated B6.Sst1S macrophages in agreement with the paracrine effect of Ifnβ, whose increased production by TNF-stimulated B6.Sst1S macrophages we have described previously (Bhattacharya *et al.*, 2021). Interestingly, the expression of *Irf7* and several IFN-inducible genes, such as *B2m, Cxcl10*, and *Ube2l6* was reduced in the sp5 cells, suggesting partial dampening of their IFN-I responsiveness (**Suppl.Fig.1C**).

Taken together, the single cell trajectory analysis revealed that sp5 represented a terminal state of the aberrant B6.Sst1S macrophage activation by TNF that was characterized the coordinated upregulation of stress, pro-apoptotic and immunosuppression genes. Unexpectedly, the stress escalation coincided with paradoxical activity of Myc and E2F pathways. Transition to

this state in the susceptible macrophage population was preceded by IFN-I pathway upregulation (sp2 – sp4). In contrast, the sp2 – sp3 transition in the wild type macrophages was coincident with upregulation of both the *Sp110* and *Sp140* genes and was accompanied by the termination of cell cycle and the upregulation of antioxidant defense pathways. Therefore, we concluded that in resistant TNF-stimulated macrophages the *sst1* locus-encoded genes promoted the activation of the AOD pathway either directly, or by suppressing the IFN-I pathway.

To begin exploring the hierarchy and crosstalk of these pathways, we used an unbiased computational approach to define the *Sp110* and *Sp140* regulatory networks. First, we inferred a mouse macrophage gene regulatory network using the GENIE3 algorithm (Huynh-Thu & Geurts, 2018) and external gene expression data for mouse macrophages derived from Gene Expression Omnibus (GEO) (Clough & Barrett, 2016). This network represents co-expression dependencies between transcription factors and their potential target genes, calculated based on mutual variation in expression level of gene pairs (Huynh-Thu *et al*, 2010; Zhernovkov *et al*, 2019). This analysis revealed that in mouse macrophages the *Sp110* and *Sp140* genes co-expressed with targets of Nfe2l1/2 (Nuclear Factor Erythroid 2 Like 1/2) and Mtf (metal-responsive transcription factor) TFs that are involved in regulating macrophage responses to oxidative stress and heavy metals, respectively (**Fig.1I**). Taken together, our experimental data and the unbiased network analysis suggested that in TNF-stimulated macrophages the *sst1*-encoded *Sp110* and/or *Sp140* gene(s) might be primarily involved in regulating AOD.

2. Dysregulated AOD activation in B6.Sst1S macrophages

Next, we compared the expression of upstream regulators of AOD in B6 and B6.Sst1S macrophages during TNF activation. Our previous studies demonstrated that the earliest differences between the B6 and B6.Sst1S BMDMs occurred between 8 and 12 h of TNF stimulation, concomitant with the upregulation of the Sp110 protein in the B6 macrophages and heat shock proteins in the mutant cells(Bhattacharya *et al.*, 2021). Comparing the time course of major transcriptional regulators of AOD in TNF-stimulated B6 and B6.Sst1S macrophages during this critical time interval, we observed higher upregulation of Nrf2 protein in TNF stimulated B6 BMDMs (**Fig.2A**). The Nrf1 levels were not substantially upregulated after TNF stimulation and were similar in B6 and B6.Sst1S BMDMs (**Suppl.Fig.2A and B**).

The Nrf2 difference was observed both in cytoplasmic and nuclear fractions (**Fig.2B** and **C**, respectively). The levels of Nrf2 negative regulators Keap1 and β-TrCP (**Suppl. Fig.2A**), and Bach1 (**Fig.2B** and **C**) were similar in both backgrounds and did not notably change after TNF stimulation. Quantitative microscopy confirmed that at 12 h of TNF stimulation the cytoplasmic and nuclear Nrf2 levels significantly increased in B6 but not in B6.Sst1S BMDMs (**Fig.2D**, **E** and **Suppl.Fig.2C**). In contrast, the levels of *Nfe2l1/2* mRNA induced by TNF were higher in the mutant macrophages suggesting post transcriptional regulation(**Fig.2F**). Therefore, we measured the rates of Nrf2 protein degradation 6 – 8 h after TNF stimulation but found no difference (**Fig.2G** and **2H**).

Using EMSA, we demonstrated that binding activity of nuclear Nrf2 to its target DNA at 8 and 12 h after TNF stimulation was greater in the resistant B6 BMDMs (**Fig.2I**). To identify core pathways controlled by the *sst1* locus during this critical period, we compared global mRNA expression profiles of the B6 and B6.Sst1S macrophages after 12 h of TNF stimulation using bulk RNA-seq. This analysis confirmed that the *Sp110* and *Sp140* genes were strongly upregulated by TNF stimulation exclusively in the B6 macrophages (**Fig.2J**). Gene set enrichment analysis (GSEA) of genes differentially expressed between TNF-stimulated B6.Sst1S and B6 macrophages

at this critical junction revealed that the IFN response, Myc, E2F target gene, Hypoxia, UV response and DNA repair pathways were upregulated in the mutant macrophages, while the detoxification of reactive oxygen species, cholesterol homeostasis, fatty acid metabolism and oxidative phosphorylation, peroxisome and lysosome pathways were downregulated (**Suppl.Table 3**). Functional pathway profiling using KEGG and Reactome databases also highlighted the upregulation of genes involved in oxidative stress and cellular senescence in mutant macrophages. In contrast, the wild type macrophages upregulated genes involved in detoxification of reactive oxygen species, inhibition of ferroptosis and peroxisome function (**Suppl.Table 4**). Supporting these findings, the total antioxidant capacity of the B6 macrophages after TNF stimulation increased to significantly higher levels, as compared to the B6.Sst1S (**Suppl.Fig.2D**).

Transcription factor binding site analysis of genes specifically upregulated by TNF in B6, but not B6.Sst1S, macrophages (B6-specific cluster) revealed an enrichment of Nfe2l1/Nfe2l2, Bach1 and Mafk sequence motifs, i.e. binding sites of transcription factors regulating AOD. In contrast, overrepresentation of E2F, Egr1 and Pbx3 transcription factor binding sites was found for genes in the Sst1S-specific cluster (**Suppl.Table 5**). A master regulator analysis using Virtual Inference of Protein Activity by Enriched Regulon Analysis (VIPER) algorithm also revealed a key role for Nfe2l1/2 (NF-E2-like) transcription factors (TFs) as regulators of genes differentially induced by TNF in B6 and B6.Sst1S BMDMs (**Suppl. Table 6**).

To further investigate this inference, we analyzed the expression of a gene ontology set "response to oxidative stress" (GO0006979, 416 genes) and observed clear separation of these genes in two clusters in a *sst1*-dependent manner (**Fig.2J** and **Suppl.Fig.2G**). This analysis demonstrated that the response to oxidative stress in the *sst1* mutant macrophages was dysregulated, but not paralyzed. For example, the upregulation of well-known Nrf2 target genes Heme oxygenase 1 (*Hmox1*) and (NAD(P)H quinone dehydrogenase 1 (*Nqo1*) were similar in B6 and B6.Sst1S BMDMs (**Suppl.Fig.2E** and **2F**, respectively).

A subset of antioxidant defense genes whose expression was concordant with *Sp110* and *Sp140* in B6 macrophages represented genes that are known to be involved in iron storage (ferritin light and heavy chains, *Ftl* and *Fth*), ROS detoxification and maintenance of redox state (*Cat, G6pdx, Sod2, Gstm1, Gpx4, Prdx6, Srxn1, Txn2* and *Txnrd1*) **(Fig.2J)**. We hypothesized that their coordinate downregulation in TNF-stimulated B6.Sst1S macrophages sensitized the mutant cells to iron-mediated oxidative damage and played a pivotal role in shaping their divergent activation trajectory.

3. Persistent TNF stimulation of B6.Sst1S macrophages leads to increased accumulation of lipid peroxidation products and IFN-I pathway hyperactivity.

To test this hypothesis, first we explored the intracellular iron storage. Both the ferritin light (*Ftl*) and heavy (*Fth*) chain genes were dysregulated in TNF-stimulated B6.Sst1S BMDMs. While the *Fth* mRNA was upregulated by TNF in B6 BMDMs, it remained at a basal level in the B6.Sst1S cells (**Fig.3A**). The *Ftl* mRNA level was significantly reduced after TNF stimulation in B6.Sst1S macrophages but remained at the basal level in B6 (**Fig.3B**). Accordingly, the expression of Ftl protein was reduced in B6.Sst1S BMDMs after 12 h of TNF stimulation, and both Ftl and Fth proteins were reduced at 24 h (**Fig.3C**). In parallel, the levels of Gpx1 and Gpx4 proteins were also substantially reduced by 24 h in B6.Sst1S(**Fig.3D**). The glutathione peroxidase 4 (Gpx4) protein plays a central role in preventing ferroptosis because of its unique ability to reduce hydroperoxide in complex membrane phospholipids and, thus, limit self-catalytic lipid

peroxidation (Stockwell *et al*, 2017). Thus, TNF-stimulated B6.Sst1S BMDMs had reduced intracellular iron storage capacity accompanied by the decline of the major lipid peroxidation inhibitor Gpx4. Accordingly, we observed increases in an intracellular labile iron pool (LIP, **Fig.3E**), an intracellular accumulation of oxidized lipids (**Fig.3F),** a toxic terminal lipid peroxidation (LPO) products malondialdehyde (MDA, **Fig.3G**) and 4-hydroxynonenal (4-HNE, **Fig.3H** and **Suppl.Fig.3A**). Treatment with the LPO inhibitor Ferrostatin-1 (Fer-1) prevented the 4-HNE accumulation (**Fig.3H** and **Suppl.Fig.3F**). The levels of the labile iron pool (LIP) and LPO remained significantly elevated in B6.Sst1S macrophages after 48h of TNF stimulation (**Suppl.Fig.3B – F**). We also observed an increased ROS production in the B6.Sst1S macrophages during persistent TNF stimulation **(Fig.3I, 3J ,** and **Suppl. Fig.3G).** The ASK1 - JNK – cJun stress kinase axis was upregulated in B6.Sst1S macrophages, as compared to B6, 12 – 36 h of TNF stimulation, i.e. during the aberrant activation stage confirming persistent stress (**Fig.3K**). By 48h of TNF stimulation, we noted moderate cell death in B6.Sst1S macrophage cultures (**Fig.3L, Suppl. Fig.3H**). Treatments with Fer-1, the antioxidant butylated hydroxyanisole (BHA), or IFNAR1 blockade each prevented the cell death (**Fig.3M**) suggesting that both persistent stress and macrophage death were mediated by ROS, lipid peroxidation and IFN-I pathway.

Next, we wanted to test whether the IFN-I pathway hyperactivity in TNF stimulated B6.Sst1S macrophages was responsible for the initial dysregulation of the *Ftl*, *Fth* and AOD gene expression, i.e. at 8 – 12 h of TNF stimulation. The IFNAR1 blockade, however, did not restore the Nrf2 and Ftl protein levels, or the *Fth*, *Ftl* and *Gpx1* mRNA levels to the wild type B6 levels (**Fig.4A – C**). Additionally, we observed that LPO production was increased as early as 6 h under TNF stimulated condition in both B6 and B6.Sst1S prior to *Ifnb1* superinduction (**Suppl. Fig.4A** and **B**). These data suggest that type I IFN signaling does not initiate LPO in our model.

Of note, the IFNAR1 blockade did not prevent the *Ifnb1* mRNA superinduction (**Fig.4D**), thus rejecting a hypothesis that the *Ifnb1* superinduction in B6.Sst1S macrophages was driven via an Ifnβ – IFNAR1 positive feedback(Ivashkiv, 2014). The mRNA expression of the interferon-inducible gene *Rsad2*, however, was suppressed, demonstrating the efficiency of the IFNAR1 blockade (**Fig.4E**).

In contrast, treatment of B6.Sst1S macrophages with Fer-1 or the iron chelator DFO during initial TNF stimulation inhibited both the *Ifnb1* and *Rsad2* mRNAs upregulation (**Fig.4F** and **Suppl. Fig.4C,** respectively). Importantly, Fer-1 treatment also reduced the *Ifnb1* and *Rsad2* levels in B6.Sst1S macrophages when added at 18 h after TNF stimulation, i.e. during established aberrant response (**Fig. 4G** and **Suppl. Fig.4D**). Thus, lipid peroxidation was involved in both the initial *Ifnb1* superinduction and in maintenance of the and IFN-I pathway hyperactivity driven by prolonged TNF stimulation.

Next, we wanted to test whether continuous IFN-I signaling was required for the accumulation of 4-HNE. during prolonged macrophage activation. Indeed, the blockade of type I IFN receptor (IFNAR1) after 2, 12 or 24 h after TNF stimulation prevented the 4-HNE accumulation at 48 h (**Fig.4H and I,** and **Suppl.Fig.4E - G**). Thus, *Ifnb1* super-induction and IFN-I pathway hyperactivity in B6.Sst1S macrophages follow the initial LPO production, and maintain and amplify it during prolonged TNF stimulation.

The *sst1*-encoded *Sp110* and *Sp140* genes were described as interferon-induced genes, and Sp140 protein was implicated in maintenance of heterochromatin silencing in activated macrophages (Fraschilla & Jeffrey, 2020a; Mehta *et al.*, 2017). Therefore, we hypothesized that their deficiency in the TNF-stimulated B6.Sst1S mutants may lead to the upregulation of silenced transposons and, thus, trigger the Ifnβ upregulation via intracellular RNA sensors, i.e. by an

autonomous mechanism unrelated to the AOD dysregulation. We examined the transcriptomes of B6 and B6.Sst1S macrophages before and after TNF stimulation for the presence of persistent viruses or transposons using a custom bioinformatics pipeline (Ma *et al*, 2021). No exogenous mouse viral RNAs were detected. A select set of mouse LTR-containing endogenous retroviruses (ERV's) (Jayewickreme *et al*, 2021), and non-retroviral LINE L1 elements were expressed at a basal level before and after TNF stimulation, but their levels in the B6.Sst1S BMDMs were similar to or lower than those seen in B6 (**Suppl.Fig.5A - C**). We also tested the accumulation of dsRNA using deep sequencing of macrophage small RNAs and failed to detect evidence of transposon-derived dsRNAs (**Suppl.Fig.5D**). We concluded from these findings that the majority of the basal transposon RNAs in macrophages exist primarily as single-stranded mRNAs that evade triggering interferon pathway. The above analyses allowed us to exclude the overexpression of persistent viral or transposon RNAs as a primary mechanism of the IFN-I pathway hyperactivity.

Taken together, the above experiments allowed us to reject the hypothesis that IFN-I hyperactivity caused the *sst1*-dependent AOD dysregulation. In contrast, they established that the hyperactivity of the IFN-I pathway in TNF-stimulated B6.Sst1S macrophages was itself driven by the *initial* dysregulation of AOD and iron-mediated lipid peroxidation. During prolonged TNF stimulation, however, the IFN-I pathway was upregulated, possibly via ROS/LPO-dependent JNK activation, and acted as a potent amplifier of lipid peroxidation.

4. Hyperactivity of Myc in susceptible macrophages after TNF stimulation fuels lipid peroxidation

We wanted to determine whether the AOD genes were regulated by the *sst1*-encoded genes directly or indirectly via an intermediary regulator. Previously, we identified two transcription factors whose binding activities were exclusively upregulated in the susceptible macrophages after 12h of TNF stimulation: Myc and HSF1 (Bhattacharya *et al.*, 2021). The bulk RNA-seq analysis at this timepoint (12 h) also demonstrated the upregulation of Myc pathway along with E2F target genes and stress responses specifically in TNF-stimulated B6.Sst1S BMDMs, as compared to B6 (**Fig.2**). Of note, the scRNA-seq analysis above also demonstrated the association of Myc and stress response pathways in the mutant cells at 24 h (**Fig.1**). Therefore, we hypothesized that in susceptible macrophages Myc might be involved in the dysregulation of AOD and iron storage.

First, we observed that Myc was regulated in an *sst1*-dependent manner: in TNF-stimulated B6 wild type BMDMs, *c-Myc* mRNA was downregulated, while in the susceptible macrophages c-*Myc* mRNA was upregulated (**Fig.5A**). The c-Myc protein levels were also higher in the B6.Sst1S cells in unstimulated BMDMs and 6 – 12 h of TNF stimulation (**Fig.5B**). Next, we tested whether suppression of Myc activity could "normalize" the susceptible phenotype using Myc-Max dimerization inhibitor 10058-F4 (F4). Indeed, this treatment increased the levels of Fth and Ftl proteins in TNF-stimulated susceptible macrophages (**Fig.5C**) and decreased the labile iron pool (**Fig.5D**). Accordingly, the levels of MDA, oxidized lipids and 4-HNE also significantly decreased (**Fig.5E – G, Suppl.Fig.6A and B**), as well as the levels of *Ifnb1*, *Rsad2* and the ISR markers *Trib3* and *Chac1* (**Fig.5H**). Possibly, the ISR activation serves as an alternative pathway of Myc inhibition, as it is known to inhibit the oncogene protein translation(Wolfe *et al*, 2014).

Next, we wanted to determine whether the upregulation of Myc is driven by TNF alone or in synergy with CSF1, a growth factor that also stimulates Myc. In vitro, we observed the upregulation of Myc shortly after the addition of fresh CSF1-containing media, but no difference in the Myc protein dynamics between B6 and B6.Sst1S BMDMs in the absence of TNF (**Suppl.Fig.6C**). In addition, we tested whether CSF1R inhibitors could prevent the superinduction

of *Ifnb1* and *Rsad2* mRNAs in TNF-stimulated B6.Sst1S macrophages. The CSF1R inhibitors were used at concentrations that did not cause macrophage death (**Suppl. Fig.6D**). Neither of these inhibitors prevented the *Ifnb1* and *Rsad2* upregulation (**Suppl.Fig.6E** and **F**). Because Myc induction by CSF1 and TNF is conducted via distinct relays of receptor signaling and transcription factors, we concluded that the *sst1* locus specifically controls Myc expression induced by inflammatory signaling. Indeed, Myc promoter has multiple predicted NF-κB and/or AP-1 transcription factors binding sites. To test this hypothesis, we used specific JNK inhibitor D-JNK1, but it only partially reduced Myc protein levels in TNF-stimulated B6.Sst1S macrophages (**Fig.5I and J**). Because both *Sp110* and *Sp140* mRNAs and proteins are upregulated during extended TNF stimulation, one of them may participate in feedback regulation of TNF-induced Myc, either directly or via yet unknown intermediates.

5. Myc hyperactivity and lipid peroxidation compromise the cell autonomous and T cell-mediated control of Mtb infection by B6.Sst1S macrophages.

Next, we tested whether the described facets of the aberrant macrophage activation conferred by the *sst1S* allele were relevant to Mtb susceptibility. After macrophage infection with virulent Mtb in vitro, gradual accumulation of LPO product 4-HNE was observed in BMDMs of both B6 and B6Sst1S genetic backgrounds at 3 – 5 days post infection (dpi). It occurred either in the presence or absence of exogenous TNF (**Fig.6A,** and **Suppl.Fig.7A and B**). By day 5 post infection, TNF stimulation significantly increased LPO accumulation only in the B6.Sst1S macrophages (**Fig.6A**). Both Mtb-infected and bystander non-infected B6.Sst1S macrophages showed 4-HNE accumulation (**Fig. 6B**).

TNF stimulation improved the control of Mtb growth in B6 but not in B6.Sst1S macrophages, as quantified using an Mtb replication reporter strain (**Fig.6B**, **Suppl. Fig.7C and D**) and quantitative PCR of Mtb genomes (**Fig.6C**). The LPO inhibition using Fer-1 improved the survival of the Mtb-infected BMDMs (**Fig.6D - E**) and prevented the intracellular Mtb growth (**Fig.6F**) during the five-day in vitro infection. The iron chelator DFO also significantly reduced the Mtb growth, although restricting iron availability may also directly affect the bacterial replication. Importantly, the survival of Mtb-infected BMDMs was also improved, and the bacterial loads were significantly reduced by the Myc inhibitor, F4 (**Fig.6G and H**). Of note, the effects of the lipid peroxidation inhibitors became prominent between days 3 and 5 post infection (**Suppl.Fig.7E**) suggesting that these inhibitors do not directly boost the bacterial killing by activated macrophages, but rather prevent macrophage damage.

Next, we tested whether the *sst1* susceptible allele compromised responsiveness of Mtb-infected macrophages to mycobacteria-specific T cells. The immune T cells were isolated from the regional lymph nodes of the resistant B6 mice vaccinated with live attenuated BCG vaccine, and added either to the B6 or B.Sst1S BMDM monolayers infected with Mtb the day before. The BMDMs were either treated with TNF prior to infection or not. After co-culture with the immune T cells for one or two days, Mtb loads were significantly reduced in T cell co-cultures with the resistant B6 macrophages. The susceptible B6.Sst1S BMDMs did not respond to the same T cells either in the presence or absence of exogenous TNF (**Fig.6I - J** and **Suppl.Fig.7F**). The B6.Sst1S BMDM responsiveness to T cells was improved by inhibitors of lipid peroxidation (Fer1) and Myc (F4): the bacterial loads were significantly reduced 48 h after co-culture with the immune T cells (**Fig.6K, Suppl. Fig.7G**). This T cell-mediated Mtb control was specific for T cells isolated from BCG-immunized mice (**Suppl. Fig.7H**). The IFNAR1 blockade improved the ability of TNF-stimulated B6.Sst1S macrophages to control Mtb with and without T help (**Fig.6L, Suppl. Fig.7I**).

It also restored their responsiveness to soluble Ifnγ that was inhibited by pre-stimulation with TNF (**Fig.6M**). These data demonstrate that during prolonged TNF stimulation of B6.Sst1S macrophages the Myc-driven lipid peroxidation and subsequent IFN-I hyperactivity compromise both the cell autonomous and T cell-mediated Mtb control.

6. Loss of Mtb control in pulmonary TB lesions is associated with the accumulation of lipid peroxidation products and stress escalation in intralesional macrophages

We wanted to determine whether the aberrantly activated macrophages accumulate within pulmonary TB lesions in vivo. We used a mouse model of pulmonary TB where the lung lesions develop after hematogenous spread from the primary site of infection and progress exclusively in the lungs, despite systemic immunity and control of infection in other organs. Microscopic pulmonary lesions develop in the lungs of both B6 and B6.Sst1S mice, but advanced multibacillary TB lesions develop exclusively in the B6.Sst1S(Yabaji *et al*, 2025a; Yabaji *et al*, 2025b; Yabaji *et al.*, 2023).

Based on Mtb loads, TB lesions were classified in two categories: the Mtb-controlling paucibacillary lesions, and multibacillary lesions, in which the control of Mtb growth was compromised (**Suppl.Fig.8**). The 4-HNE levels dramatically increased in multibacillary lesions (**Fig.7A** and **Suppl. Fig.9A**). The majority of the 4-HNE+ cells were CD11b+ myeloid cells (**Fig.7B** and **Suppl. Fig.9B**).

To characterize macrophages in TB lesions and identify pathways associated with the loss of Mtb control, we performed spatial transcriptomics analysis of intralesional macrophages (Iba1+) using the Nanostring GeoMX Digital Spatial Profiler (DSP) system(Merritt *et al*, 2020)(**Suppl.Fig.10**).

Comparing the Iba1+ macrophage gene expression profiles in the mutibacillary vs paucibacillary lesions, we identified 192 upregulated and 376 downregulated genes at a two and above fold change (**Suppl.Table 7**). Pathway analysis demonstrated a highly significant upregulation of Hypoxia, TNF and IL6/STAT3 Signaling, Glycolysis, Complement and Coagulation pathways in the multibacillary lesions consistent with the escalation of hypoxia, inflammation and macrophage activation in the advanced lesions. Mechanistically, top transcription factors associated with genes upregulated in the multibacillary lesions were NFKB1, JUN, STAT1, STAT3 and SP1 (**Suppl.Fig.11A - C**).

To specifically interrogate the interferon pathways in paucibacillary vs multibacillary lesions, we compiled a list of 430 interferon type I and type II inducible genes from public databases that were also included in Nanostring Whole Transcriptome Analysis (WTA) probes. Among these, 70 genes were differentially regulated between the Iba1+ macrophages in multi- vs paucibacillary lesions (**Fig.7C**). Among the upregulated genes were metalloprotease *Mmp12, IL6* and *Socs3*, chemokines *Cxcl10, Ccl2, Ccl3, Ccl4, Ccl19*, cell stress and senescence marker p21 (*Cdkn1a*), and many known IFN-I target genes. The most upregulated pathways in Iba1+ cells within multibacillary lesions were Interferon, TNF, and IL6/STAT3 Signaling, and top transcription factors associated with upregulation of these pathways were NFKB1, STAT3, STAT1 and IRF1 (**Suppl.Fig.11D – E**).

Among the IFN-inducible genes upregulated in paucibacillary lesions were *Ifi44l*, a recently described negative regulator of IFN-I that enhances control of Mtb in human macrophages(DeDiego *et al*, 2019; Jiang *et al*, 2021) and *Ciita*, a regulator of MHC class II inducible by Ifnγ, but not IFN-I (**Suppl.Table 8**). Thus, the loss of local Mtb control in advanced pulmonary TB lesions was associated with the accumulation of aberrantly activated macrophages

that contained lipid peroxidation products, with upregulation of the IFN-I pathway and downregulation of Ifnγ-inducible genes.

To detect the Ifnβ-expressing cells within TB lesions, we introduced the *Ifnb1*-YFP reporter described previously (Scheu *et al*, 2008) in the B6.Sst1S background. The B6.Sst1S,*Ifnb1*-YFP reporter mice were infected with virulent Mtb (*smyc'* :: mCherry) constitutively expressing the red fluorescent protein reporter (Lavin & Tan, 2022). We validated the Ifnβ reporter in vitro using co-staining of TNF-stimulated B6.Sst1S,*Ifnb1*-YFP BMDMs with YFP-specific antibodies (**Suppl.Fig.12A**). We demonstrated the accumulation of Ifnβ expressing cells in pulmonary TB lesions of B6.Sst1S, *Ifnb1*-YFP mice using both the YFP reporter and in situ hybridization with the *Ifnb1* probe (**Suppl.Fig.12B**). The majority of the YFP+ cells in TB lesions were Iba1+ macrophages a fraction of which were iNOS positive (**Fig. 7D, Suppl. Fig.13A**). The mice with paucibacillary lesions had 62% and multibacillary lesions had 80% activated macrophages expressing YFP. These findings clearly demonstrated the production of Ifnβ by activated M1-like macrophages.

Next, we assessed the expression of stress markers phospho-cJun and Chac1 in total, IFN-I producing and activated macrophages in TB lesions. These markers were primarily expressed by activated macrophages (Iba1+) expressing iNOS and/or Ifnβ (YFP+)(**Fig.7E, Suppl. Fig.13B - F**). We also documented the upregulation of PKR in the multibacillary lesions, which is consistent with the upregulation of the upstream IFN-I and downstream Integrated Stress Response (ISR) pathways, as described in our previous studies (Bhattacharya *et al.*, 2021) (**Suppl.Fig.14A**).

Thus, progression from the Mtb-controlling paucibacillary to non-controlling multibacillary TB lesions in the lungs of TB susceptible mice was mechanistically linked with a pathological state of macrophage activation characterized by escalating stress (as evidenced by the upregulation phospho-cJun, PKR and Chac1), the upregulation of Ifnβ and the IFN-I pathway hyperactivity, with a concurrent reduction of Ifnγ responses. In our in vitro experiments, these stressed macrophages were unresponsive to T cell help (**Fig.6J**). Consequently, the administration of BCG vaccine to Mtb-infected B6.Sst1S mice did not increase their survival (**Suppl.Fig.14B**).

7. Myc upregulated genes are enriched in TB patients who fail treatment

Next, we tested whether the upregulation of Myc pathway is associated with pulmonary TB progression in human TB patients. We used blood samples obtained from 41 individuals recently (<90 days) diagnosed with TB that were enrolled in the Regional Prospective Observational Research for Tuberculosis (RePORT)-India consortium. Patients were infected with drug susceptible Mtb and treated with rifampicin, isoniazid, ethambutol, and pyrazinamide, per Technical and Operational Guidelines for TB Control by the Ministry of Health and Family Welfare, Government of India, 2016. Blood samples were collected before or within a week of the antibiotic treatment commencement. Patients were monitored for two years during and post-treatment. Individuals who failed the antibiotic treatment (n=21) were identified by positive sputum culture or clinical diagnosis of symptoms at any time after 4 full months of treatment and symptoms determined to not be from another cause. Cured TB patients (controls) remained culture-negative and symptom-negative for the two-year observation period.

Several oncogene signatures identified previously(Bild *et al*, 2006) were analyzed with the TBSignatureProfiler(Johnson *et al*, 2021) to determine their ability to differentiate between treatment failures and controls based on bootstrapped AUC scores. Myc_up ranked within the top 3 signatures with an AUC of 0.74 and p-value of 0.008 (**Suppl.Fig.15A**). Boxplots of ssGSEA

scores were created to determine whether the myc signatures were differentially enriched between treatment failures and controls. Myc_upregulated genes were enriched in the treatment failure group relative to the treatment control group (**Suppl.Fig.15B, Suppl.Table 9**). The ROC curve used to generate the AUC scores for myc_up is depicted in **Suppl.Fig.15C**, and a heatmap of the genes used to generate the ssGSEA scores is depicted in **Suppl.Fig.15D**, with ssGSEA scores of each patient sample. These data indicate that the upregulation of Myc pathway in peripheral blood cells of TB patients was associated with poor prognosis and TB persistence even in patients infected with antibiotic sensitive Mtb. Although pathological evaluation was not included in this study, treatment failures in immunocompetent patients are often associated with massive fibro-necrotic pulmonary TB lesions.

DISCUSSION

This study revealed a mechanistic connection between susceptibility to TB conferred by the *sst1* locus, hyperactivity of the IFN-I pathway and unresolving stress in activated macrophages. We have shown that the aberrant activation of the *sst1*-susceptible macrophages and persistent stress in response to TNF form a vicious cycle shaped by disbalance of anabolic (Myc), homeostatic (antioxidant defense and proteostasis) and immune pathways (TNF and type I IFN).

Previous studies demonstrated that the IFN-I pathway hyperactivity underlies the Mtb susceptibility mediated by the *sst1* locus(Moreira-Teixeira *et al.*, 2018; O'Garra *et al.*, 2013). Indeed, the IFN-I pathway inactivation in B6.Sst1S mice increased their resistance to Mtb infection, but it did not restore it to the wildtype B6 level(Ji *et al.*, 2019). Thus, the IFN-I pathway hyperactivity was insufficient to explain the *sst1*-mediated susceptibility.

Exploring additional mechanisms controlled by the *sst1* locus in activated macrophages we revealed deficient activation of a fraction of the antioxidant defense genes, including genes involved in glutathione and thioredoxin antioxidant systems, NADPH regeneration and ferroptosis resistance, such as ferritin light and heavy chains *Ftl* and *Fth*, subunits of glutamate–cysteine ligase subunits *Gclm*, gluthathione peroxidases *Gpx1* and *Gpx4* and stearoyl-Coenzyme A desaturase 2 *Scd2*. These experimental findings are consistent with an unbiased computational analysis that considered genes co-regulated with the *sst1*-encoded *Sp110* and *Sp140* genes in mouse macrophage datasets and suggested their primary association with antioxidant response pathways.

Blockade of IFNAR1 did not restore the AOD gene expression. In contrast, ROS scavengers, iron chelators and inhibitors of lipid peroxidation prevented the *Ifnb1* superinduction suggesting that the dysregulated oxidative stress response of B6.Sst1S macrophages was upstream of the IFN-I pathway hyperactivity. Boosting antioxidant defense in B6.Sst1S mice by knockout of the *Bach1* gene, a negative regulator of Nrf2, not only reduced lung inflammatory damage, but also decreased the expression of the IFN-I pathway genes (Amaral *et al*, 2023).

Taken together these data are consistent with our previous observations that the initial *Ifnb1* super-induction in the *sst1*-susceptible macrophages was driven by the synergy of TNF/NFκB and a JNK pathway activated by oxidative stress (Bhattacharya *et al.*, 2021). Here we found that the prolonged TNF stimulation of the *sst1* mutant macrophages led to the IFN-I dependent accumulation of toxic low molecular weight lipid peroxidation products MDA and 4-HNE. The *Ifnb1* superinduction also resulted in the downstream activation of the integrated stress response markers Trb3 and Chac1. Thus, IFN-I pathway did not initiate, but amplified the AOD dysregulation.

Among pathways upregulated in TNF-stimulated B6.Sst1S macrophages was Myc pathway. In actively growing cells, Myc promotes ribosome biogenesis, cap-dependent protein translation and also suppresses expression of ferritins, most likely to provide labile iron for anabolic metabolism(Torti & Torti, 2002; Wu *et al*, 1999). Myc hyperactivity is associated with cell senescence and maladaptive activity mTOR pathway(Alic & Partridge, 2015; Hofmann *et al*, 2015). In macrophages, Myc promotes the development of myeloid derived suppressor cells and alternatively activated macrophages(Kumar *et al*, 2016; Pello *et al*, 2012). Here we have shown that Myc hyperactivity was responsible for the initiation of the aberrant macrophage activation trajectory leading to increased intracellular labile iron pool (Fe^{+2}) and lipid peroxidation. Myc inhibition also prevented the *Ifnb1* superinduction and activation of the integrated stress response markers *Trb3* and *Chac1*.

The above findings allowed us to reconstruct the regulatory cascade driving the aberrant macrophage activation (**Suppl.Fig.16**). During prolonged TNF stimulation of the B6.Sst1S macrophages, Myc hyperactivity and the impairment of AOD lead a coordinated downregulation of the Ferritin heavy and light chains and lipid peroxidation inhibitor genes. In the absence of terminators, the intracellular peroxidation of polyunsaturated fatty acids (PUFA) is catalyzed by ferrous iron (Fe^{+2}) via the Fenton reaction and proceeds in an autocatalytic manner damaging cell membranes containing tightly packed PUFA (Mortensen *et al*, 2023). This autocatalytic lipid peroxidation fuels persistent oxidative stress and, likely, sustains the activity of JNK. Downstream, *Ifnb1* superinduction in B6.Sst1S macrophages leads to the upregulation of interferon-inducible genes, including PKR. The subsequent PKR-dependent ISR activation leads to the upregulation of Chac1(Bhattacharya *et al.*, 2021)(Bhattacharya *et al.*, 2021) - a glutathione degrading enzyme gamma-glutamylcyclotransferase 1(Crawford *et al*, 2015) that further compromises the AOD. This stepwise escalation eventually locks the susceptible macrophages in a state of unresolving stress which is maintained by continuous stimulation with TNF and boosted by IFN-I signaling. Thus, during prolonged stimulation of the B6.Sst1S macrophages with TNF the autocatalytic lipid peroxidation and IFN-I hyperactivity form a positive feedback loop sustaining the unresolving oxidative stress. Unlike ferroptosis, however, this did not immediately result in massive cell death but sustained a state of the aberrant macrophage activation that reduced their ability to control Mtb both in a cell autonomous and a T cell-dependent manner. In contrast, in the wild type B6 macrophages Myc was inhibited more readily, and ferritin proteins were upregulated to sequester free iron in parallel with the upregulation of Nrf2. Their combined effects increased stress resilience of activated macrophages. Recent in vivo studies also demonstrated that ferritins and antioxidant pathways were upregulated in inflammatory macrophages isolated from Mtb-infected wild type B6 mice (Pisu *et al*, 2020).

At the molecular level, the detailed characterization of the *sst1*-mediated regulation of macrophage activation provides proximal phenotypes for deeper understanding of the functions of the *sst1*-encoded Sp110 and Sp140 proteins. The *Sp110* and *Sp140* genes and proteins are upregulated exclusively in the wild type cells 8 - 12h after TNF stimulation, i.e. the time interval during which the divergence between the wild type and mutant macrophages occurs(Bhattacharya *et al.*, 2021). Their transcription and protein stability are regulated by interferons and stress kinases(Fraschilla & Jeffrey, 2020a). Their activities can modulate i) responses to inflammatory stimuli via CARD domain(Fraschilla & Jeffrey, 2020b), ii) metabolism, via the activated nuclear receptor interaction domain LXXLL, iii) regulation of chromatin silencing(Mehta *et al.*, 2017), transcriptional elongation(Amatullah *et al.*, 2022) via chromatin interacting PHD, BRD and SAND domains and indirect regulation of the *Ifnb1* mRNA stability(Witt *et al.*, 2024). Potentially, they may interact with intracellular nucleic acids via the DNA interaction domain SAND(Bottomley *et al*, 2001; Carles & Fletcher, 2010).

Our data suggest that one of them might be involved in regulation of the Nrf2 protein biosynthesis either at the levels of *Nfe2l1/2* mRNA splicing (Goldstein *et al*, 2016) or cap-independent translation (Li *et al*, 2010;Shay *et al*, 2012) (**Fig.2**). Recent experimental evidence suggest that a specialized translation machinery is involved in context-dependent regulation of protein biosynthesis(Shi & Barna, 2015). Ribosome modifications, such as protein composition and rRNA methylation, were shown to be involved in control of selective IRES-dependent translation in myeloid cells(Basu *et al*, 2011; Mazumder *et al*, 2003) and regulation of inflammation(Basu *et al*, 2014; Poddar *et al*, 2013; Poddar *et al*, 2015). Recently, enrichment of Sp100 and Sp110 proteins in ribosomes was observed during B6 macrophage activation with

LPS(Susanto *et al*, 2023). These findings suggest that the Sp110 protein may be involved in fine tuning of protein biosynthesis in activated macrophages favoring the IRES-dependent Nrf2 translation.

More generally, the Sp110 and Sp140 proteins may serve as context-dependent regulators (possibly, both as sensors and tunable controllers) of macrophage activation and stress resilience via a coordinated upregulation of AOD and downregulating Myc and IFN-I pathways. Hypothetically, downregulating this mechanism may also play physiological roles in eliminating infected(Rothchild *et al*, 2019) or transformed cells(Gorbunova *et al*, 2012; Leonova *et al*, 2013). By coordinately increasing free iron pool for non-enzymatic free radical generation, and simultaneously decreasing the buffering capacity of intracellular antioxidants, this activation state promotes generation and unopposed spread of free radicals. However, the inappropriate activation of its build-in amplification mechanisms, such as IFN-I, may drive immunopathologies in the face of chronic stimulation, as occurs with Mtb infection.

In the mouse model of chronic TB infection, lipid peroxidation products did not appear to significantly affect the long term Mtb survival: the mycobacterial cell wall and multiple mycobacterial antioxidant pathways exist to allow for the survival of, at least, a fraction of mycobacterial population in highly oxidative environments (Pacl *et al*, 2018; Piddington *et al*, 2001). The accumulation of stressed macrophages and LPO products within TB lesions, however, gradually degraded local immunity that allowed for Mtb replication and provided a fodder for growing mycobacteria(Mahamed *et al*, 2017). Thus, in the mouse model that recapitulate key pathomorphological features of pulmonary TB in human patients, the aberrant macrophage activation state was responsible for both the inflammatory tissue damage and the failure of local immunity.

The above mechanistic dissection of the aberrant macrophage activation drivers provides therapeutic targets for interrupting their vicious cycle in vivo. For example, monocytes recruited to inflammatory lesions may be particularly vulnerable to the dysregulation of Myc. Prior to terminal differentiation within inflammatory milieu, these immature cells undergo several cycles of replication. Cell growth requires labile iron that is provided by Myc via downregulation of ferritins(Stockwell *et al.*, 2017; Torti & Torti, 2002). Recently we found that lung epithelial cells embedded within TB lesions express CSF1 – a macrophage growth factor known to stimulate Myc expression (Yabaji *et al.*, 2023). Thus, the coincidence of TNF and CSF1 – Myc stimulation may initiate and propagate the aberrant activation state in monocytes recruited to chronic pulmonary TB lesions. Similarly, growth factors produced locally within inflamed tissues may sustain Myc hyperactivity and the aberrant activation state of monocytes/macrophages in other chronic inflammatory pathologies.

Further understanding the specific roles of the SP100 family proteins, as well as other signals and checkpoints that regulate the pathological macrophage activation state transitions, will allow for their rational therapeutic modulation - to boost host defenses and mitigate the collateral tissue damage.

Resource availability

Lead contact

Further information and requests for resources and reagents should be directed to and will be fulfilled by the lead contact, Igor Kramnik (ikramnik@bu.edu).

Materials availability

All unique/stable reagents generated in this study are available from the Lead Contact with a completed Materials Transfer Agreement.

Data and code availability

This study did not generate datasets/code and any additional information will be available from the lead contact upon request.

Inclusion and Diversity

We support inclusive, diverse, and equitable conduct of research.

MATERIALS and METHODS

Reagents

Recombinant mouse TNF (Cat# 315-01A) and IL-3 (Cat# 213-13) were procured from Peprotech. The mouse monoclonal antibody to mouse TNF (MAb; clone XT22), isotype control, and mouse monoclonal antibody to mouse Ifnβ (Clone: MAR1-5A3) were obtained from Thermo Scientific. BHA (Cat# B1253) and Deferoxamine mesylate (Cat#D9533]) were sourced from Sigma Aldrich. PLX3397 (Cat# S7818), Myc inhibitor (10058-F4) (Cat# S7153), and ferrostatin-1 (Cat# S7243) were purchased from Selleckchem. D-JNK1 (Cat# HY-P0069), GW2580 (Cat# HY-10917), and BLZ945 (Cat# HY-12768) were acquired from Med Chem Express. Fetal bovine serum (FBS) for cell culture medium was sourced from HyClone. Middlebrook 7H9 and 7H10 mycobacterial growth media were purchased from BD and prepared following the manufacturer's instructions. A 50 µg/mL hygromycin solution was utilized for reporter strains of Mtb Erdman (SSB-GFP, smyc′::mCherry).

Animals

C57BL/6J inbred mice were obtained from the Jackson Laboratory (Bar Harbor, Maine, USA). The B6J.C3-*Sst1*$^{C3HeB/Fej}$ Krmn congenic mice were created by transferring the *sst1* susceptible allele from C3HeB/FeJ mouse strain on the B6 (C57BL/6J) genetic background using twelve backcrosses (referred to as B6.Sst1S in the text). The B6.Sst1S,*Ifnb1*-YFP mice were produced by breeding B6.Sst1S mice with a reporter mouse containing a Yellow Fluorescent Protein (YFP) reporter gene inserted after the *Ifnb1* gene promoter (Scheu *et al.*, 2008). The YFP serves as a substitute for Interferon beta (*Ifnb1*) gene expression. All animal procedures were performed with the full knowledge and approval by the Institutional Animal Care and Use Committee (IACUC) of Boston University. Mice were euthanized by CO_2 asphyxiation in accordance with IACUC-approved protocols.

BMDMs culture and Treatment

The isolation of mouse bone marrow and the cultivation of bone marrow-derived macrophages (BMDMs) were conducted following the procedures outlined in a prior study (Yabaji *et al*, 2022). BMDMs were plated in tissue culture plates, followed by treatment with TNF and incubation for 16 hours at 37°C with 5% CO2. Various inhibitors were applied to the cells until the point of harvest.

Infection of BMDM with *M. tuberculosis*

For infection experiments, M. tuberculosis H37Rv (Mtb) was cultured in 7H9 liquid media for three days and subsequently harvested. The bacteria were then diluted in media containing 10% L929 cell culture medium (LCCM) without antibiotics to achieve the desired Multiplicity of Infection (MOI). Following this, 100 µL of Mtb-containing media with the specified MOI was added to BMDMs cultivated in a 96-well plate format that had been pre-treated with TNF or inhibitors. The plates underwent centrifugation at 500xg for 5 minutes, followed by an incubation period of 1 hour at 37°C. To eliminate any extracellular bacteria, cells were treated with Amikacin at 200 µg/µL for 45 minutes. Subsequently, cells were washed and maintained with inhibitors, as applicable, in DMEM/F12 containing 10% FBS medium without antibiotics at 37°C in 5% CO2 for the duration of each experiment. Media changes and inhibitor replacements were carried out

every 48 hours. The confirmation of MOIs was achieved by counting colonies on 7H10 agar plates. All procedures involving live Mtb were conducted within Biosafety Level 3 containment, adhering to regulations from Environmental Health and Safety at the National Emerging Infectious Disease Laboratories, the Boston Public Health Commission, and the Center for Disease Control.

Cytotoxicity and Mycobacterial growth assays

The cytotoxicity, cell loss, and Mtb growth assays were conducted in accordance with the procedures outlined by (Yabaji *et al.*, 2022). In brief, BMDMs were subjected to inhibitor treatment or Mtb infection as previously described for specified time points. Upon harvesting, samples were treated with Live-or-Dye™ Fixable Viability Stain (Biotium) at a 1:1000 dilution in 1X PBS/1% FBS for 30 minutes. Following staining, samples were carefully washed to prevent any loss of dead cells from the plate and subsequently treated with 4% paraformaldehyde (PFA) for 30 minutes. After rinsing off the fixative, samples were replaced with 1X PBS. Following decontamination, the sample plates were safely removed from containment. Utilizing the Operetta CLS HCA System (PerkinElmer), both infected and uninfected cells were quantified. The intracellular bacterial load was assessed through quantitative PCR (qPCR) employing a specific set of Mtb and *M. bovis*-BCG primer/probes, with BCG spikes included as an internal control, as previously described(Yabaji *et al.*, 2022). The percentage of cell numbers were calculated based on the number of cells at Day 0 (immediately after Mtb infection). The fold change of Mtb was calculated after normalization using Mtb load at Day 0 after infection and washes. We quantified the percentage of replicating Mtb using a replication reporter strain, Mtb Erdman (SSB-GFP, *smyc′*::mCherry). Replicating Mtb was identified by counting the number of SSB-GFP puncta-positive Mtb, while the total number of Mtb per field was determined by counting mCherry-expressing bacteria (red).

RNA Isolation and quantitative PCR

The extraction of total RNA was carried out utilizing the RNeasy Plus mini kit (Qiagen). Subsequently, cDNA synthesis was conducted using the Invitrogen™ SuperScript™ III First-Strand Synthesis SuperMix (Cat#18080400). Real-time PCR was executed with the GoTaq qPCR Mastermix (Promega) employing the CFX-96 real-time PCR System (Bio-Rad). Oligonucleotide primers were designed using Integrated DNA Technologies. Either 18S or β-actin expression served as an internal control, and the quantification of fold induction was computed using the ΔΔCt method.

Analysis of RNA sequencing data

Raw sequence reads were mapped to the reference mouse genome build 38 (GRCm38) by STAR (Dobin *et al*, 2013). The read count per gene for analysis was generated by featureCounts (Liao *et al*, 2014). Read counts were normalized to the number of fragments per kilobase of transcript per million mapped reads (FPKM) using the DESeq2 Bioconductor R package (Love *et al*, 2014). Pathway analysis was performed using the GSEA method implemented in the camera function from the limma R package (Wu & Smyth, 2012). Databases KEGG, MSigDB Hallmark, Reactome were used for the GSEA analysis . Transcripts expressed in either 3 conditions with FPKM > 1 were included in the pathway analyses. To infer mice macrophage gene regulatory network, we used ARCHS4 collected list of RNE-seq data for mice macrophages cells from Gene Expression Omnibus (GEO) (Lachmann *et al*, 2018). The total number of analyzed experimental datasets was 1960. This gene expression matrix was utilized as input for the GENIE3 algorithm, which

calculated the most likely co-expression partners for transcription factors. The list of transcription factors was derived from the Animal TFDB 3.0 database (Hu *et al*, 2019). The Virtual Inference of Protein Activity by Enriched Regulon Analysis (VIPER) algorithm was used to estimate the prioritized list of transcription factors (Alvarez *et al*, 2016). The software Cytoscape (version 3.4.0) was used for network visualization (Shannon *et al*, 2003). The i-cisTarget web service was used to identify transcription factor binding motifs that were over-represented on a gene list (Imrichova *et al*, 2015). Statistical analysis and data processing were performed with R version 3.6.1 (https://www.r-project.org/) and RStudio version 1.1.383 (https://www.rstudio.com).

Generation and sequencing of single-cell RNA libraries

Single cell suspensions of mouse bone marrow derived macrophages were loaded on a 10X genomics chip G at concentrations varying between 1,240,000 – 1,575,000 cells/mL aiming for a targeted cell recovery of 5,000 cells per sample and processed using the 10X Genomics 3'v3.1 Dual index kit according to the manufacturer protocol (10x Genomics, CA, USA). Following the 10X Genomics Chromium controller run the Gel-beads in emulsion (GEMs) were transferred to strip tubes and subsequently put into a thermal cycler using the following parameters: 45 min at 53 °C, 5 min at 85 °C, hold at 4 °C. The samples were then stored in a -20˚C freezer overnight. The next day samples were thawed at room temperature before adding the recovery agent to break the GEMs. Subsequently the cDNA was purified and amplified, and the gene expression libraries were generated and purified. The size distribution and molarity of these libraries were assessed using the Bioanalyzer High Sensitivity DNA Assay (Agilent Technologies, Lexington, MA, USA). The libraries were then pooled at 5nM and sequenced on an Illumina NextSeq 2000 instrument at a 600pM input and 2% PhiX spike in using a P3 100 cycle flow cell (Illumina, San Diego, CA, USA) resulting in 36000-58000 reads per cell.

Processing of scRNA-seq data

The 10x Genomics Cell Ranger pipeline v6.0.1 was used for demultiplexing, alignment, identification of cells, and counting of unique molecular indices (UMIs). The Cell Ranger mkfastq pipeline was used to demultiplex raw base call (BCL) files generated by Illumina sequencers into FASTQ files. The Cell Ranger count pipeline was used to perform alignment and create UMI count matrices using reference genome mm10 (Ensembl 84) and parameters –expect-cells = 5000. Droplets with at least 500 UMIs underwent further quality control with the SCTK-QC pipeline(Hong *et al*, 2022). The median number of UMIs was 9,927, the median number of genes detected was 2,637, the median percentage of mitochondrial reads was 5.43%, and the median contamination estimated by decontX was 0.17 across cells from all samples(Yang *et al*, 2020). Cells with less than 500 counts, less than 500 genes detected, or more than 25% mitochondrial counts were excluded leaving a total of 14,658 cells for the downstream analysis.

Clustering of single-cell data

The Seurat package was used to cluster the cells into subpopulations(Stuart *et al*, 2019). The 2,000 most variable genes were selected using the FindVariableFeatures function, after removing features with fewer than 3 counts in 3 cells. Cells were embedded in two dimensions with UMAP using the RunUMAP function. The clustering was performed at resolution 0.8 resulting in 15 clusters. Markers for each cluster were identified with the FindAllMarkers function using the Wilcoxon Rank Sum test and default parameters: log fold-change threshold = 0.25 and min.pct = 0.1. The trajectory analysis was performed using the slingshot package; the pseudotime trajectory was computed using the slingshot function and selecting the PCA (considering 50 PCA) and

unweighted cluster labels as inputs(Street *et al*, 2018). The pathway analysis was performed using the VAM package in combination with MSigDB's Hallmark geneset collection. The genesets were scored using the vamForSeurat function, and the top pathways were found by running the FindAllMarkers analysis on the CDF assay. The following package versions were used: Seurat v4.0.4, VAM v1.0.0, Slingshot v2.3.0, SingleCellTK v2.4.1, Celda v1.10.0.

Western Blot Analysis

Equal amounts of protein extracts were separated by SDS-PAGE and transferred to a PVDF membrane (Millipore). Following a 2-hour blocking period in 5% skim milk in TBS-T buffer [20 mM Tris-HCl (pH 7.5), 150 mM NaCl, and 0.1% Tween20], the membranes were incubated overnight with the primary antibody at 4°C. Subsequently, bands were acquired using the chemiluminescence (ECL) kit (Thermo Scientific) and GE ImageQuant LAS-4000 Multi-Mode imager. A loading control, either β-actin or β-tubulin, was assessed on the same membrane. Secondary antibodies used included HRP-conjugated goat anti-mouse and anti-rabbit antibodies. Densiometric analysis was performed by quantification of area using Image J.

Half-life determination of Nrf2 protein

The B6 and B6.Sst1S BMDM were stimulated with TNF (10 ng/ml) for 6 h. Cycloheximide (2 uM) was added to the cultures and cells were harvested after 15, 30, 45, 60, 90, and 120 min. Western blotting was carried out for Nrf2 and β-tubulin as described. The densitometry analysis was performed using ImageJ software (NIH, USA). The linear regression curve was plotted using GraphPad Prism software, and the half-life of Nrf2 protein was derived."

Electrophoretic Mobility Shift Assay

The nuclear extracts were prepared using a nuclear extraction kit (Signosis Inc.) according to the instructions provided. The EMSA was carried out using the EMSA assay kit (Signosis Inc.) following the instructions provided. Briefly, 5 μg of nuclear extract was incubated with biotin-conjugated Nrf2 antioxidant response element (ARE) probe in 1X binding buffer for 30 min. The reaction mixture was electrophoresed in 6.5% non-denaturing polyacrylamide gel and then blotted onto a nylon membrane. The protein-bound probe and free probe were immobilized on the membrane by UV light mediated cross-linking. After blocking the membrane, the probes were detected using streptavidin-HRP mediated chemiluminescence method. The images were captured using ImageQuant LAS 4000.

Quantification of intracellular labile iron

The method used to measure Labile Intracellular Iron (LIP) involved the Calcein acetoxymethyl (AM) ester (Invitrogen) quenching technique with some modifications, as described in (Amaral *et al*, 2019; Picard *et al*, 1998; Thomas *et al*, 1999). BMDMs were plated in 96 well plates and washed with 1× DPBS before being lysed with 0.05% saponin for 10 minutes. Next, the cell lysates were incubated with 125 nM calcein AM at 37°C for 30 minutes. A negative control was established by incubating the lysates with the iron chelator deferoxamine (Sigma-Aldrich) at room temperature for 30 minutes, while FeSO4-treated cells served as the positive control. The fluorescence of Calcein AM was measured using a fluorescence microplate reader, and the differential MFI of calcein AM between untreated and deferoxamine-treated samples was calculated to determine intracellular labile iron and represented as fold change.

MDA assay

The amount of MDA in the BMDMs were measured using a Lipid Peroxidation (MDA) Assay Kit (Abcam, ab118970) according to the manufacturer's protocols. Briefly, $2x10^6$ cells were lysed in Lysis Solution containing butylated hydroxytoluene (BHT). The insoluble fraction was removed by centrifugation, and the supernatant was collected, protein concentrations were estimated and used for analysis. The equal amount of supernatants (Based on protein concentration) were mixed with thiobarbituric acid (TBA) solution reconstituted in glacial acetic acid and then incubated at 95˚C for 60 min. The supernatants containing MDA-TBA adduct were added into a 96-well microplate for analysis. A microplate reader was used to measure the absorbance at OD 532 nm.

Lipid peroxidation by C11-Bodipy 581/591

Briefly, the cells were washed 3 times with 1X PBS and treated with 1 μM C11-Bodipy 581/591 dye (Invitrogen) suspended in 1X PBS for 30 min in the dark at 37oC. The LPOs were measured fluorometrically using Spectramax M5 microplate reader (Molecular Devices).

Measurement of total antioxidant capacity

The total antioxidant capacity was quantified using the Antioxidant assay kit (Cayman chemical) according to the instructions provided. A standard curve was generated by using various concentrations of Trolox (0.068-0.495 mM). 10 μg of the cell lysate was used to determine the Trolox equivalent antioxidant capacity. The percentage of induced antioxidant capacity was calculated using the formula, (Trolox $equivalent_{TNF\ stimulated}$-Trolox $equivalent_{unstimulated}$)/ Trolox equivalent $_{unstimulated}$ X 100.

Immunofluorescence imaging

BMDMs were cultured on coverslips and subjected to treatment with or without TNF, followed by processing for inhibitor treatment or Mtb infection. Subsequently, cells were fixed with 4% paraformaldehyde (PFA) for 10 minutes (non-infected) or 30 minutes (Mtb infected) at room temperature and then blocked for 60 minutes with 1% BSA containing 22.52 mg/mL glycine in PBST (PBS + 0.1% Tween 20). After the blocking step, cells were incubated overnight with primary antibodies (4-HNE, Nrf2, or Nrf-1 specific), washed, and then incubated with Alexa Fluor 594-conjugated Goat anti-Rabbit IgG (H+L) secondary Antibody (Invitrogen) in 1% BSA in the dark for 1 hour. The cells were mounted using ProlongTM Gold antifade reagent (Thermo Fisher Scientific), and images were captured using an SP5 confocal microscope. All images were processed using ImageJ software.

Detection of lipid peroxidation by Click-iT linoleamide alkyne (LAA) method

To investigate the lipid peroxidation, the Click-iT™ lipid peroxidation imaging kit (C10446, ThermoFisher) was used. The BMDMs were cultured on 12 mm coverslips in 24-well plates. Following a 6 h of TNF treatment, 50 μM Click-iT linoleamide alkyne (LAA) was added to the cell culture and incubated at 37oC for 1 h under 5 % CO2. The cells were washed, fixed, permeabilized, blocked, and stained with Alexa fluor 488 azide according to the manufacturer's instructions. Subsequently, the coverslips were mounted onto the microscope slide with ProLongTM Diamond Antifade mountant with DAPI (P36962, ThermoFisher). The images were captured using the Leica SP5 confocal microscope and further the signal quantification was carried out using ImageJ software (Version 1.53k, NIH).

Quantification of oxidative stress
B6 and B6.Sst1S cells were seeded in a 96-well plate and stimulated with TNF (10 ng/mL) or left untreated for 6, 24, and 36 hours. For ROS inhibition, cells were treated with BHA (100 µM) 2 h post TNF stimulation. At each time point, CellROX® Oxidative Stress Reagent (Cat#C10444, Invitrogen™) at 5 µM final concentration was added to the cells and incubated for 30 minutes at 37°C, protected from light. After incubation, cells were washed twice with warm PBS, and fluorescence was analyzed using a fluorescence microscope or flow cytometer. ROS levels were quantified by comparing the fluorescence intensity across treatment groups and time points.

Analysis of Small RNAs in Macrophages
Small RNA libraries were prepared from size fractionation of 10ug of total macrophage RNA on a denaturing polyacrylamide gel to purify 18-35nt small RNAs, and converted into Illumina sequencing libraries with the NEBNext Small RNA Library kit (NEB). Libraries were sequenced on the Illumina NextSeq-550 in the Boston University Microarray and Sequencing Core. We applied long RNAs and small RNAs RNAseq fastq files to a transposon and small RNA genomics analysis pipeline previously developed for mosquitoes (Dayama *et al*, 2022; Ma *et al.*, 2021) with the mouse transposon consensus sequences loaded instead. Mouse transposon consensus sequences were downloaded from RepBase (Bao *et al*, 2015), and RNA expression levels were normalized internally to each library's depth by the Reads Per Million counting method.

Infection of mice with *Mycobacterium tuberculosis* and collection of organs
The subcutaneous infection of mice was conducted following the procedure outlined in (Yabaji *et al.*, 2023). In brief, mice were anesthetized using a ketamine-xylazine solution administered intraperitoneally. Each mouse was subcutaneously injected in the hock, specifically in the lateral tarsal region just above the ankle (by placing the animal in the restrainer), with 50 µl of 1X PBS containing 10^6 CFU of Mtb H37Rv or Mtb Erdman (SSB-GFP, smyc′::mCherry). At the designated time points, the mice were anesthetized, lung perfusion was performed using 1X PBS/heparin (10 U/ml), and organs were collected.
Female mice were used unless otherwise specified and mice were randomly assigned to experimental groups. No animals were excluded after enrollment. Investigators were blinded to group assignments during outcome assessment. Sample size was determined based on prior studies.

Confocal immunofluorescence microscopy of tissue sections
Immunofluorescence of thick lung sections (50-100 µm) was conducted following the detailed procedures outlined earlier (Yabaji *et al.*, 2023). Briefly, lung slices were prepared by embedding formalin fixed lung lobes in 4% agarose and cutting 50 µm sections using a Leica VT1200S vibratome. Sections were permeabilized in 2% Triton X-100 for 1 day at room temperature, followed by washing and blocking with 3% BSA in PBS and 0.1% Triton X-100 for 1 hour. Primary antibodies were applied overnight at room temperature, followed by washing and incubation with secondary antibodies for 2 hours. Samples were stained with Hoechst solution for nuclei detection, cleared using RapiClear® 1.47 solution for 2 days, and mounted with ProLong Gold Antifade Mountant. Imaging was performed using a Leica SP5 spectral confocal microscope. Primary rabbit anti-4-HNE, anti-Iba1, and anti-iNOS polyclonal antibodies were detected using goat anti-rabbit antibodies labelled with Alexa Fluor 647.

Mycobacterial staining of lung sections
Paraffin-embedded 5µm sections were stained using New Fuchsin method (Poly Scientific R and D Corp., cat no. K093) and counterstained with methylene blue following the manufacturer's instructions.

Tissue inactivation, processing, and histopathologic interpretation
Tissue samples were submersion fixed for 48 h in 10% neutral buffered formalin, processed in a Tissue-Tek VIP-5 automated vacuum infiltration processor (Sakura Finetek , Torrance, CA, USA), followed by paraffin embedding with a HistoCore Arcadia paraffin embedding machine (Leica, Wetzlar, Germany) to generate formalin-fixed, paraffin-embedded (FFPE) blocks, which were sectioned to 5 µm, transferred to positively charged slides, deparaffinized in xylene, and dehydrated in graded ethanol. A subset of slides from each sample were stained with hematoxylin and eosin (H&E) and consensus qualitative histopathology analysis was conducted by a board-certified veterinary pathologist (N.A.C.) to characterize the overall heterogeneity and severity of lesions.

Chromogenic Monoplex Immunohistochemistry
A rabbit specific HRP/DAB detection kit was employed (Abcam catalog #ab64261, Cambridge, United Kingdom). In brief, slides were deparaffinized and rehydrated, endogenous peroxidases were blocked with hydrogen peroxidase, antigen retrieval was performed with a citrate buffer for 40 minutes at 90°C using a NxGen Decloaking chamber (Biocare Medical, Pacheco, California), non-specific binding was blocked using a kit protein block, the primary antibody was applied at a 1.200 dilution, which cross-reacts with mycobacterium species (Biocare Medical catalog#CP140A,C) and was incubated for 1 h at room temperature, followed by an anti-rabbit antibody, DAB chromogen, and hematoxylin counterstain. Uninfected mouse lung was examined in parallel under identical conditions with no immunolabeling observed serving as a negative control.

Multiplex fluorescent immunohistochemistry (mfIHC)
A Ventana Discovery Ultra (Roche, Basel, Switzerland) tissue autostainer was used for brightfield and multiplex fluorescent immunohistochemistry (fmIHC). In brief tyramide signaling amplification (TSA) was used in an iterative approach to covalently bind Opal fluorophores (Akoya Bioscience, Marlborough, MA) to tyrosine residues in tissue sections, with subsequent heat stripping of primary-secondary antibody complexes until all antibodies were developed. Before multiplex-IHC was performed, each antibody was individually optimized using a single-plex-IHC assay using an appropriate positive control tissue. Optimizations were performed to determine ideal primary antibody dilution, sequential order of antibody development, assignment of each primary antibody to an Opal fluorophore, and fluorophore dilution. Once an optimal protocol was established, 5µm tissue sections were cut from FFPE lung arrays. All Opal TSA-conjugated fluorophore reactions took place for 20 minutes. Fluorescent slides were counterstained with spectral DAPI (Akoya Biosciences) for 16 minutes before being mounted with ProLong gold antifade (ThermoFischer, Waltham, MA). Antibodies utilized in 4-plex 5 color (DAPI counterstained) analysis included: Iba1, iNOS, YFP, Chac1, and P-c-Jun. All rabbit antibodies were developed with a secondary goat anti-rabbit HRP-polymer antibody (Vector Laboratories, Burlingame, CA) for 20min at 37C and all mouse derived antibodies were developed with a secondary goat anti-mouse HRP-polymer antibody (Vector Laboratories).

Brightfield Immunohistochemistry
Antigen retrieval was conducted using a Tris based buffer-Cell Conditioning 1 (CC1)-Catalog # 950-124 (Roche). The MHCII primary was of mouse origin, so a goat anti-mouse HRP-polymer antibody (Vector Laboratories) was utilized. Brightfield slides utilized A ChromoMap DAB (3,3′-Diaminobenzidine) Kit-Catalog #760-159 (Roche) to form a brown precipitate at the site of primary-secondary antibody complexes containing HRP. Slides were counterstained with hematoxylin and mounted.

Multispectral whole slide microscopy
Fluorescent and chromogen labeled slides were imaged at 40X using a Vectra Polaris™ Quantitative Pathology Imaging System (Akoya Biosciences). For fluorescently labeled slides, exposures for all Opal dyes were set based upon regions of interest with strong signal intensities to minimize exposure times and maximize the specificity of signal detected. A brightfield acquisition protocol at 40X was used for chromogenically labeled slides.

Digitalization and linear unmixing of multiplex fluorescent immunohistochemistry
Whole slide fluorescent images were segmented into QPTIFFs, uploaded into Inform software version 2.4.9 (Akoya Biosciences), unmixed using spectral libraries affiliated with each respective opal fluorophore including removal of autofluorescence, then fused together as a single whole slide image in HALO (Indica Labs, Inc., Corrales, NM).

Quantitative analysis of immunohistochemistry
View settings were adjusted to allow for optimal visibility of immunomarkers and to reduce background signal by setting threshold gates to minimum signal intensities. After optimizing view settings, annotations around the entire tissue were created to define analysis area using the flood tool and artifacts were excluded using the exclusion pen tool. To analyze lesions independently, a tissue classifier that uses a machine-learning approach was utilized to identify lesions. The outputs from this classifier were annotations for each lesion, which were then isolated into independent layers, which were analyzed separately from other layers. For quantifying myeloid markers in multiplexes, an algorithm called the HALO (v3.4.2986.151, Indica Labs, Albuquerque, NM, USA) Area Quantification (AQ) module was created and finetuned to quantify the immunoreactivity for all targets. Thresholds were set to define positive staining based on a real-time tuning feature. AQ outputted the percentage of total area displaying immunoreactivity across the annotated whole slide scan in micrometers squared (μm^2). AQ output the total percentage positive for each phenotype. AQ and HP algorithms were run across all layers for each individual lesion and exported as a .csv file.

Spatial transcriptomics
To perform spatial transcriptomics analysis, we used the Nanostring GeoMX Digital Spatial Profiler (DSP) system (Nanostring, Seattle, WA) (Danaher *et al*, 2022; Merritt *et al.*, 2020). To identify pathways dominating early vs. late (advanced) lesions, we selected lungs from 2 mice with paucibacilarly early lesions and 2 mice with advanced multibacilarly lesions with necrotic areas. Slides were stained with fluorescent CD45-, pan-keratin-specific antibodies, and Iba1-specific antibodies (sc-32725, Santa Cruz Biotechnology, CA, USA) and DAPI. Diseased regions of interest (ROI) for expression profiling of Iba1+ cells were selected to focus on myeloid-rich

areas avoiding areas of micronecrosis and tertiary lymphoid tissue (**Suppl.Fig.9**). Eight ROI each of normal lung, early and late lesions (respectively) were studied. The profiling used the Mouse Whole Transcriptome Atlas (WTA) panel which targets ~21,000+ transcripts for mouse protein coding genes plus ERCC negative controls to profile the whole transcriptome, excluding uninformative high expressing targets such as ribosomal subunits. A subsequent study focused on gene expression within macrophages identified by Iba1 labeling in lung sections showing uncontrolled (advanced multibacillary) lesions in comparison to controlled (paucibacillary stage). Samples from each ROI were packaged into library for sequencing (NextSeq550, Illumina) following the procedure recommended by Nanostring. After sequencing, the data analysis workflow began with QC evaluation of each ROI based on thresholds for number of raw and aligned reads, sequencing saturation, negative control probe means, and number of nuclei and surface area. Background correction is performed using subtraction of the mean of negative probe counts. Q3 normalization (recommended by Nanostring) results in scaling of all ROIs to the same value for their 3rd quartile value. The count matrix was imported into the Qlucore Genomics Explorer software package (Qlucore, Stockholm, Sweden) and log2 transformed for further analysis. Statistical analysis was then performed to identify differentially expressed genes (typically unpaired t-test with Benjamini-Hochberg control for FDR rate at $q < .05$). Lists of differentially expressed genes (DEGs) from comparisons of distinct stages were further analyzed for enrichment of pathways or predicted transcription factors using the Enrichr online tool (Chen *et al*, 2013; Liberzon *et al*, 2015; Xie *et al*, 2021). To specifically explore interferon-related gene expression in Iba1+ macrophages, we used: 1) a list of genes unique to type I genes derived by pooling four common type I and type II interferon gene list respectively and identifying the non-overlapping (unique) genes for each type (see **Suppl.Table 8, Suppl. Fig. 10**); 2) using the GSEA analysis tool of the Qlucore software to evaluate enrichment of the MSigDB Hallmark collection of pathways (which include Interferon-alpha and Interferon-gamma, and other pathways of interest(Liberzon *et al.*, 2015).

Human blood transcriptome analysis

Ethics approval

Ethics approval for the study was obtained from the Institutional Ethics Committee of the participating institutions, and written informed consent was obtained prior to enrollment. This study utilized data from four longitudinal observational studies collected at five clinical sites within the Regional Prospective Observational Research for Tuberculosis (RePORT)-India consortium: Byramjee Jeejeebhoy Government Medical College (BJMC), Pune; the Jawaharlal Institute of Postgraduate Medical Education and Research (JIPMER, Puducherry); National Institute for Research in Tuberculosis (NIRT), Chennai; Prof. M. Viswanathan Diabetes Research Centre (MVDRC), Chennai; and the Christian Medical College (CMC), Vellore(Ayiraveetil *et al*, 2020; Christopher *et al*, 2021; Gupte *et al*, 2016; Kornfeld *et al*, 2016).

Blood sample collection and processing

Participant demographics including age, sex, body mass index (BMI), diabetes status, alcohol use, and tobacco use were recorded and matched for Blood collection. Blood samples were collected from 41 individuals and recently (<90 days) diagnosed with TB, within one week of treatment commencement from five clinical sites within the Regional Prospective Observational Research

for Tuberculosis (RePORT)-India consortium. Individuals for this study were newly diagnosed with TB (within 90 days; sputum smear-positive or Xpert MTB/RIF assay positive (Cepheid, Sunnyvale, CA, USA)), at least 15 years of age, multi-drug-resistant negative, and had received less than one week of treatment. Sociodemographic data such as age, sex, behavioral characteristics (smoking, alcohol use (using the Alcohol Use Disorders Identification Test [AUDIT-C]), tobacco use, and body mass index (BMI) were obtained through a questionnaire and the medical history of the participants. There were no significant differences in risk factors for TB or treatment failure, including sex, risky alcohol use, tobacco use, BMI, or diabetes. Patients were monitored for two years during and post-treatment with Rifampicin, isoniazid, ethambutol, and pyrazinamide, per India national guidelines[Division CT. Technical and Operational Guidelines for TB Control in India 2016. Central TB Division, Directorate General of Health Service, Ministry of Health and Family Welfare; Government of India, New Delhi. 2016 (Bush *et al*, 1998). Individuals who failed treatment (n=21) were identified by positive sputum culture or clinical diagnosis of symptoms at any time after 4 full months of treatment and symptoms determined to not be from another cause. Treatment controls were determined by those who remained culture-negative and symptom-negative for the two-year observation period.

Blood samples from each person were collected and stored in PAXgene tubes (Cat #762165, BD Biosciences, San Jose, CA, USA) at -80C until processing using the PAXgene Blood RNA kit (Cat #762164, Qiagen, Hilden, Germany). PAXgene tubes were sent to MedGenome (Bangalore, India) for processing. Library preparation and sequencing were performed at the GenoTypic Technology Pvt. Ltd. Genomics facility in Bangalore, India, with the SureSelect Strand-Specific mRNA Library Prep kit (Cat #5190–6411, Agilent, Santa Clara, USA). One µg of RNA was used for mRNA enrichment by poly(A) selection and fragmented using RNAseq Fragmentation Mix containing divalent cations at 94 degrees C for 4 minutes. Enriched mRNA underwent fragmentation through exposure to RNASeq Fragmentation Mix with divalent cations at 94 °C for 4 min. Subsequently, single-strand cDNA was synthesized in the presence of Actinomycin D (Gibco, Life Technologies, Carlsbad, CA, USA) and purified utilizing HighPrep magnetic beads (Magbio Genomics Inc., USA). Following this step, double-stranded cDNA was synthesized, and the ends were repaired before undergoing further purification. Adenylation of the 3′-ends of cDNA preceded the ligation of Illumina Universal sequencing adaptors, which were then purified and amplified with 10 PCR cycles. The final cDNA sequencing libraries were purified and quantified using Qubit, while the fragment size distribution was assessed using Agilent TapeStation. Subsequently, the libraries were combined in equimolar proportions, and the resulting multiplexed library pools were sequenced utilizing the Illumina NextSeq 500 platform for 75 bp single-end reads.

RNA-sequencing data processing of human samples

QC and alignment

Raw sequencing FASTQ files were assessed for data quality using FastQC[S. A. FastQC: a quality control tool for high throughput sequence data. Babraham Bioinformatics, Babraham Institute. 2010]. Trimmomatic was used to trim the reads (SLIDINGWINDOW:4:20 LEADING:3 TRAILING:3 MINLEN:36) (Bolger *et al*, 2014). Rsubread (Liao *et al*, 2013)]was used to align reads to the human genome hg39 and to determine expression counts for each gene. Genes missing (or with 0 counts) in more than 20% of the samples were excluded before batch correction, as well

as one outlier identified with Principal Components Analysis (PCA) before batch correction and could not be rectified using batch correction (unpublished data).

Batch correction and normalization

The RNA samples were processed sequentially in two batches. Batch effects created by combining the two batches were removed using ComBat-Seq(Zhang *et al*, 2020)). The ComBat-Seq adjusted counts were normalized using a $\log_2$-counts per million (logCPM) adjustment, and the logCPM values were used for downstream analysis.

Differential expression

Differential expression was performed on batch-corrected counts/logcpm using limma(Ritchie *et al*, 2015) and signature genes were selected from the limma results to obtain logFC, p-values, and p-adjusted values (using a Benjamini-Hochberg false-discovery rate).

Oncogene signatures

Normal Human mammary epithelial cells (HMEC) were transfected with adenoviruses containing either the gene of interest or GFP as described in(Bild *et al.*, 2006; McQuerry *et al*, 2019). Differentially expressed genes between transfected cells and controls with a Benjamini-Hochberg cutoff of < 0.05 were used in for the signatures of each transfected oncogene.

TBSignatureProfiler Platform

Heatmaps, boxplots, receiver-operating characteristic (ROC) curve, and area under the ROC curve (AUC) were calculated and depicted using the functions within the TBSignatureProfiler (Johnson *et al.*, 2021). Bootstrapping was used to iteratively calculate AUC values using leave-one-out cross-validation to obtain mean AUCs and 95% confidence intervals (CI) for 100 repeats for each signature. We generated mean AUC values for the predictive performance of collected oncogene-specific signatures(Bild *et al.*, 2006; McQuerry *et al.*, 2019) in terms of their ability to distinguish between treatment-failure individuals and control samples in our cohort. The single sample Gene Set Enrichment Analysis (ssGSEA) (Barbie *et al*, 2009) was used to generate enrichment scores for each signature.

Statistical Analysis

Statistical analyses were performed using GraphPad Prism 9 software (RRID:SCR_002798). Differences among groups involving two or more variables were assessed using two-way analysis of variance (ANOVA) with adjustments for multiple post hoc comparisons. For comparisons across multiple groups based on a single variable, one-way ANOVA with post hoc testing was applied. Two-tailed paired or unpaired t-tests were used for comparisons between two groups after verifying data normality. For non-parametric datasets, the Wilcoxon Rank Sum test (Mann-Whitney U test equivalent) was employed. Statistical significance was defined as $p < 0.05$. Significance levels are indicated as follows: *, $p < 0.05$; **, $p < 0.01$; ***, $p < 0.001$; and ****, $p < 0.0001$.

Acknowledgements:

The authors would like to acknowledge expert support of Boston University Avedisian and Chobanian School of Medicine Sequencing and Single Cell Sequencing Cores. This work was supported by the National Institutes of Health grant R01HL126066 (to IK), R01HL133190 (to IK and WRB), National Institutes of Health grant R01CA244660 and EU grant no. 101136926 MULTIR" (to BK), and National Institutes of Health grant R01GM114864 (to AAG.). NIH grants R01-AG052465 and R01-GM135215 to NCL. National Library of Medicine grant R01LM013154 to JDC, NIH grant R01: 5R01GM127430-07 to WEJ.

Author contributions: Conceptualization: IK, LK, SMY, WEJ, WRB; Methodology : SMY, VZ, PBA, SL, LK, OSR, AAG, YA, JDC, NAC, NCL, SL, WEJ; Validation and formal analysis: SMY, SAA, PBA, VZ, OSR, AAG, BNK, LK, NCL, QM, GD, AV; Investigation: SMY, PBA, SL, GD, AV; Resources: IK, LK, AAG, BK, NCL, JDC, NAC, WEJ; Writing – original draft: SMY, PBA, IK, LK; Writing – review & editing: IK, LK, WRB, WEJ; Supervision: IK; Funding acquisition: IK, LK, AAG, BNK, NCL, WRB, WEJ.

Declaration of interests:
The authors have declared that no conflict of interest exists.

References

Alic N, Partridge L (2015) Myc mouse and anti-ageing therapy. *Trends in Endocrinology & Metabolism* 26: 163 - 164

Alvarez MJ, Shen Y, Giorgi FM, Lachmann A, Ding BB, Ye BH, Califano A (2016) Functional characterization of somatic mutations in cancer using network-based inference of protein activity. *Nat Genet* 48: 838-847

Amaral EP, Costa DL, Namasivayam S, Riteau N, Kamenyeva O, Mittereder L, Mayer-Barber KD, Andrade BB, Sher A (2019) A major role for ferroptosis in Mycobacterium tuberculosis-induced cell death and tissue necrosis. *J Exp Med* 216: 556-570

Amaral EP, Namasivayam S, Queiroz ATL, Fukutani E, Hilligan KL, Aberman K, Fisher L, Bomfim CCB, Kauffman K, Buchanan J *et al* (2023) BACH1 promotes tissue necrosis and Mycobacterium tuberculosis susceptibility. *Nat Microbiol*

Amatullah H, Fraschilla I, Digumarthi S, Huang J, Adiliaghdam F, Bonilla G, Wong LP, Rivard M-E, Beauchamp C, Mercier V *et al* (2022) Epigenetic reader SP140 loss of function drives Crohn's disease due to uncontrolled macrophage topoisomerases. *Cell* 185: 3232-3247.e3218

Apt A, Kramnik I (2009) Man and mouse TB: contradictions and solutions. *Tuberculosis (Edinburgh, Scotland)* 89: 195 - 198

Ayiraveetil R, Sarkar S, Chinnakali P, Jeyashree K, Vijayageetha M, Thekkur P, Lakshminarayanan S, Knudsen S, Hochberg NS, Horsburgh CR *et al* (2020) Household food insecurity among patients with pulmonary tuberculosis and its associated factors in South India: a cross-sectional analysis. *BMJ Open* 10: e033798

Bao W, Kojima KK, Kohany O (2015) Repbase Update, a database of repetitive elements in eukaryotic genomes. *Mob DNA* 6: 11

Barbie DA, Tamayo P, Boehm JS, Kim SY, Moody SE, Dunn IF, Schinzel AC, Sandy P, Meylan E, Scholl C *et al* (2009) Systematic RNA interference reveals that oncogenic KRAS-driven cancers require TBK1. *Nature* 462: 108-112

Basu A, Das P, Chaudhuri S, Bevilacqua E, Andrews J, Barik S, Hatzoglou M, Komar Aa, Mazumder B (2011) Requirement of rRNA methylation for 80S ribosome assembly on a cohort of cellular internal ribosome entry sites. *Molecular and Cellular Biology* 31: 4482 - 4499

Basu A, Poddar D, Robinet P, Smith JD, Febbraio M, Baldwin WM, Mazumder B (2014) Ribosomal Protein L13a Deficiency in Macrophages Promotes Atherosclerosis by Limiting Translation Control-Dependent Retardation of Inflammation. *Arteriosclerosis, Thrombosis, and Vascular Biology* 34: 533 - 542

Behr MA, Kaufmann E, Duffin J, Edelstein PH, Ramakrishnan L (2021) Latent Tuberculosis: Two Centuries of Confusion. *Am J Resp Crit Care* 204: 142-148

Bhattacharya B, Xiao S, Chatterjee S, Urbanowski M, Ordonez A, Ihms EA, Agrahari G, Lun S, Berland R, Pichugin A *et al* (2021) The integrated stress response mediates necrosis in murine Mycobacterium tuberculosis granulomas. *J Clin Invest* 131

Bild AH, Yao G, Chang JT, Wang Q, Potti A, Chasse D, Joshi MB, Harpole D, Lancaster JM, Berchuck A *et al* (2006) Oncogenic pathway signatures in human cancers as a guide to targeted therapies. *Nature* 439: 353-357

Blaser H, Dostert C, Mak TW, Brenner D (2016) TNF and ROS Crosstalk in Inflammation. *Trends Cell Biol* 26: 249-261

Boccuni L, Podgorschek E, Schmiedeberg M, Platanitis E, Traxler P, Fischer P, Schirripa A, Novoszel P, Nebreda AR, Arthur JSC *et al* (2022) Stress signaling boosts interferon-induced gene transcription in macrophages. *Sci Signal* 15: eabq5389

Bolger AM, Lohse M, Usadel B (2014) Trimmomatic: a flexible trimmer for Illumina sequence data. *Bioinformatics* 30: 2114-2120
Bottomley MJ, Collard MW, Huggenvik JI, Liu Z, Gibson TJ, Sattler M (2001) The SAND domain structure defines a novel DNA-binding fold in transcriptional regulation. *Nature structural biology* 8: 626 - 633
Boyartchuk V, Rojas M, Yan BS, Jobe O, Hurt N, Dorfman DM, Higgins DE, Dietrich WF, Kramnik I (2004) The host resistance locus sst1 controls innate immunity to Listeria monocytogenes infection in immunodeficient mice. *J Immunol* 173: 5112-5120
Bush K, Kivlahan DR, McDonell MB, Fihn SD, Bradley KA (1998) The AUDIT alcohol consumption questions (AUDIT-C): an effective brief screening test for problem drinking. Ambulatory Care Quality Improvement Project (ACQUIP). Alcohol Use Disorders Identification Test. *Arch Intern Med* 158: 1789-1795
Buskiewicz IA, Montgomery T, Yasewicz EC, Huber SA, Murphy MP, Hartley RC, Kelly R, Crow MK, Perl A, Budd RC *et al* (2016) Reactive oxygen species induce virus-independent MAVS oligomerization in systemic lupus erythematosus. *Sci Signal* 9: ra115 - ra115
Bussi C, Gutierrez MG (2019) Mycobacterium tuberculosis infection of host cells in space and time. *FEMS Microbiol Rev* 43: 341-361
Carles CC, Fletcher JC (2010) Missing links between histones and RNA Pol II arising from SAND? *Epigenetics : official journal of the DNA Methylation Society* 5: 381 - 385
Chen EY, Tan CM, Kou Y, Duan Q, Wang Z, Meirelles GV, Clark NR, Ma'ayan A (2013) Enrichr: interactive and collaborative HTML5 gene list enrichment analysis tool. *BMC Bioinformatics* 14: 128
Christopher DJ, Coelho V, Ebby GS, Shankar D, Gupta R, Thangakunam B (2021) Incremental yield of Xpert((R)) MTB/RIF Ultra over Xpert((R)) MTB/RIF in the diagnosis of extrapulmonary TB. *Int J Tuberc Lung Dis* 25: 939-944
Clough E, Barrett T (2016) The Gene Expression Omnibus Database. *Methods Mol Biol* 1418: 93-110
Cohen SB, Gern BH, Urdahl KB (2022) The Tuberculous Granuloma and Preexisting Immunity. *Annual Review of Immunology* 40: 589-614
Crawford RR, Prescott ET, Sylvester CF, Higdon AN, Shan J, Kilberg MS, Mungrue IN (2015) Human CHAC1 Protein Degrades Glutathione, and mRNA Induction Is Regulated by the Transcription Factors ATF4 and ATF3 and a Bipartite ATF/CRE Regulatory Element. *The Journal of biological chemistry* 290: 15878 - 15891
Danaher P, Kim Y, Nelson B, Griswold M, Yang Z, Piazza E, Beechem JM (2022) Advances in mixed cell deconvolution enable quantification of cell types in spatial transcriptomic data. *Nat Commun* 13: 385
Dayama G, Bulekova K, Lau NC (2022) Extending and Running the Mosquito Small RNA Genomics Resource Pipeline. *Methods Mol Biol* 2509: 341-352
DeDiego ML, Martinez-Sobrido L, Topham DJ (2019) Novel Functions of IFI44L as a Feedback Regulator of Host Antiviral Responses. *J Virol* 93
DiNardo AR, Nishiguchi T, Grimm SL, Schlesinger LS, Graviss EA, Cirillo JD, Coarfa C, Mandalakas AM, Heyckendorf J, Kaufmann SHE *et al* (2021) Tuberculosis Endotypes to Guide Stratified Host-Directed Therapy. *Med* 2: 217-232
Dobin A, Davis CA, Schlesinger F, Drenkow J, Zaleski C, Jha S, Batut P, Chaisson M, Gingeras TR (2013) STAR: ultrafast universal RNA-seq aligner. *Bioinformatics* 29: 15-21

Donovan ML, Schultz TE, Duke TJ, Blumenthal A (2017) Type I Interferons in the Pathogenesis of Tuberculosis: Molecular Drivers and Immunological Consequences. *Front Immunol* 8: 1633
Drain PK, Bajema KL, Dowdy D, Dheda K, Naidoo K, Schumacher SG, Ma S, Meermeier E, Lewinsohn DM, Sherman DR (2018) Incipient and Subclinical Tuberculosis: a Clinical Review of Early Stages and Progression of Infection. *Clin Microbiol Rev* 31
Ernst JD (2018) Mechanisms of M. tuberculosis Immune Evasion as Challenges to TB Vaccine Design. *Cell host & microbe* 24: 34-42
Flynn JL, Chan J (2022) Immune cell interactions in tuberculosis. *Cell* 185: 4682-4702
Fraschilla I, Jeffrey KL (2020a) The Speckled Protein (SP) Family: Immunity's Chromatin Readers. *Trends Immunol* 41: 572-585
Fraschilla IR, Jeffrey KL (2020b) Speckled Protein (SP)140, an immune-specific chromatin reader, contains a CARD and chromatin-interacting domains that dictate subnuclear localization and macrophage identity. *The Journal of Immunology* 204: 69.27 - 69.27
Gupte A, Padmapriyadarsini C, Mave V, Kadam D, Suryavanshi N, Shivakumar SV, Kohli R, Gupte N, Thiruvengadam K, Kagal A *et al* (2016) Cohort for Tuberculosis Research by the Indo-US Medical Partnership (CTRIUMPH): protocol for a multicentric prospective observational study. *BMJ Open* 6: e010542
He X, Berland R, Mekasha S, Christensen TG, Alroy J, Kramnik I, Ingalls RR (2013) The sst1 resistance locus regulates evasion of type I interferon signaling by Chlamydia pneumoniae as a disease tolerance mechanism. *PLoS Pathog* 9: e1003569
Hofmann JW, Zhao X, Cecco MD, Peterson AL, Pagliaroli L, Manivannan J, Hubbard GB, Ikeno Y, Zhang Y, Feng B *et al* (2015) Reduced Expression of MYC Increases Longevity and Enhances Healthspan. *Cell* 160: 477 - 488
Hong R, Koga Y, Bandyadka S, Leshchyk A, Wang Y, Akavoor V, Cao X, Sarfraz I, Wang Z, Alabdullatif S *et al* (2022) Comprehensive generation, visualization, and reporting of quality control metrics for single-cell RNA sequencing data. *Nat Commun* 13: 1688
Horsburgh CR, Jr., Rubin EJ (2011) Clinical practice. Latent tuberculosis infection in the United States. *N Engl J Med* 364: 1441-1448
Hu H, Miao YR, Jia LH, Yu QY, Zhang Q, Guo AY (2019) AnimalTFDB 3.0: a comprehensive resource for annotation and prediction of animal transcription factors. *Nucleic Acids Res* 47: D33-D38
Hunter RL (2011) Pathology of post primary tuberculosis of the lung: An illustrated critical review. *Tuberculosis* 91: 497 - 509
Huynh-Thu VA, Geurts P (2018) dynGENIE3: dynamical GENIE3 for the inference of gene networks from time series expression data. *Sci Rep* 8: 3384
Huynh-Thu VA, Irrthum A, Wehenkel L, Geurts P (2010) Inferring regulatory networks from expression data using tree-based methods. *PLoS One* 5
Imrichova H, Hulselmans G, Atak ZK, Potier D, Aerts S (2015) i-cisTarget 2015 update: generalized cis-regulatory enrichment analysis in human, mouse and fly. *Nucleic Acids Res* 43: W57-64
Ivashkiv LTDLB (2014) Regulation of type I interferon responses. *Nature Reviews Immunology* 14: 36 - 49
Jayewickreme R, Mao T, Philbrick W, Kong Y, Treger RS, Lu P, Rakib T, Dong H, Dang-Lawson M, Guild WA *et al* (2021) Endogenous Retroviruses Provide Protection Against Vaginal HSV-2 Disease. *Front Immunol* 12: 758721

Ji DX, Witt KC, Kotov DI, Margolis SR, Louie A, Chevee V, Chen KJ, Gaidt MM, Dhaliwal HS, Lee AY *et al* (2021) Role of the transcriptional regulator SP140 in resistance to bacterial infections via repression of type I interferons. *Elife* 10
Ji DX, Yamashiro LH, Chen KJ, Mukaida N, Kramnik I, Darwin KH, Vance RE (2019) Type I interferon-driven susceptibility to Mycobacterium tuberculosis is mediated by IL-1Ra. *Nat Microbiol* 4: 2128-2135
Jiang H, Tsang L, Wang H, Liu C (2021) IFI44L as a Forward Regulator Enhancing Host Antituberculosis Responses. *J Immunol Res* 2021: 1-12
Johnson WE, Odom A, Cintron C, Muthaiah M, Knudsen S, Joseph N, Babu S, Lakshminarayanan S, Jenkins DF, Zhao Y *et al* (2021) Comparing tuberculosis gene signatures in malnourished individuals using the TBSignatureProfiler. *BMC Infect Dis* 21: 106
Kamata H, Honda S-I, Maeda S, Chang L, Hirata H, Karin M (2005) Reactive Oxygen Species Promote TNFα-Induced Death and Sustained JNK Activation by Inhibiting MAP Kinase Phosphatases. *Cell* 120: 649 - 661
Karin M, Gallagher E (2005) From JNK to Pay Dirt: Jun Kinases, their Biochemistry, Physiology and Clinical Importance. *IUBMB Life* 57: 283-295
Kornfeld H, West K, Kane K, Kumpatla S, Zacharias RR, Martinez-Balzano C, Li W, Viswanathan V (2016) High Prevalence and Heterogeneity of Diabetes in Patients With TB in South India: A Report from the Effects of Diabetes on Tuberculosis Severity (EDOTS) Study. *Chest* 149: 1501-1508
Kotov DI, Lee OV, Fattinger SA, Langner CA, Guillen JV, Peters JM, Moon A, Burd EM, Witt KC, Stetson DB *et al* (2023) Early cellular mechanisms of type I interferon-driven susceptibility to tuberculosis. *Cell*
Kramnik I, Beamer G (2016) Mouse models of human TB pathology: roles in the analysis of necrosis and the development of host-directed therapies. *Semin Immunopathol* 38: 221-237
Kramnik I, Demant P, Bloom BB (1998) Susceptibility to tuberculosis as a complex genetic trait: analysis using recombinant congenic strains of mice. *Novartis Found Symp* 217: 120-131; discussion 132-127
Kramnik I, Dietrich WF, Demant P, Bloom BR (2000) Genetic control of resistance to experimental infection with virulent Mycobacterium tuberculosis. *Proc Natl Acad Sci U S A* 97: 8560-8565
Kumar V, Patel S, Tcyganov E, Gabrilovich DI (2016) The Nature of Myeloid-Derived Suppressor Cells in the Tumor Microenvironment. *Trends in immunology* 37: 208 - 220
Lachmann A, Torre D, Keenan AB, Jagodnik KM, Lee HJ, Wang L, Silverstein MC, Ma'ayan A (2018) Massive mining of publicly available RNA-seq data from human and mouse. *Nat Commun* 9: 1366
Lavin RC, Tan S (2022) Spatial relationships of intra-lesion heterogeneity in Mycobacterium tuberculosis microenvironment, replication status, and drug efficacy. *PLoS Pathog* 18: e1010459
Lee MN, Roy M, Ong S-E, Mertins P, Villani A-C, Li W, Dotiwala F, Sen J, Doench JG, Orzalli MH *et al* (2012) Identification of regulators of the innate immune response to cytosolic DNA and retroviral infection by an integrative approach. *Nature Immunology* 14: 179 - 185
Lei Y, Martinez CG, Torres-Odio S, Bell SL, Birdwell CE, Bryant JD, Tong CW, Watson RO, West LC, West AP (2021) Elevated type I interferon responses potentiate metabolic dysfunction, inflammation, and accelerated aging in mtDNA mutator mice.
Levy S, Forman HJ (2010) C-Myc is a Nrf2-interacting protein that negatively regulates phase II genes through their electrophile responsive elements. *IUBMB Life* 62: 237-246

Liao Y, Smyth GK, Shi W (2013) The Subread aligner: fast, accurate and scalable read mapping by seed-and-vote. *Nucleic Acids Res* 41: e108
Liao Y, Smyth GK, Shi W (2014) featureCounts: an efficient general purpose program for assigning sequence reads to genomic features. *Bioinformatics* 30: 923-930
Liberzon A, Birger C, Thorvaldsdottir H, Ghandi M, Mesirov JP, Tamayo P (2015) The Molecular Signatures Database (MSigDB) hallmark gene set collection. *Cell Syst* 1: 417-425
Love MI, Huber W, Anders S (2014) Moderated estimation of fold change and dispersion for RNA-seq data with DESeq2. *Genome Biol* 15: 550
Ma Q, Srivastav SP, Gamez S, Dayama G, Feitosa-Suntheimer F, Patterson EI, Johnson RM, Matson EM, Gold AS, Brackney DE *et al* (2021) A mosquito small RNA genomics resource reveals dynamic evolution and host responses to viruses and transposons. *Genome Res* 31: 512-528
Mahamed D, Boulle M, Ganga Y, Arthur CM, Skroch S, Oom L, Catinas O, Pillay K, Naicker M, Rampersad S *et al* (2017) Intracellular growth of Mycobacterium tuberculosis after macrophage cell death leads to serial killing of host cells. *eLife* 6: 5210
Matesanz F, Potenciano V, Fedetz M, Ramos-Mozo P, Abad-Grau MdM, Karaky M, Barrionuevo C, Izquierdo G, Ruiz-Peña JL, García-Sánchez MI *et al* (2015) A functional variant that affects exon-skipping and protein expression of SP140as genetic mechanism predisposing to multiple sclerosis. *Human molecular genetics* 24: 5619 - 5627
Mazumder B, Sampath P, Seshadri V, Maitra RK, Dicorleto PE, Fox PL (2003) Regulated Release of L13a from the 60S Ribosomal Subunit as A Mechanism of Transcript-Specific Translational Control 9500 Euclid Avenue 2121 Euclid Avenue. *Cell* 115: 187 - 198
McQuerry JA, Jenkins DF, Yost SE, Zhang Y, Schmolze D, Johnson WE, Yuan Y, Bild AH (2019) Pathway activity profiling of growth factor receptor network and stemness pathways differentiates metaplastic breast cancer histological subtypes. *BMC Cancer* 19: 881
Mehta S, Cronkite DA, Basavappa M, Saunders TL, Adiliaghdam F, Amatullah H, Morrison SA, Pagan JD, Anthony RM, Tonnerre P *et al* (2017) Maintenance of macrophage transcriptional programs and intestinal homeostasis by epigenetic reader SP140. *Sci Immunol* 2
Merritt CR, Ong GT, Church SE, Barker K, Danaher P, Geiss G, Hoang M, Jung J, Liang Y, McKay-Fleisch J *et al* (2020) Multiplex digital spatial profiling of proteins and RNA in fixed tissue. *Nat Biotechnol* 38: 586-599
Moreira-Teixeira L, Mayer-Barber K, Sher A, O'Garra A (2018) Type I interferons in tuberculosis: Foe and occasionally friend. *J Exp Med* 215: 1273-1285
Mortensen MS, Ruiz J, Watts JL (2023) Polyunsaturated Fatty Acids Drive Lipid Peroxidation during Ferroptosis. *Cells* 12
North RJ, Jung Y-J (2004) Immunity to Tuberculosis. *Immunology* 22: 599-623
O'Garra A, Redford PS, McNab FW, Bloom CI, Wilkinson RJ, Berry MP (2013) The immune response in tuberculosis. *Annu Rev Immunol* 31: 475-527
Ogongo P, Ernst JD (2023) Finding antigens for TB vaccines: the good, the bad and the useless. *Nat Med* 29: 35-36
Orgeur M, Brosch R (2018) Evolution of virulence in the Mycobacterium tuberculosis complex. *Curr Opin Microbiol* 41: 68-75
Pacl HT, Reddy VP, Saini V, Chinta KC, Steyn AJC (2018) Host-pathogen redox dynamics modulate Mycobacterium tuberculosis pathogenesis. *Pathog Dis* 76
Pagan AJ, Ramakrishnan L (2018) The Formation and Function of Granulomas. *Annu Rev Immunol* 36: 639-665

Pai M, Behr MA, Dowdy D, Dheda K, Divangahi M, Boehme CC, Ginsberg A, Swaminathan S, Spigelman M, Getahun H *et al* (2016) Tuberculosis. *Nat Rev Dis Primers* 2: 16076
Pan H, Yan BS, Rojas M, Shebzukhov YV, Zhou H, Kobzik L, Higgins DE, Daly MJ, Bloom BR, Kramnik I (2005) Ipr1 gene mediates innate immunity to tuberculosis. *Nature* 434: 767-772
Pello OM, Pello OM, Pizzol MD, Pizzol MD, Mirolo M, Mirolo M, Soucek L, Soucek L, Zammataro L, Zammataro L *et al* (2012) Role of c-MYC in alternative activation of human macrophages and tumor-associated macrophage biology. *Blood* 119: 411 - 421
Picard V, Epsztejn S, Santambrogio P, Cabantchik ZI, Beaumont C (1998) Role of ferritin in the control of the labile iron pool in murine erythroleukemia cells. *J Biol Chem* 273: 15382-15386
Pichugin AV, Yan BS, Sloutsky A, Kobzik L, Kramnik I (2009) Dominant role of the sst1 locus in pathogenesis of necrotizing lung granulomas during chronic tuberculosis infection and reactivation in genetically resistant hosts. *Am J Pathol* 174: 2190-2201
Piddington DL, Fang FC, Laessig T, Cooper AM, Orme IM, Buchmeier NA (2001) Cu,Zn superoxide dismutase of Mycobacterium tuberculosis contributes to survival in activated macrophages that are generating an oxidative burst. *Infect Immun* 69: 4980-4987
Pisu D, Huang L, Grenier JK, Russell DG (2020) Dual RNA-Seq of Mtb-Infected Macrophages In Vivo Reveals Ontologically Distinct Host-Pathogen Interactions. *Cell Rep* 30: 335-350 e334
Poddar D, Basu A, Baldwin WM, Kondratov RV, Barik S, Mazumder B (2013) An Extraribosomal Function of Ribosomal Protein L13a in Macrophages Resolves Inflammation. *Journal of immunology (Baltimore, Md : 1950)* 190: 3600 - 3612
Poddar D, Kaur R, Baldwin WM, Mazumder B (2015) L13a-dependent translational control in macrophages limits the pathogenesis of colitis. *Cellular and Molecular Immunology*
Reichler MR, Khan A, Sterling TR, Zhao H, Moran J, McAuley J, Bessler P, Mangura B, Tuberculosis Epidemiologic Studies Consortium Task Order T (2018) Risk and Timing of Tuberculosis Among Close Contacts of Persons with Infectious Tuberculosis. *J Infect Dis* 218: 1000-1008
Riedelberger M, Penninger P, Tscherner M, Seifert M, Jenull S, Brunnhofer C, Scheidl B, Tsymala I, Bourgeois C, Petryshyn A *et al* (2020) Type I Interferon Response Dysregulates Host Iron Homeostasis and Enhances Candida glabrata Infection. *Cell host & microbe* 27: 454 - 466.e458
Ritchie ME, Phipson B, Wu D, Hu Y, Law CW, Shi W, Smyth GK (2015) limma powers differential expression analyses for RNA-sequencing and microarray studies. *Nucleic Acids Res* 43: e47-e47
Rothchild AC, Olson GS, Nemeth J, Amon LM, Mai D, Gold ES, Diercks AH, Aderem A (2019) Alveolar macrophages generate a noncanonical NRF2-driven transcriptional response to Mycobacterium tuberculosis in vivo. *Sci Immunol* 4
Scheu S, Dresing P, Locksley RM (2008) Visualization of IFNbeta production by plasmacytoid versus conventional dendritic cells under specific stimulation conditions in vivo. *Proc Natl Acad Sci U S A* 105: 20416-20421
Shannon P, Markiel A, Ozier O, Baliga NS, Wang JT, Ramage D, Amin N, Schwikowski B, Ideker T (2003) Cytoscape: a software environment for integrated models of biomolecular interaction networks. *Genome Res* 13: 2498-2504
Shi Z, Barna M (2015) Translating the Genome in Time and Space: Specialized Ribosomes, RNA Regulons, and RNA-Binding Proteins. *Annual review of cell and developmental biology* 31: 31 - 54

Simmons JD, Stein CM, Seshadri C, Campo M, Alter G, Fortune S, Schurr E, Wallis RS, Churchyard G, Mayanja-Kizza H *et al* (2018) Immunological mechanisms of human resistance to persistent Mycobacterium tuberculosis infection. *Nature Reviews Immunology* 282: 677
Sissons J, Yan BS, Pichugin AV, Kirby A, Daly MJ, Kramnik I (2009) Multigenic control of tuberculosis resistance: analysis of a QTL on mouse chromosome 7 and its synergism with sst1. *Genes Immun* 10: 37-46
Stanley SA, Johndrow JE, Manzanillo P, Cox JS (2007) The Type I IFN response to infection with Mycobacterium tuberculosis requires ESX-1-mediated secretion and contributes to pathogenesis. *J Immunol* 178: 3143-3152
Stockwell BR, Friedmann Angeli JP, Bayir H, Bush AI, Conrad M, Dixon SJ, Fulda S, Gascon S, Hatzios SK, Kagan VE *et al* (2017) Ferroptosis: A Regulated Cell Death Nexus Linking Metabolism, Redox Biology, and Disease. *Cell* 171: 273-285
Street K, Risso D, Fletcher RB, Das D, Ngai J, Yosef N, Purdom E, Dudoit S (2018) Slingshot: cell lineage and pseudotime inference for single-cell transcriptomics. *BMC Genomics* 19: 477
Stuart T, Butler A, Hoffman P, Hafemeister C, Papalexi E, Mauck WM, 3rd, Hao Y, Stoeckius M, Smibert P, Satija R (2019) Comprehensive Integration of Single-Cell Data. *Cell* 177: 1888-1902 e1821
Susanto TT, Hung V, Levine AG, Kerr CH, Yoo Y, Chen Y, Oses-Prieto JA, Fromm L, Fujii K, Wernig M *et al* (2023) RAPIDASH: A tag-free enrichment of ribosome-associated proteins reveals compositional dynamics in embryonic tissues and stimulated macrophages. *bioRxiv*: 2023.2012.2007.570613
Thomas F, Serratrice G, Beguin C, Aman ES, Pierre JL, Fontecave M, Laulhere JP (1999) Calcein as a fluorescent probe for ferric iron. Application to iron nutrition in plant cells. *J Biol Chem* 274: 13375-13383
Torti FM, Torti SV (2002) Regulation of ferritin genes and protein. *Blood* 99: 3505 - 3516
Ulrichs T, Lefmann M, Reich M, Morawietz L, Roth A, Brinkmann V, Kosmiadi GA, Seiler P, Aichele P, Hahn H *et al* (2005) Modified immunohistological staining allows detection of Ziehl–Neelsen-negative Mycobacterium tuberculosis organisms and their precise localization in human tissue.
WHO (2022) Global Health TB Report. *https://wwwwhoint/tb/publications/global_report/en/*
Witt KC, Dziulko A, An J, Lee OV, Liu G, Lari A, Chavez R, Turner DJ, Cheng A, Kotov DI *et al* (2024) The SP140-RESIST pathway regulates interferon mRNA stability and antiviral immunity. *bioRxiv*: 2024.2008.2028.610186
Wolfe AL, Singh K, Zhong Y, Drewe P, Rajasekhar VK, Sanghvi VR, Mavrakis KJ, Jiang M, Roderick JE, Meulen JVd *et al* (2014) RNA G-quadruplexes cause eIF4A-dependent oncogene translation in cancer. *Nature* 513: 65 - 70
Wu D, Smyth GK (2012) Camera: a competitive gene set test accounting for inter-gene correlation. *Nucleic Acids Res* 40: e133
Wu KJ, Polack A, Dalla-Favera R (1999) Coordinated regulation of iron-controlling genes, H-ferritin and IRP2, by c-MYC. *Science (New York, NY)* 283: 676 - 679
Xie Z, Bailey A, Kuleshov MV, Clarke DJB, Evangelista JE, Jenkins SL, Lachmann A, Wojciechowicz ML, Kropiwnicki E, Jagodnik KM *et al* (2021) Gene Set Knowledge Discovery with Enrichr. *Curr Protoc* 1: e90
Yabaji SM, Chatterjee S, Waligursky E, Gimelbrant A, Kramnik I (2022) Medium throughput protocol for genome-based quantification of intracellular mycobacterial loads and macrophage survival during in vitro infection. *STAR Protoc* 3: 101241

Yabaji SM, Lata S, Gavrish I, Lo M, O'Connell AK, Gertje HP, Thurman CE, Crossland NA, Kobzik L, Kramnik I (2025a) Protocol for Developing a Mouse Model of Post Primary Pulmonary Tuberculosis after Hematogenous Spread in Native Lungs and Lung Implants. *bioRxiv*: 2025.2002.2028.640830

Yabaji SM, Lata S, Tseng AE, Araveti PB, Lo M, Gavrish I, O'Connell AK, Gertje HP, Belkina AC, Thurman CE *et al* (2025b) Aberrant macrophage activation and maladaptive lung repair promote tuberculosis progression uniquely in the lung. *bioRxiv*: 2023.2010.2017.562695

Yabaji SM, Lo M, Lata S, Gavrish I, Tseng AE, O'Connell AK, Gertje HP, Mazzilli S, Tan S, Thurman CE *et al* (2023) Aberrant macrophage activation and failed regeneration of pulmonary epithelium promote tuberculosis progression uniquely in lung tissue. 2023.2010.2017.562695

Yan BS, Kirby A, Shebzukhov YV, Daly MJ, Kramnik I (2006) Genetic architecture of tuberculosis resistance in a mouse model of infection. *Genes Immun* 7: 201-210

Yan BS, Pichugin AV, Jobe O, Helming L, Eruslanov EB, Gutierrez-Pabello JA, Rojas M, Shebzukhov YV, Kobzik L, Kramnik I (2007) Progression of pulmonary tuberculosis and efficiency of bacillus Calmette-Guerin vaccination are genetically controlled via a common sst1-mediated mechanism of innate immunity. *J Immunol* 179: 6919-6932

Yang S, Corbett SE, Koga Y, Wang Z, Johnson WE, Yajima M, Campbell JD (2020) Decontamination of ambient RNA in single-cell RNA-seq with DecontX. *Genome Biol* 21: 57

Zhang Y, Parmigiani G, Johnson WE (2020) ComBat-seq: batch effect adjustment for RNA-seq count data. *NAR Genom Bioinform* 2: lqaa078

Zhernovkov V, Santra T, Cassidy H, Rukhlenko O, Matallanas D, Krstic A, Kolch W, Lobaskin V, Kholodenko BN (2019) An Integrative Computational Approach for a Prioritization of Key Transcription Regulators Associated With Nanomaterial-Induced Toxicity. *Toxicol Sci* 171: 303-314

Zimmerli D, Brambillasca CS, Talens F, Bhin J, Linstra R, Romanens L, Bhattacharya A, Joosten SEP, Silva AMD, Padrao N *et al* (2022) MYC promotes immune-suppression in triple-negative breast cancer via inhibition of interferon signaling. *Nature Communications* 13: 6579

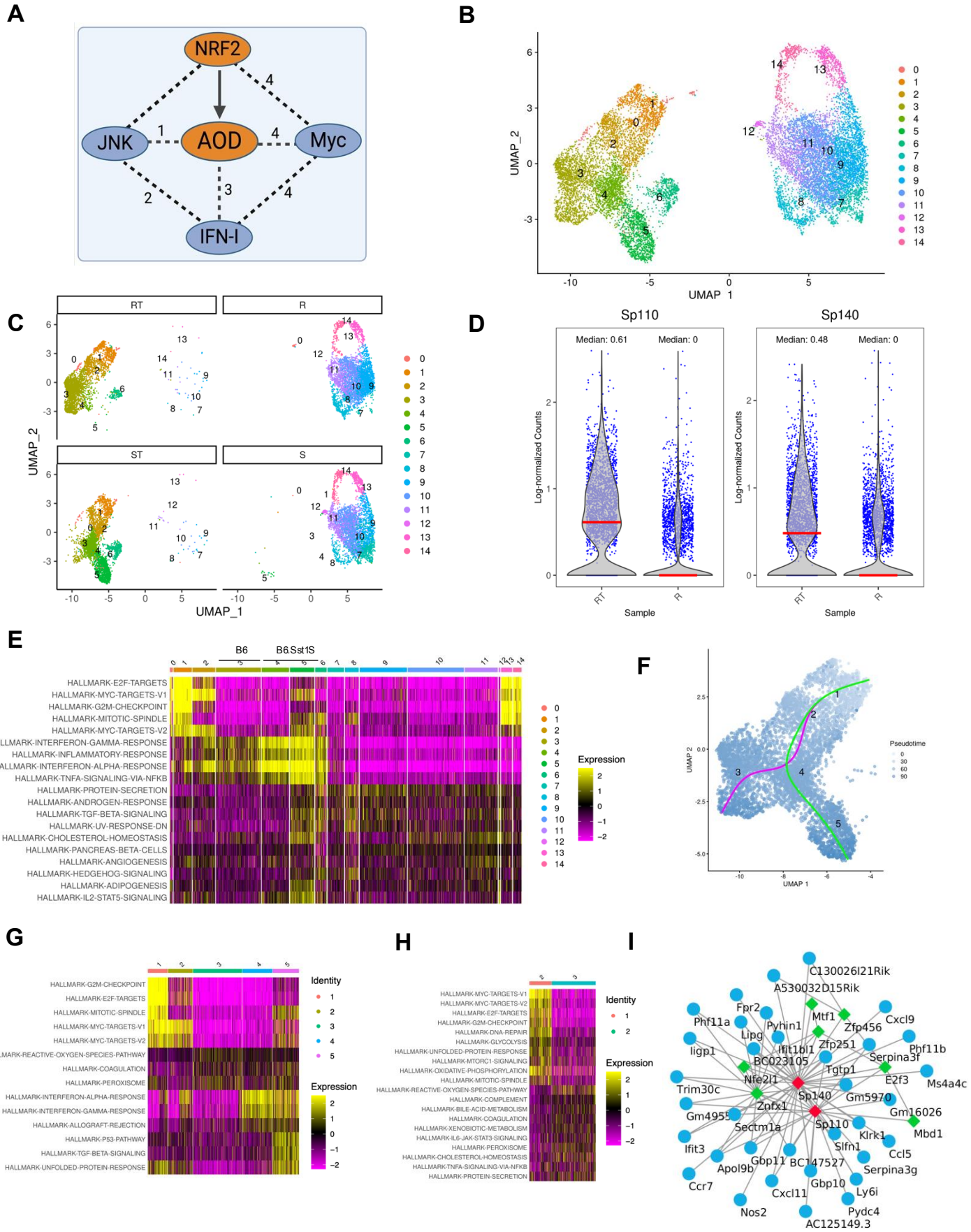
A
NRF2
JNK
AOD
Myc
IFN-I
B
UMAP_2
UMAP_1
C
RT
R
ST
S
D
Sp110
Sp140
Median: 0.61
Median: 0
Median: 0.48
Median: 0
Log-normalized Counts
Sample
E
B6
B6.Sst1S
HALLMARK-E2F-TARGETS
HALLMARK-MYC-TARGETS-V1
HALLMARK-G2M-CHECKPOINT
HALLMARK-MITOTIC-SPINDLE
HALLMARK-MYC-TARGETS-V2
HALLMARK-INTERFERON-GAMMA-RESPONSE
HALLMARK-INFLAMMATORY-RESPONSE
HALLMARK-INTERFERON-ALPHA-RESPONSE
HALLMARK-TNFA-SIGNALING-VIA-NFKB
HALLMARK-PROTEIN-SECRETION
HALLMARK-ANDROGEN-RESPONSE
HALLMARK-TGF-BETA-SIGNALING
HALLMARK-UV-RESPONSE-DN
HALLMARK-CHOLESTEROL-HOMEOSTASIS
HALLMARK-PANCREAS-BETA-CELLS
HALLMARK-ANGIOGENESIS
HALLMARK-HEDGEHOG-SIGNALING
HALLMARK-ADIPOGENESIS
HALLMARK-IL2-STAT5-SIGNALING
Expression
F
UMAP 2
UMAP 1
Pseudotime
G
HALLMARK-G2M-CHECKPOINT
HALLMARK-E2F-TARGETS
HALLMARK-MITOTIC-SPINDLE
HALLMARK-MYC-TARGETS-V1
HALLMARK-MYC-TARGETS-V2
HALLMARK-REACTIVE-OXYGEN-SPECIES-PATHWAY
HALLMARK-COAGULATION
HALLMARK-PEROXISOME
HALLMARK-INTERFERON-ALPHA-RESPONSE
HALLMARK-INTERFERON-GAMMA-RESPONSE
HALLMARK-ALLOGRAFT-REJECTION
HALLMARK-P53-PATHWAY
HALLMARK-TGF-BETA-SIGNALING
HALLMARK-UNFOLDED-PROTEIN-RESPONSE
Identity
Expression
H
HALLMARK-MYC-TARGETS-V1
HALLMARK-MYC-TARGETS-V2
HALLMARK-E2F-TARGETS
HALLMARK-G2M-CHECKPOINT
HALLMARK-DNA-REPAIR
HALLMARK-GLYCOLYSIS
HALLMARK-UNFOLDED-PROTEIN-RESPONSE
HALLMARK-MTORC1-SIGNALING
HALLMARK-OXIDATIVE-PHOSPHORYLATION
HALLMARK-MITOTIC-SPINDLE
HALLMARK-REACTIVE-OXYGEN-SPECIES-PATHWAY
HALLMARK-COMPLEMENT
HALLMARK-BILE-ACID-METABOLISM
HALLMARK-COAGULATION
HALLMARK-XENOBIOTIC-METABOLISM
HALLMARK-IL6-JAK-STAT3-SIGNALING
HALLMARK-PEROXISOME
HALLMARK-CHOLESTEROL-HOMEOSTASIS
HALLMARK-TNFA-SIGNALING-VIA-NFKB
HALLMARK-PROTEIN-SECRETION
Identity
Expression
I
C130026I21Rik
A530032D15Rik
Fpr2
Mtf1
Cxcl9
Phf11a
Pyhin1
Zfp456
Lipg
Ifit1bl1
Zfp251
Phf11b
Iigp1
BC023105
Serpina3f
Tgtp1
E2f3
Ms4a4c
Nfe2l1
Trim30c
Sp140
Gm5970
Znfx1
Gm16026
Gm4955
Sp110
Mbd1
Sectm1a
Klrk1
Ifit3
Slfn1
Ccl5
Gbp11
BC147527
Apol9b
Serpina3g
Ccr7
Gbp10
Ly6i
Cxcl11
Nos2
Pydc4
AC125149.3

Figure 1

Figure 1. Single cell RNAseq analysis of the population dynamics of B6 and B6.Sst1S macrophages after TNF stimulation

(**A**). Connectivity of antioxidant defense (AOD) with the Myc-, Nrf2-, JNK-, and IFN-I-regulated pathways: 1) stress kinase activation by oxidative stress; 2) promotion of IFN-I responses by stress kinases; 3) suppression of AOD by IFN-I; 4) inhibition of Nrf2, AOD and IFN responses by Myc.

(B and **C)**. scRNA-seq analysis (UMAP and individual clusters) of B6 (R) and B6.Sst1S (S) BMDMs either naïve (R and S) or after 24 h of stimulation with TNF (RT and ST, respectively).

(**D**). Expression of the *sst1*-encoded *Sp110* and *Sp140* genes in the population of either naïve (R) or TNF-stimulated (RT) B6 BMDMs.

(**E**). Heatmap showing differentially expressed pathways in all cell clusters identified using scRNA-seq. Rows represent pathways and columns represent individual clusters with color intensity indicating the relative expression.

(**F)**. Reconstruction of the activation trajectories of TNF-stimulated resistant (RT) and susceptible (ST) macrophage populations using pseudotime analysis. magenta line indicates B6 and green line indicates B6.Sst1S BMDMs.

(**G**). Heatmap showing differentially expressed pathways in subpopulations 1 to 5 identified using pseudotime analysis. Rows represent pathways and columns represent individual subpopulations with color intensity indicating the relative expression.

(**H)**. Pathway heatmap representing transition from subpopulation 2 to unique subpopulation 3 in TNF-stimulated B6 macrophages.

(**I**). The *Sp110* and *Sp140* gene regulatory network analysis. The mouse macrophage gene regulatory network was inferred using GENIE3 algorithm from mouse macrophages gene expression data sets obtained from Gene Expression Omnibus (GEO). First neighbors of *Sp110/Sp140* genes were selected to infer a subnetwork of *Sp110/Sp140* co-regulated genes. Green nodes represent transcription factors, blue nodes denote their potential targets.

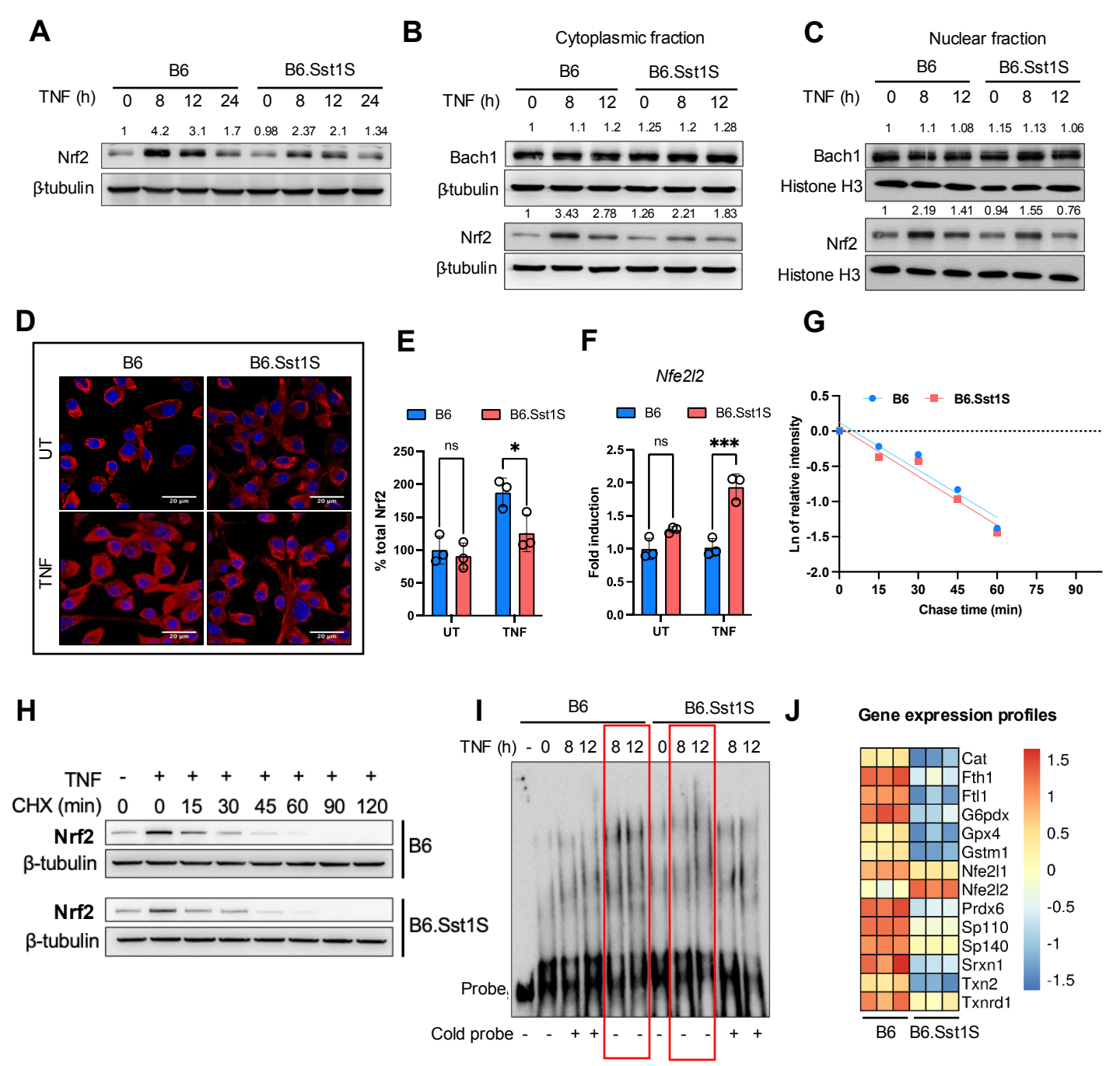
A
B6
B6.Sst1S
TNF (h)
0 8 12 24 0 8 12 24
1 4.2 3.1 1.7 0.98 2.37 2.1 1.34
Nrf2
β-tubulin
B
Cytoplasmic fraction
B6
B6.Sst1S
TNF (h)
0 8 12 0 8 12
1 1.1 1.2 1.25 1.2 1.28
Bach1
β-tubulin
1 3.43 2.78 1.26 2.21 1.83
Nrf2
β-tubulin
C
Nuclear fraction
B6
B6.Sst1S
TNF (h)
0 8 12 0 8 12
1 1.1 1.08 1.15 1.13 1.06
Bach1
Histone H3
1 2.19 1.41 0.94 1.55 0.76
Nrf2
Histone H3
D
B6
B6.Sst1S
UT
TNF
20 µm
E
B6
B6.Sst1S
% total Nrf2
ns
*
UT
TNF
F
Nfe2l2
B6
B6.Sst1S
Fold induction
ns
***
UT
TNF
G
B6
B6.Sst1S
Ln of relative intensity
Chase time (min)
H
TNF - + + + + + + +
CHX (min) 0 0 15 30 45 60 90 120
Nrf2
β-tubulin
B6
Nrf2
β-tubulin
B6.Sst1S
I
B6
B6.Sst1S
TNF (h) - 0 8 12 8 12 0 8 12 8 12
Probe
Cold probe - - + + - - - - - + +
J
Gene expression profiles
Cat
Fth1
Ftl1
G6pdx
Gpx4
Gstm1
Nfe2l1
Nfe2l2
Prdx6
Sp110
Sp140
Srxn1
Txn2
Txnrd1
B6
B6.Sst1S

Figure 2

Figure 2: Gene expression profiling comparing B6 and B6.Sst1.S BMDMs stimulated with TNF and regulation of NRF2.

(**A**). Total level of Nrf2 protein in B6 and B6.Sst1S BMDMs stimulated with TNF (10 ng/ml) for 8, 12 and 24 h (Western blotting). Average densitometric values from 2 independent experiment were included above the blot.

(**B**). Cytoplasmic Nrf2 and Bach1 proteins in B6 and B6.Sst1S BMDMs stimulated with TNF (10 ng/ml) for 8 and 12 h (Western blotting). Average densitometric values from 2 independent experiment were included above the blot.
(**C**). Nuclear Nrf2 and Bach1 protein levels in B6 and B6.Sst1S BMDMs treated with TNF (10 ng/ml) for 8 and 12 h (Western blotting). Average densitometric values from 2 independent experiment were included above the blot.

(**D** and **E**). Confocal microscopy of Nrf2 protein in B6 and B6.Sst1S BMDMs stimulated with TNF (10 ng/ml) for 12 h (scale bar 20 μm). The data shows staining with Nrf2-specific antibody and performed area quantification using ImageJ to calculate the Nrf2 total signal intensity per field. Each dot in the graph represents the average intensity of 3 fields in a representative experiment. The experiment was repeated 3 times.

(**F**). B6 and B6.Sst1S BMDMs were stimulated with TNF (10 ng/ml) for 8 h. The *Nfe2l2* mRNA levels were quantified using quantitative RT-PCR. Fold induction was calculated by DDCt method, and b-actin was used as internal control and normalized the fold change using B6 UT.

(**G** and **H**). The Nrf2 protein stability in TNF-stimulated (10 ng/ml) B6 and B6.Sst1S BMDMs. BMDMs were stimulated with TNF. After 6 h, 25 μg/ml of cycloheximide (CHX) was added and cells were harvested after 15, 30, 45, 60, 90, ad 120 min. The Nrf2 protein levels after TNF stimulation and degradation after cycloheximide addition were determined by Western blotting. I - Linear regression curves of Nrf2 degradation after addition of CHX. Band intensities were measured by densitometry using ImageJ. No significant difference in the Nrf2 half-life was found: B6: 15.14 ± 2.5 min and B6.Sst1S: 13.35 ± 0.6 min.

(**I**). Nuclear Nrf2 binding to target sequence. Nuclear extracts were prepared from BMDMs treated with TNF (10 ng/ml) for 8 and 12 h. The binding activity of Nrf2 was monitored by EMSA using biotin conjugated Nrf2 specific probe (hot probe, red frames). Competition with the unconjugated NRF2 probe (cold probe) was used as specificity control.

(**J**). Anti-oxidant genes co-regulated with *Sp110* and *Sp140* after stimulation with TNF (10 ng/ml) for 12 h. The heatmap was generated using FPKM values obtained from RNA-seq expression profiles of B6.Sst1S and B6 BMDMs after 12 h of TNF stimulation.

The data are presented as means ± standard deviation (SD) from three-five samples per experiment, representative of three independent experiments. The statistical significance was performed by two-way ANOVA using Tukey's multiple comparison test (Panel E, F). Significant differences are indicated with asterisks (*, $P < 0.05$; **, $P < 0.01$; ***, $P < 0.001$; ****, $P < 0.0001$).

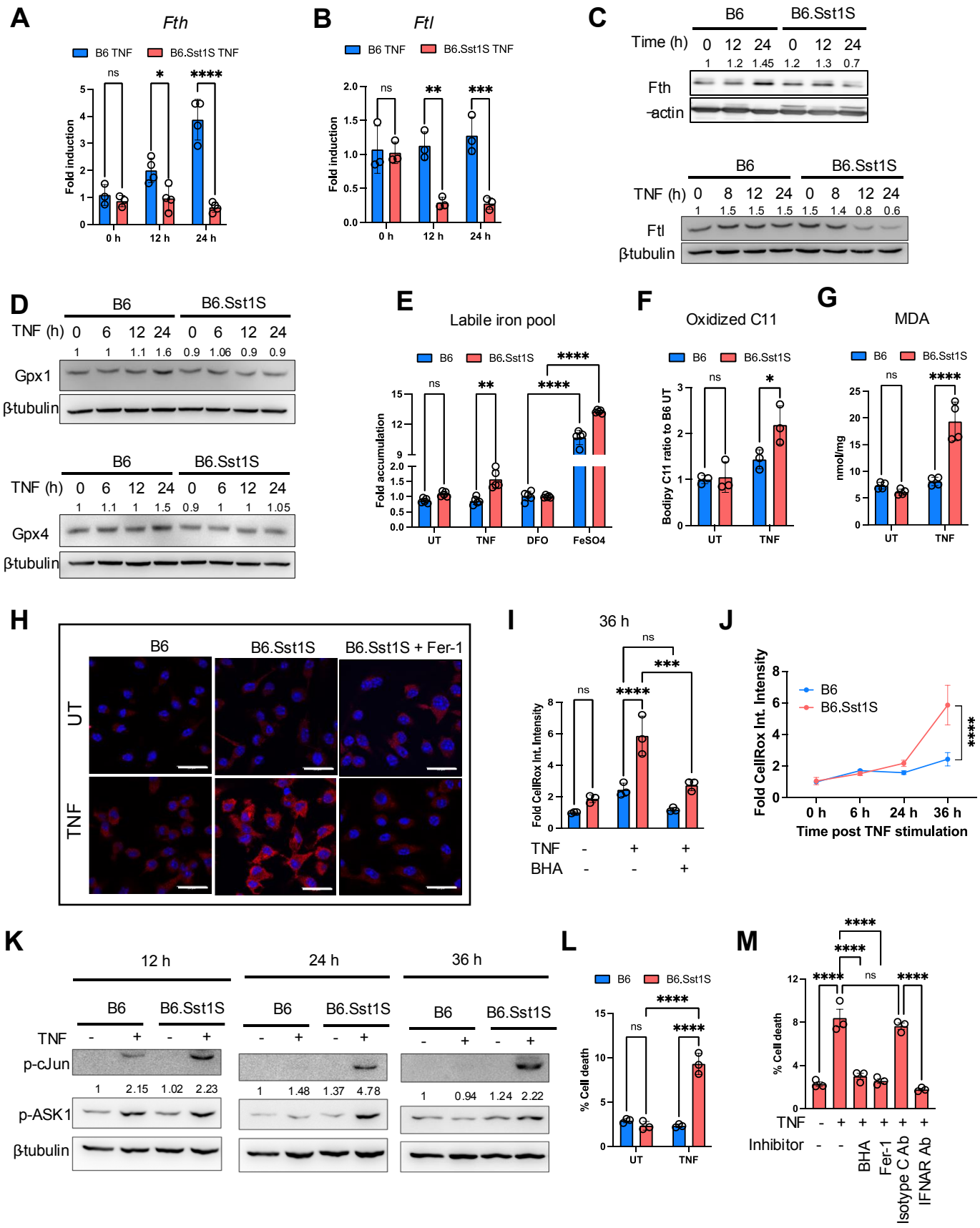
A
Fth
B6 TNF
B6.Sst1S TNF
Fold induction
ns
*
****
0 h
12 h
24 h
B
Ftl
B6 TNF
B6.Sst1S TNF
Fold induction
ns
**
***
0 h
12 h
24 h
C
B6
B6.Sst1S
Time (h) 0 12 24 0 12 24
1 1.2 1.45 1.2 1.3 0.7
Fth
-actin
B6
B6.Sst1S
TNF (h) 0 8 12 24 0 8 12 24
1 1.5 1.5 1.5 1.5 1.4 0.8 0.6
Ftl
β-tubulin
D
B6
B6.Sst1S
TNF (h) 0 6 12 24 0 6 12 24
1 1 1.1 1.6 0.9 1.06 0.9 0.9
Gpx1
β-tubulin
B6
B6.Sst1S
TNF (h) 0 6 12 24 0 6 12 24
1 1.1 1 1.5 0.9 1 1 1.05
Gpx4
β-tubulin
E
Labile iron pool
B6
B6.Sst1S
Fold accumulation
ns
**
****
****
UT
TNF
DFO
FeSO4
F
Oxidized C11
B6
B6.Sst1S
Bodipy C11 ratio to B6 UT
ns
*
UT
TNF
G
MDA
B6
B6.Sst1S
nmol/mg
ns
****
UT
TNF
H
B6
B6.Sst1S
B6.Sst1S + Fer-1
UT
TNF
I
36 h
Fold CellRox Int. Intensity
ns
***
ns
****
TNF - + +
BHA - - +
J
B6
B6.Sst1S
Fold CellRox Int. Intensity
****
0 h
6 h
24 h
36 h
Time post TNF stimulation
K
12 h
24 h
36 h
B6
B6.Sst1S
TNF - + - +
p-cJun
1 2.15 1.02 2.23
1 1.48 1.37 4.78
1 0.94 1.24 2.22
p-ASK1
β-tubulin
L
B6
B6.Sst1S
% Cell death
****
ns
****
UT
TNF
M
% Cell death
****
****
ns
****
****
TNF - + + + + +
Inhibitor - - BHA Fer-1 Isotype C Ab IFNAR Ab

Figure 3

Figure 3. Regulation of iron and lipid peroxidation in B6 and B6.Sst1.S BMDMs.

(**A** and **B**). The expression of *Fth* and *Ftl* genes in B6 and B6.Sst1S BMDMs treated with 10 ng/mL TNF for 12 and 24 h was determined using qRT-PCR. Fold induction was calculated normalizing with B6 untreated control using ΔΔCt method, and 18S was used as internal control.

(**C**). The Fth and Ftl protein levels in B6 and B6.Sst1S BMDMs treated with 10 ng/mL TNF for 0, 12 and 24 h (Fth) and 0, 8, 12 and 24 h (for Ftl) (Western blot). Average densitometric values from 3 independent experiment were included above the blot.
(**D**). The Gpx1 and Gpx4 protein levels in B6 and B6.Sst1S BMDMs stimulated with TNF (10 ng/mL) for 0, 6, 12, and 24 h (Western blot). Average densitometric values from 2 independent experiment were included above the blot.

(**E**). The labile iron pool (LIP) in TNF-stimulated B6 and B6.Sst1S BMDMs from were treated with 10 ng/mL TNF for 24 h. UT - untreated control. The LIP was determined using Calcein AM method and represented as fold change as compared to B6 untreated. DFO was used as negative control and FeSo4 was used as positive control.

(**F**). The lipid peroxidation levels were determined by fluorometric method using C11-Bodipy 581/591. BMDMs from B6 and B6.Sst1S were treated with 10 ng/mL TNF for 30 h. UT - untreated control.

(**G**). Production of lipid peroxidation metabolite malondialdehyde (MDA) by B6 and B6.Sst1S BMDMs treated with 10 ng/mL TNF for 30 h. UT - untreated control.

(**H**). The accumulation of the intracellular lipid peroxidation product 4-HNE in B6 and B6.Sst1S BMDMs treated with 10 ng/mL TNF for 48 h. The lipid peroxidation (ferroptosis) inhibitor, Fer-1 (10 μM) was added 2 h post TNF stimulation in B6.Sst1S macrophages. The 4HNE accumulation was detected using 4-HNE specific antibody and confocal microscopy.

(**I**). Reactive oxygen species (ROS) levels were observed using the CellROX assay and quantified by automated microscopy in B6 and B6.Sst1S BMDMs either treated with TNF (10 ng/mL) or left untreated for 36 h. BHA (100 μM) was used as a positive control. Data are presented as fold mean fluorescence intensity (MFI) normalized by B6 UT, representing ROS levels.

(**J**). Time course of ROS accumulation in B6 and B6.Sst1S BMDMs during TNF stimulated condition. Reactive oxygen species (ROS) levels were observed using the CellROX assay after 0, 6, 24 and 36 h of TNF stimulation and quantified by automated microscopy.

(**K**). Induction of c-Jun and ASK1 phosphorylation by TNF in B6 and B6.Sst1S BMDMs. The B6 and B6.Sst1S BMDMs were treated with TNF (10 ng/ml) or left untreated for 12, 24, and 36 h and the c-Jun and ASK1 phosphorylation was determined by Western blot. Average densitometric values from 2 independent experiment were included above the blot.

(**L**). Cell death in B6 and B6.Sst1S BMDMs stimulated with 50 ng/mL TNF for 48 h. Percent of dead cells was determined by automated microscopy using Live-or-DyeTM 594/614 Fixable Viability stain (Biotium) and Hoechst staining.

(**M**). Inhibition of cell death of B6.Sst1S BMDMs stimulated with 50 ng/mL TNF for 48 h using IFNAR1 blocking antibodies (5 μg/mL), isotype C antibodies (5 μg/mL), Butylated hydroxyanisole (BHA, 100 μM) or Fer-1 (10 μM) . Percent cell death was measured as in L.

The data are presented as means ± standard deviation (SD) from three-five samples per experiment, representative of three independent experiments. Statistical analysis was performed using two-way ANOVA followed by Šídák's multiple comparison test (Panels A, B, F, G and M) and Tukey's multiple comparison test (Panel E, I, J, L).
Statistical significance is indicated by asterisks: *P < 0.05, **P < 0.01, ***P < 0.001, ****P < 0.0001.

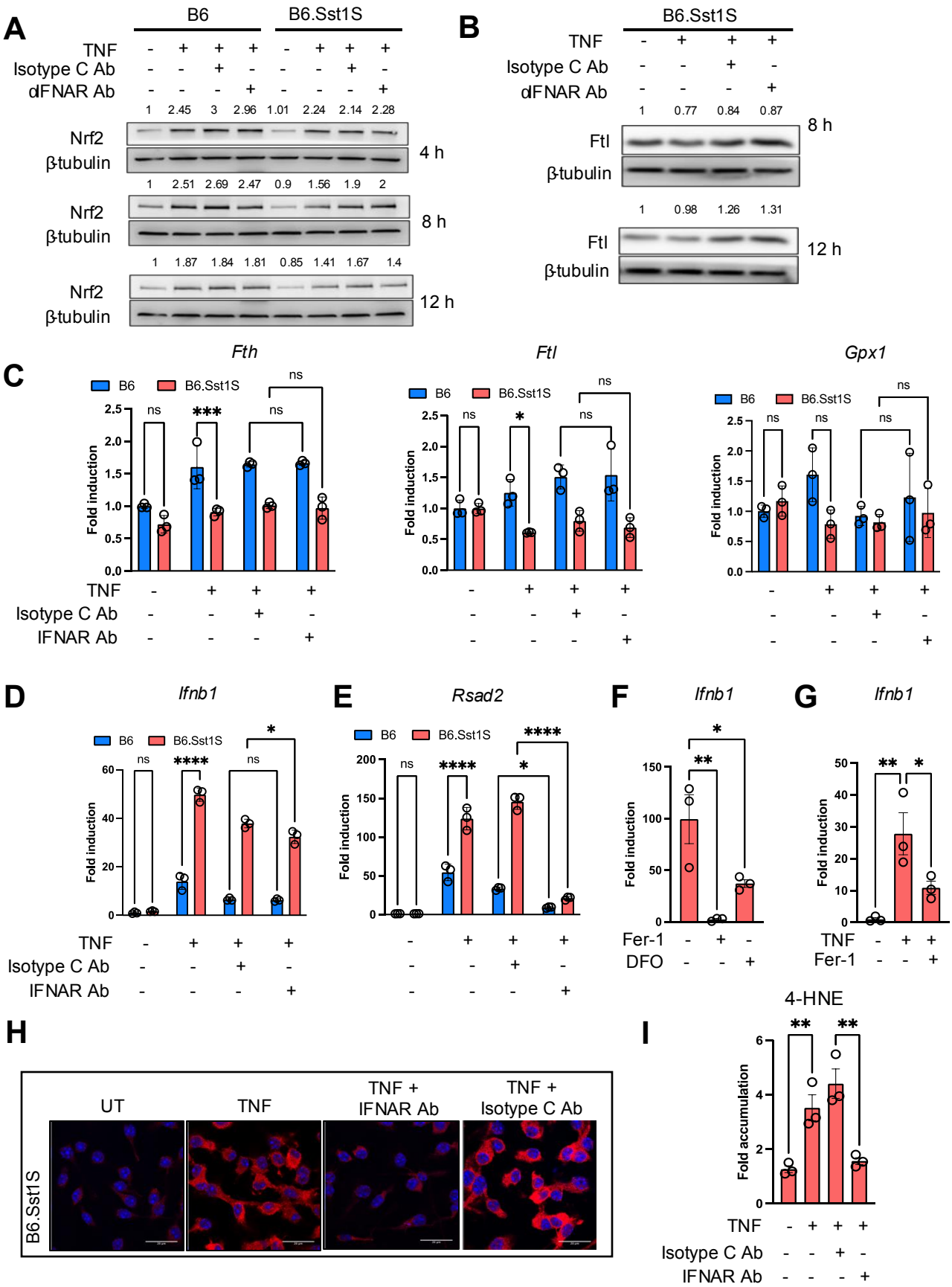
A
B6
B6.Sst1S
TNF
Isotype C Ab
αIFNAR Ab
1 2.45 3 2.96 1.01 2.24 2.14 2.28
Nrf2
β-tubulin
4 h
1 2.51 2.69 2.47 0.9 1.56 1.9 2
8 h
1 1.87 1.84 1.81 0.85 1.41 1.67 1.4
12 h
B
B6.Sst1S
1 0.77 0.84 0.87
Ftl
1 0.98 1.26 1.31
C
Fth
Ftl
Gpx1
Fold induction
ns
***
*
IFNAR Ab
D
Ifnb1
****
E
Rsad2
F
G
Fer-1
DFO
H
UT
TNF
TNF + IFNAR Ab
TNF + Isotype C Ab
I
4-HNE
Fold accumulation
**

Figure 4

Figure 4. Crosstalk of the IFN-I and AOD pathways.

(**A**) IFNAR1 blockade does not enhance Nrf2 upregulation in TNF-stimulated B6.Sst1S macrophages. B6 and B6.Sst1S BMDMs were treated with 10 ng/mL TNF, with or without IFNAR1-blocking antibodies or isotype control (Isotype C Ab) at 5 μg/mL concentration for 4, 8, and 12 hours. Nrf2 protein levels were quantified by Western blot. Average densitometric values from two separate experiments were included above the blot.

(**B**) IFNAR1 blockade does not increase Ftl expression in TNF-stimulated B6.Sst1S macrophages. B6.Sst1S BMDMs were treated with 10 ng/mL TNF, with or without IFNAR1-blocking antibodies (5 μg/mL) or Isotype C Ab (5 μg/mL), for 8 and 12 hours. Ftl protein levels were quantified by Western blot. Average densitometric values from 2 independent experiment were included above the blot.

(**C**) IFNAR1 blockade does not increase mRNA levels of *Fth*, *Ftl*, and *Gpx1*. B6 and B6.Sst1S BMDMs were treated with 10 ng/mL TNF, with or without IFNAR1-blocking antibodies or Isotype C Ab, for 12 hours. Blocking antibodies (5 μg/mL) or isotype C antibodies (5 μg/mL) were added 2 hours after TNF stimulation. Fold induction was calculated using B6 untreated control as average one-fold by utilizing the ΔΔCt method with β-actin as the internal control.

(**D and E**) IFNAR1 blockade reduces *Rsad2* mRNA levels (E) but does not affect *Ifnb1* mRNA levels (D). B6 and B6.Sst1S BMDMs were treated with 10 ng/mL TNF, with or without IFNAR1-blocking antibodies or Isotype C Ab for 16 hours. Blocking antibodies (5 μg/mL) or isotype C antibodies (5 μg/mL) were added 2 hours after TNF stimulation. Fold induction was calculated using B6 untreated control as average one-fold by utilizing the ΔΔCt method with β-actin as the internal control.

(**F**) Lipid peroxidation inhibition prevents the superinduction of *Ifnb1* mRNA. B6.Sst1S BMDMs were treated with 10 ng/mL TNF, and the lipid peroxidation inhibitor (Fer-1) was added 2 hours post-TNF stimulation. *Ifnb1* mRNA levels were measured using qRT-PCR after 16 hours of TNF treatment. Fold induction was calculated using untreated control as average one-fold by utilizing the ΔΔCt method with 18S as the internal control.

(**G**) Lipid peroxidation inhibition reverses the superinduction of *Ifnb1* mRNA. B6.Sst1S BMDMs were stimulated with 10 ng/mL TNF for 18 h, then the LPO inhibitor (Fer-1) was added for the remaining 12 h. *Ifnb1* mRNA levels were measured using qRT-PCR. Fold induction was calculated using untreated control as average one-fold by utilizing the ΔΔCt method with 18S as the internal control.

(**H and I**) IFNAR1 blockade reduces 4-HNE accumulation in B6.Sst1S BMDMs treated with TNF (10 ng/mL) for 48 hours. Blocking antibodies (5 μg/mL) or Isotype C Ab (5 μg/mL) were added 2 hours post-TNF stimulation.

The data are presented as means ± standard deviation (SD) from three-five samples per experiment, representative of three independent experiments. The statistical significance was performed by two-way ANOVA using Tukey's multiple comparison test (Panel C-E), Ordinary one-way

ANOVA using Bonferroni's multiple comparison test (Panel F-G and I). Significant differences are indicated with asterisks (*, $P < 0.05$; **, $P < 0.01$; ***, $P < 0.001$; ****, $P < 0.0001$).

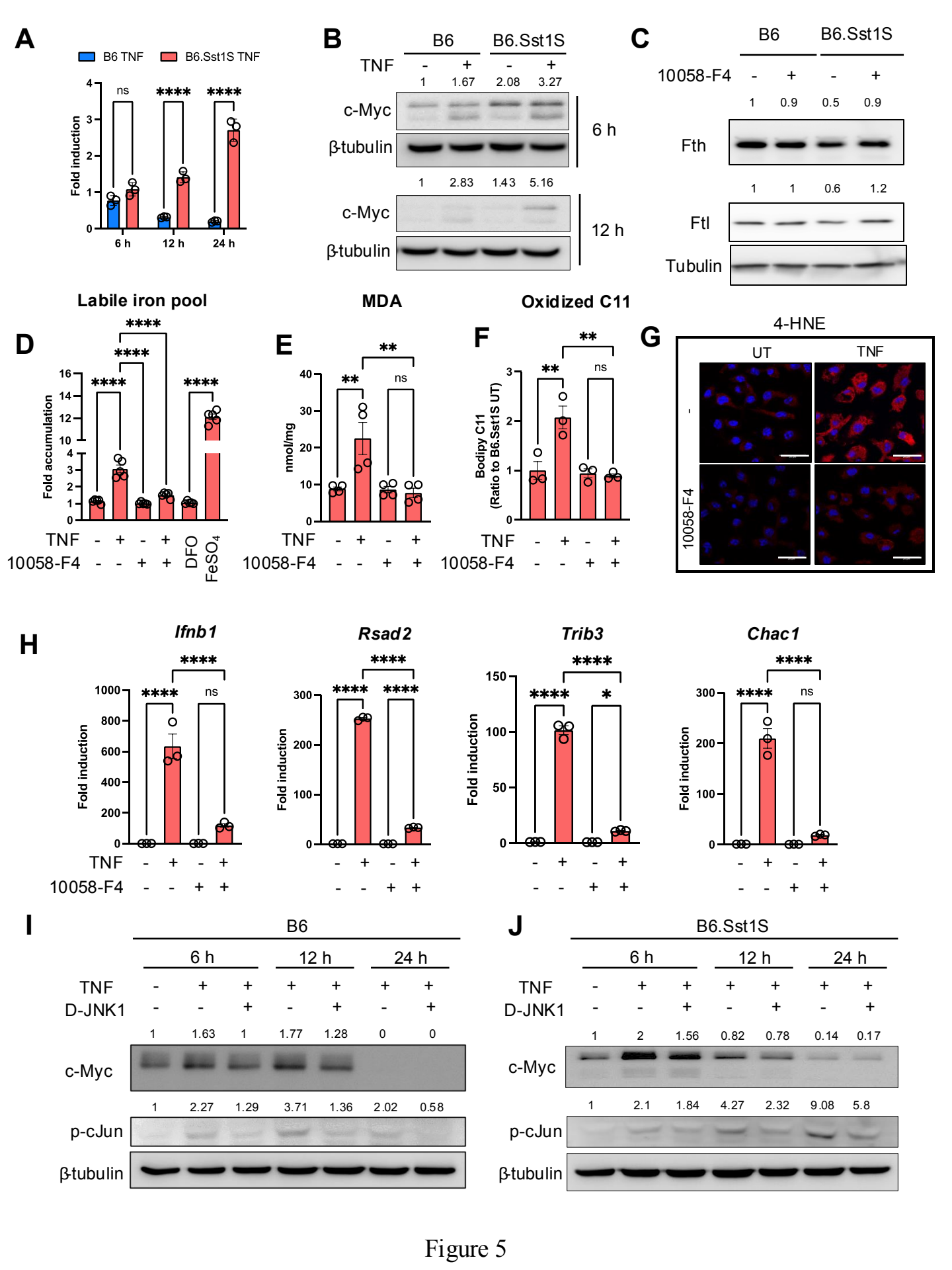
A
B6 TNF
B6.Sst1S TNF
Fold induction
ns
****
****
6 h
12 h
24 h
B
B6
B6.Sst1S
TNF
1
1.67
2.08
3.27
c-Myc
β-tubulin
6 h
1
2.83
1.43
5.16
c-Myc
β-tubulin
12 h
C
B6
B6.Sst1S
10058-F4
1
0.9
0.5
0.9
Fth
1
1
0.6
1.2
Ftl
Tubulin
Labile iron pool
D
Fold accumulation
TNF
10058-F4
DFO
FeSO4
MDA
E
nmol/mg
Oxidized C11
F
Bodipy C11 (Ratio to B6.Sst1S UT)
G
4-HNE
UT
TNF
10058-F4
H
Ifnb1
Rsad2
Trib3
Chac1
Fold induction
I
B6
6 h
12 h
24 h
TNF
D-JNK1
1
1.63
1
1.77
1.28
0
0
c-Myc
1
2.27
1.29
3.71
1.36
2.02
0.58
p-cJun
β-tubulin
J
B6.Sst1S
1
2
1.56
0.82
0.78
0.14
0.17
c-Myc
1
2.1
1.84
4.27
2.32
9.08
5.8
p-cJun
β-tubulin

Figure 5

Figure 5. Myc dysregulation drives the aberrant state of macrophage activation

(**A**). The lack of *Myc* mRNA downregulation after prolonged TNF stimulation in B6.Sst1S macrophages. BMDMs from B6 and B6.Sst1S were treated with 10 ng/mL TNF for 6, 12 and 24 h. Expression of *Myc* was quantified by the ΔΔCt method using qRT-PCR and expressed as a fold induction compared to the untreated B6 BMDMs. β-actin was used as the internal control.

(**B**). Myc protein levels expressed by B6 and B6.Sst1S BMDMs during the course of stimulation with TNF(10 ng/mL) for 6 and 12 h. (Western blot). Average densitometric values from 2 independent experiment were included above the blot.

(**C**). Myc inhibition restored the levels of Fth and Ftl proteins in TNF-stimulated B6.Sst1S macrophages to the B6 levels. B6 and B6.Sst1S BMDMs from were treated with 10 ng/mL TNF alone or in combination with Myc inhibitor, 10058-F4 (10 μM) for 24 h. 10058-F4 was added 2 h post TNF stimulation. Protein levels of Fth and Ftl were observed using Western blot. Average densitometric values from 2 independent experiment were included above the blot.

(**D**). Myc inhibition decreased the labile iron pool in TNF-stimulated B6.Sst1S macrophages. B6.Sst1S BMDMs were treated with 10 ng/mL TNF or left untreated for 48 h. The 10058-F4 inhibitor was added 2 h post TNF stimulation. The labile iron pool (LIP) was measured using Calcein AM method and represented as fold change as compared to untreated control. DFO was used as negative control and FeSo4 was used as positive control.

(**E** and **F**). Myc inhibition reduced lipid peroxidation in TNF-stimulated B6.Sst1S BMDMs. Cells were treated with 10 ng/mL TNF in presence or absence of 10058-F4 for 48 h. The inhibitor was added 2 h post TNF stimulation. The MDA production was measured using commercial MDA assay (E). The lipid peroxidation was measured by fluorometric method using C11-Bodipy 581/591 (F).

(**G**). B6.Sst1S BMDMs were treated as above in E. The accumulation of lipid peroxidation product, 4HNE after 48h was detected by confocal microscopy using 4-HNE specific antibody. The 4HNE accumulation was quantified using ImageJ and plotted as fold accumulation compared to untreated group.

(**H**). The BMDMs from B6.Sst1S were treated with 10 ng/mL TNF alone or in combination with Myc inhibitor, 10058-F4 (10 μM) for 24 h. 10058-F4 was added 2 h post TNF stimulation. Expression of *Ifnb1*, *Rsad2, Trib3* and *Chac1* was quantified by the ΔΔCt method using qRT-PCR and expressed as a fold induction compared to the untreated group. 18S was used as the internal control.

(**I** and **J**). B6 (I) and B6.Sst1S (J) BMDMs were treated with TNF (10 ng/ml) for 6, 12, and 24 h in the presence or absence of JNK inhibitor D-JNK1 (2 μM). The cells were harvested and the protein levels of c-Myc and p-cJun were determined by western blotting. JNK inhibitor D-JNK1 was added 2 h post TNF stimulation. Average densitometric values from 2 independent experiment were included above the blot.

The data are presented as means ± standard deviation (SD) from three-five samples per experiment, representative of three independent experiments. The statistical significance was performed by two-way ANOVA using Šídák's multiple comparison test (Panel A) and ordinary one-way ANOVA using Šídák's multiple comparison test (Panel D-F and H). Significant differences are indicated with asterisks (*, $P < 0.05$; **, $P < 0.01$; ***, $P < 0.001$; ****, $P < 0.0001$).

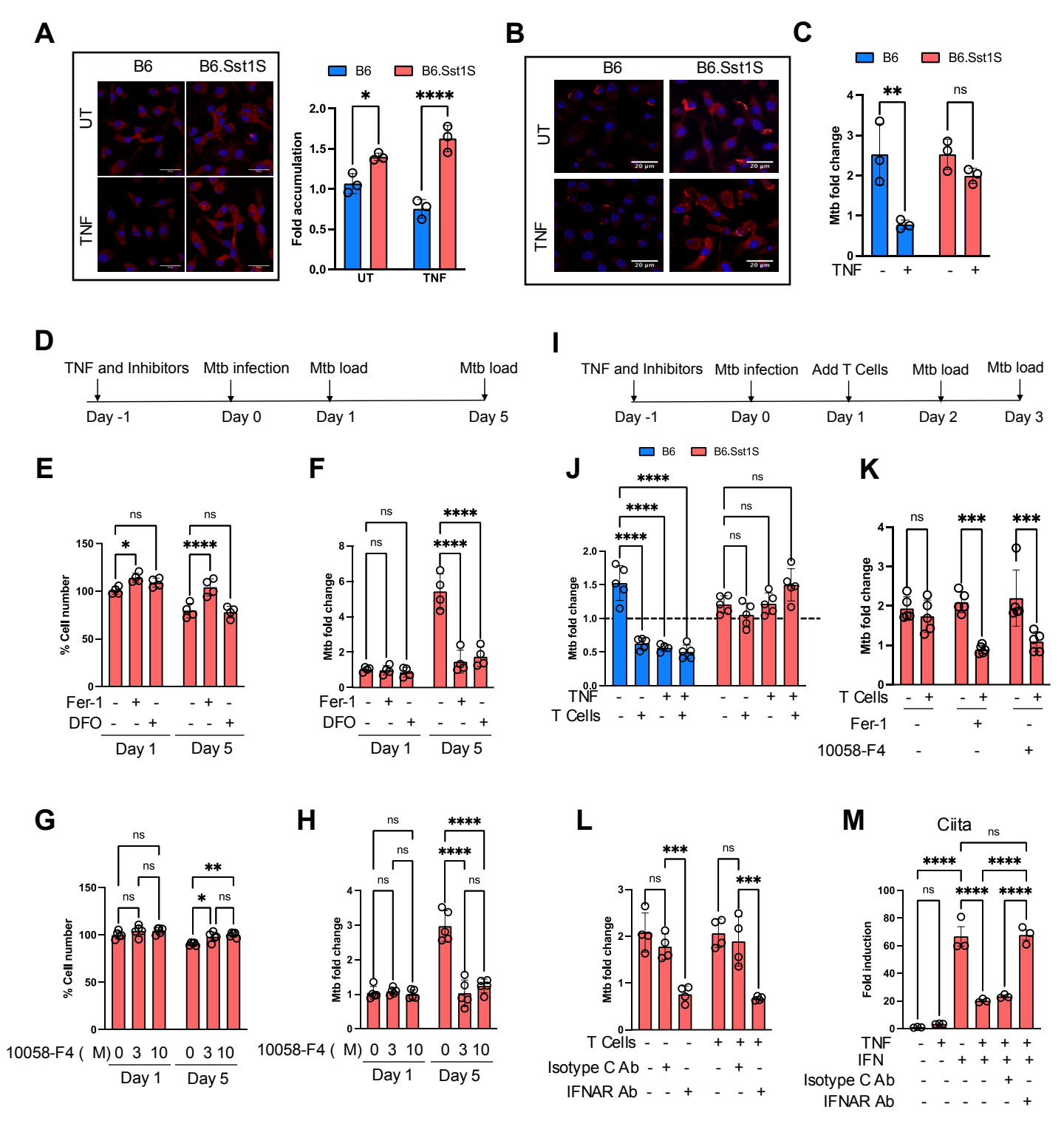
A
B6
B6.Sst1S
UT
TNF
Fold accumulation
B
C
Mtb fold change
D
TNF and Inhibitors
Mtb infection
Mtb load
Day -1
Day 0
Day 1
Day 5
I
Add T Cells
Day 2
Day 3
E
% Cell number
Fer-1
DFO
F
J
T Cells
K
10058-F4
G
10058-F4 (M)
H
L
Isotype C Ab
IFNAR Ab
M
Ciita
Fold induction
IFN

Figure 6

Figure 6. Myc and lipid peroxidation compromise control of intracellular Mtb by the B6.Sst1S macrophages.

(**A**). Accumulation of 4-HNE in Mtb-infected B6 and B6.Sst1S macrophage monolayers infected with Mtb. BMDMs were either treated with 10 ng/mL TNF or left untreated (UT), and subsequently infected with Mtb at MOI=1. 4-HNE was detected by confocal microscopy using 4-HNE specific antibody 5 dpi. The 4HNE accumulation was quantified at 5 dpi using ImageJ and plotted as fold accumulation compared to untreated B6 (UT).

(**B**). Naïve and TNF-stimulated B6 and B6.Sst1S BMDMs were infected with Mtb Erdman reporter strain (SSB-GFP, *smyc*'::mCherry) for 5 days. The accumulation of 4HNE was detected in both Mtb-infected and non-infected B6.Sst1S cells at day 5 p.i..

(**C**). Naïve and TNF-stimulated B6.Sst1S BMDMs were infected with Mtb at MOI=1. At days 4 post infection Mtb load was determined using a qPCR-based method.

(**D**). Testing the effects of LPO and Myc inhibitors on the Mtb-infected B6.Sst1S BMDM survival and Mtb control: experimental design for panels E - H.

(**E** and **F**). Prevention of iron-mediated lipid peroxidation improves the survival of and Mtb control by the B6.Sst1S macrophages. BMDMs were treated with 10 ng/mL TNF alone in combination with Fer-1 (3 μM) or DFO (50 μM) for 16 h and subsequently infected with Mtb at MOI=1. The inhibitors were added after infection for the duration of the experiment. At days 1 and 5 post infection, total cell numbers were quantified using automated microscopy (E) and Mtb loads was determined using a qPCR-based method (F). The percentage cell number were calculated based on the number of cells at Day 0 (immediately after Mtb infection and washes). The fold change of Mtb was calculated after normalization using Mtb load at Day 0 after infection.

(**G** and **H**). Myc inhibition improves the survival and Mtb control by B6.Sst1S macrophages. BMDMs were treated with 10 ng/mL TNF alone or in combination with 3 μM or 10 μM 10058-F4 for 16 h and subsequently infected with Mtb at MOI=1. At days 1 and 5 post infection, total cell numbers were quantified using automated microscopy (G) and Mtb loads was determined using a qPCR-based method (H). The percentage cell number were calculated based on the number of cells at Day 0 (immediately after Mtb infection). The fold change of Mtb was calculated after normalization using Mtb load at Day 0 after infection and washes.

(**I**). LPO and Myc inhibitors improve Mtb control by B6.Sst1S BMDMs co-cultured with BCG-induced T cells: experimental design for panels J - L.

(**J**). Differential effect of BCG-induced T cells on Mtb control by B6 and B6.Sst1S macrophages. BMDMs of both backgrounds were treated with 10 ng/mL TNF or left untreated and subsequently infected with Mtb at MOI=1. T lymphocytes purified from lymph nodes of BCG vaccinated B6 mice were added to the infected macrophage monolayers 24 h post infection. The Mtb load was calculated by qPCR based method after 2 days of co-culture with T lymphocytes (3 days post infection). The dotted line indicates the Mtb load in untreated cells at day 2 post infection.

(**K**). Inhibition of Myc and lipid peroxidation improves control of Mtb by B6.Sst1S macrophages co-cultured with immune T cells isolated from BCG-vaccinated B6 mice. BMDMs were pretreated with 10 ng/mL TNF alone or in combination with either Fer-1 (3 μM) or 10058-F4 (10 μM) for 16 h and subsequently infected with Mtb at MOI 1. At 24 h post infection the lymphocytes from BCG immunized B6 mice were added to the infected macrophage monolayers. The Mtb loads were determined by qPCR based method after 2 days of co-culture with T cells (3 days post infection).

(**L**). Inhibition of type I IFN receptor improves control of Mtb by B6.Sst1S macrophages. BMDMs were pretreated with 10 ng/mL TNF alone or in combination with IFNAR1blocking Ab or isotype C Ab for 16 h and subsequently infected with Mtb at MOI 1. At 24 h post infection the lymphocytes from BCG immunized B6 mice were added to the infected macrophage monolayers. The Mtb loads were determined by qPCR-based method after 2 days of co-culture with T cells (3 days post infection).

(**M**). TNF stimulation inhibits and IFNAR1 blockade restores the response of B6.Sst1S macrophages to IFNγ. BMDMs were pretreated with TNF (10 ng/mL) for 18 h and the IFNAR1 blocking Abs or isotype C Ab were added two hours after TNF. Subsequently, IFNγ (10 U/mL) was added for additional 12 h. The expression of the IFNγ -specific target gene *Ciita* was assessed using qRT-PCR. 18S was used as internal control.

The data are presented as means ± standard deviation (SD) from three-five samples per experiment, representative of three independent experiments.
The statistical significance was performed by two-way ANOVA using Bonferroni's multiple comparison test (Panel A, C, J and K) and Tukey's multiple comparison test (Panel E-H and L). One-way ANOVA using Bonferroni's multiple comparison test (Panel M). Significant differences are indicated with asterisks (*, $P < 0.05$; **, $P < 0.01$; ***, $P < 0.001$; ****, $P < 0.0001$).

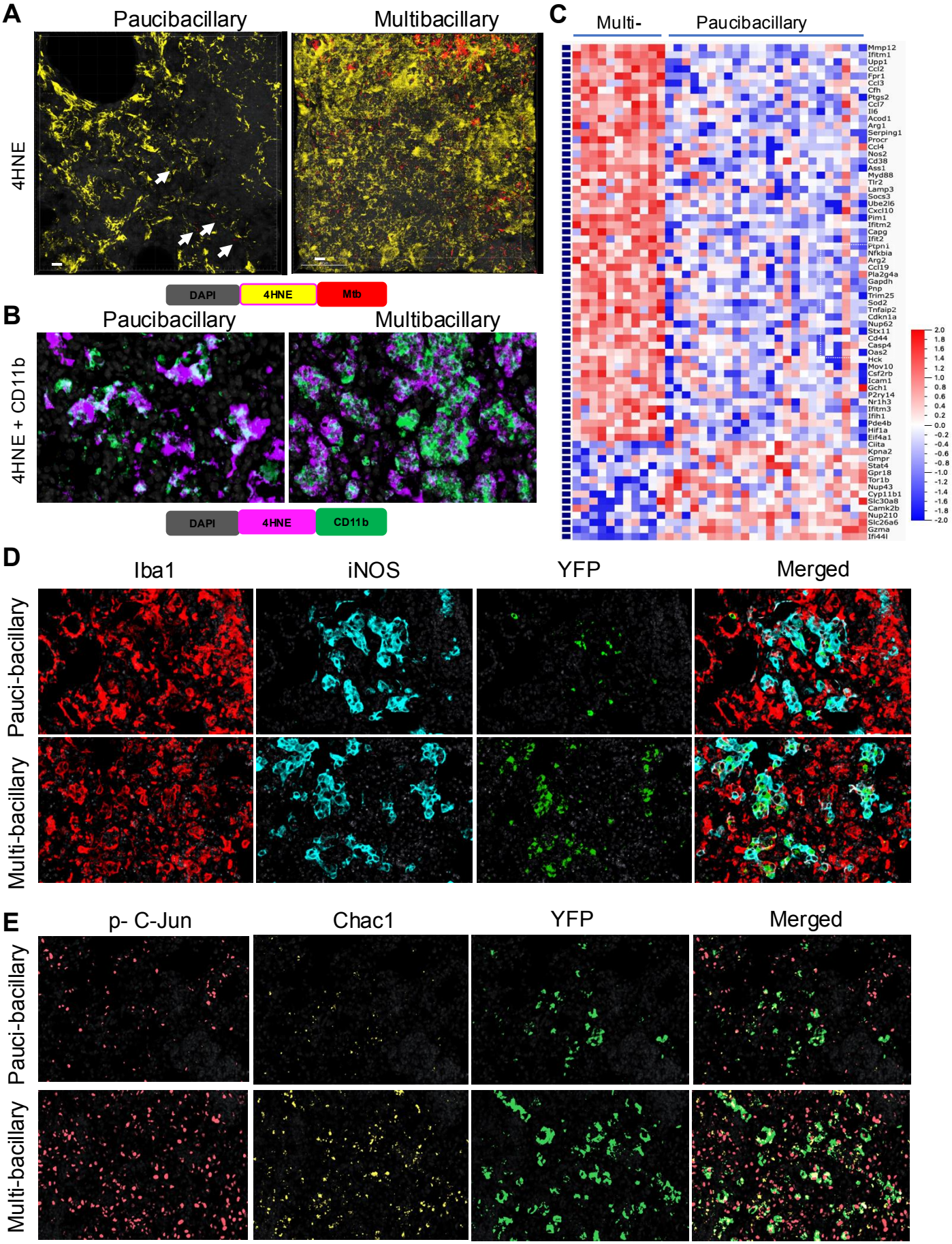
A
Paucibacillary
Multibacillary
4HNE
DAPI
4HNE
Mtb
B
Paucibacillary
Multibacillary
4HNE + CD11b
DAPI
4HNE
CD11b
C
Multi-
Paucibacillary
Mmp12
Ifitm1
Upp1
Ccl2
Fpr1
Ccl3
Cfh
Ptgs2
Ccl7
Il6
Acod1
Arg1
Serping1
Procr
Ccl4
Nos2
Cd38
Ass1
Myd88
Tlr2
Lamp3
Socs3
Ube2l6
Cxcl10
Pim1
Ifitm2
Capg
Ifit2
Ptpn1
Nfkbia
Arg2
Ccl19
Pla2g4a
Gapdh
Pnp
Trim25
Sod2
Tnfaip2
Cdkn1a
Nup62
Stx11
Cd44
Casp4
Oas2
Hck
Mov10
Csf2rb
Icam1
Gch1
P2ry14
Nr1h3
Ifitm3
Ifih1
Pde4b
Hif1a
Eif4a1
Ciita
Kpna2
Gmpr
Stat4
Gpr18
Tor1b
Nup43
Cyp11b1
Slc30a8
Camk2b
Nup210
Slc26a6
Gzma
Ifi44l
2.0
1.8
1.6
1.4
1.2
1.0
0.8
0.6
0.4
0.2
0.0
-0.2
-0.4
-0.6
-0.8
-1.0
-1.2
-1.4
-1.6
-1.8
-2.0
D
Iba1
iNOS
YFP
Merged
Pauci-bacillary
Multi-bacillary
E
p- C-Jun
Chac1
YFP
Merged
Pauci-bacillary
Multi-bacillary

Figure 7

Figure 7: Accumulation of lipid peroxidation products and stress escalation in macrophages during pulmonary TB progression.

(**A**). Representative 3D confocal images of paucibacillary (n=16) and multibacillary (n=16) pulmonary TB lesions of B6.Sst1S,*Ifnb1* -YFP reporter mice stained with anti-4HNE antibody (yellow). Cells expressing YFP are green, Mtb reporter Mtb (smyc' :: mCherry) is red. Arrows indicate Mtb reporter strain expressing mCherry. The mice were infected for 20 weeks.

(**B**). Representative Fluorescent multiplexed immunohistochemistry (fmIHC) images of pauci-bacillary and multi-bacillary PTB lesion in B6.Sst1S mice at high magnification (600X). 4-HNE (magenta), CD11b (green) and DAPI (grey). White areas showing 4-HNE and CD11b co-localization. The mice were infected for 20 weeks.

(**C**). Heatmap of interferon inducible genes differentially expressed in Iba1+ cells within multibacillary vs paucibacillary lesions (fold change 1.5 and above). Pooled gene list of IFN type I and II regulated genes was assembled using public databases (as described in Methods). The mice were infected for 14 weeks.

(**D).** Representative fmIHC images of IFN-I producing (YFP positive) myeloid cells in pauci-bacillary (n=8) and multi-bacillary (n=8) lesion of B6.Sst1S,*Ifnb1* -YFP reporter mice. The different markers are shown as Iba1 (red), iNOS (teal) and YFP (green) at 400X magnification. The mice were infected for 20 weeks.

(**E).** Representative fmIHC images of IFN-I producing (YFP positive) cells accumulating stress markers in pauci-bacillary (n=6) and multi-bacillary (n=9) lesion of B6.Sst1S,*Ifnb1* -YFP reporter mice. The different markers are shown as phospho-c-Jun (peach), Chac-1 (yellow) and YFP (green) at 400X original magnification. The mice were infected for 20 weeks.

Supplemental Materials for

Lipid peroxidation and type I interferon coupling fuels pathogenic macrophage activation causing tuberculosis susceptibility

Shivraj M. Yabaji et al.

Corresponding author Email: ikramnik@bu.edu

This PDF file includes:

Supplemental Figures 1 to 16

Supplemental Tables 1 to 6

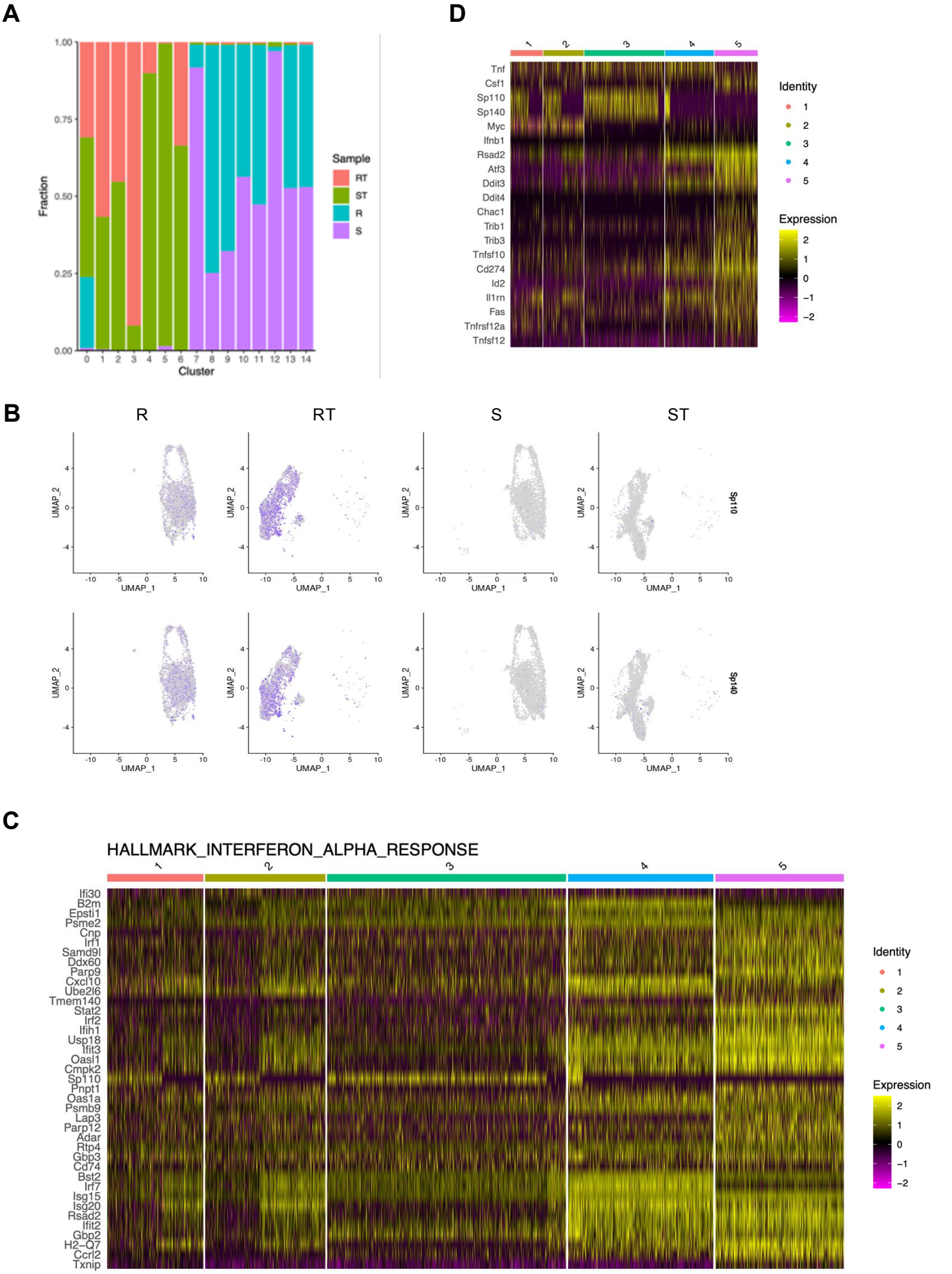

Supplemental Figure 1

Supplemental Figure 1: Single cell RNAseq analysis of the B6 and B6.Sst1S macrophages after TNF stimulation

A. Relative proportions of either naïve (R and S) or TNF-stimulated (RT and ST) B6 or B6.Sst1S macrophages within individual single cell clusters depicted in **Fig.1B**.

B. The distribution of macrophages expressing the *sst1*-encoded *Sp110* and *Sp140* genes across the populations of naïve (R and S) and TNF-stimulated (RT and ST) B6 or B6.Sst1S macrophages.

C. Heatmap of the IFN-I pathway gene expression in subpopulations 1 - 5 identified using pseudotime trajectory analysis.

D. The expression of known *sst1*-dependent genes representing IFN-I, stress response, apoptosis and immunosuppression in subpopulations 1 - 5.

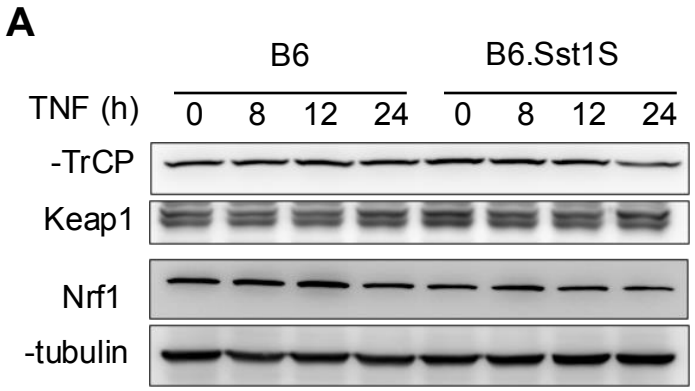

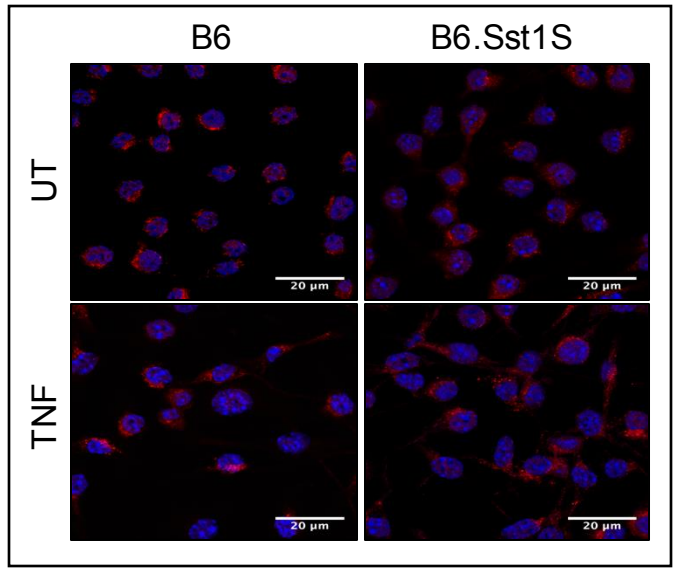

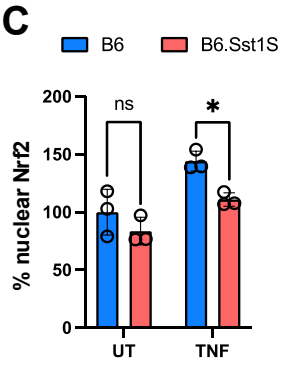

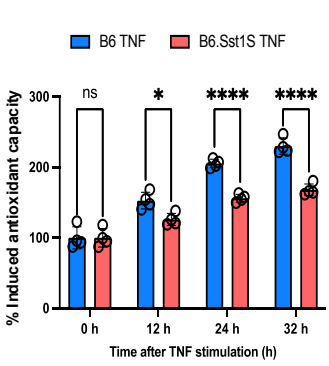

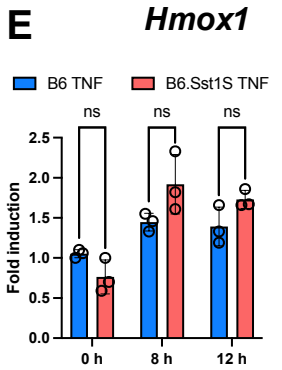

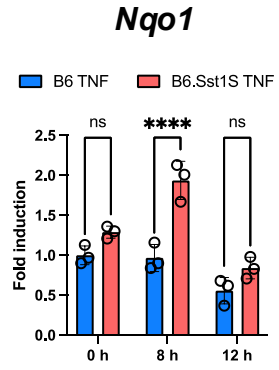

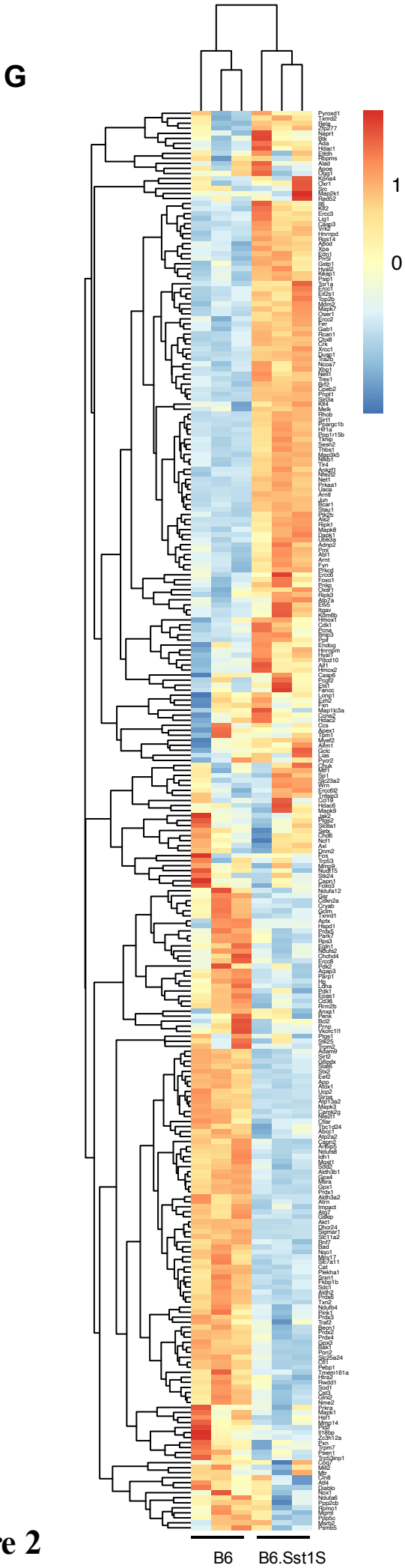

Supplemental Figure 2

Supplemental Figure 2: Anti-oxidant response of TNF-stimulated B6 and B6.Sst1.S BMDMs.

A. Total levels of Nrf1, -TrCP and Keap1 proteins in B6 and B6.Sst1S BMDMs stimulated with TNF (10 ng/ml) for 8, 12 and 24 h (Western blotting). The experiment was repeated 2 times and shown the representative blot.

B. B6 and B6.Sst1S BMDMs stimulated with TNF (10 ng/ml) for 12 h. Total NRF1 levels were evaluated using confocal microscopy. Scale bar = 20 m.

C. B6 and B6.Sst1S BMDMs stimulated with TNF (10 ng/ml) for 12 h. Nrf2 nuclear translocation was quantified using automated microscopy (Operetta CLS High Content Analysis System). Untreated samples considered 100%.

D. The total antioxidant capacity of B6 and B6.Sst1S BMDMs were measured after TNF (10 ng/ml) stimulation. The percentage of induced antioxidant capacity upon TNF stimulation was plotted (Y axis).

E and F. B6 and B6.Sst1S BMDMs stimulated with TNF (10 ng/ml) for 8 and 12 h. *Hmox1* and *Nqo1* expressions were quantified using qRT-PCR.

G. The heatmap of all genes related to response to oxidative stress (gene ontology category GO: 0006979). The heatmap was generated using FPKM values obtained using bulk RNAseq of B6.Sst1S and B6 BMDMs after 12 h of TNF stimulation. For heatmap generation, FPKM values were scaled using Z-scores for each tested gene.

The data are presented as means ± standard deviation (SD) from three-five samples per experiment, representative of three independent experiments.
The statistical significance was performed by two-way ANOVA using Tukey's multiple comparison test (Panels C-F). Significant differences are indicated with asterisks (*, $P < 0.05$; **, $P < 0.01$; ***, $P < 0.001$; ****, $P < 0.0001$).

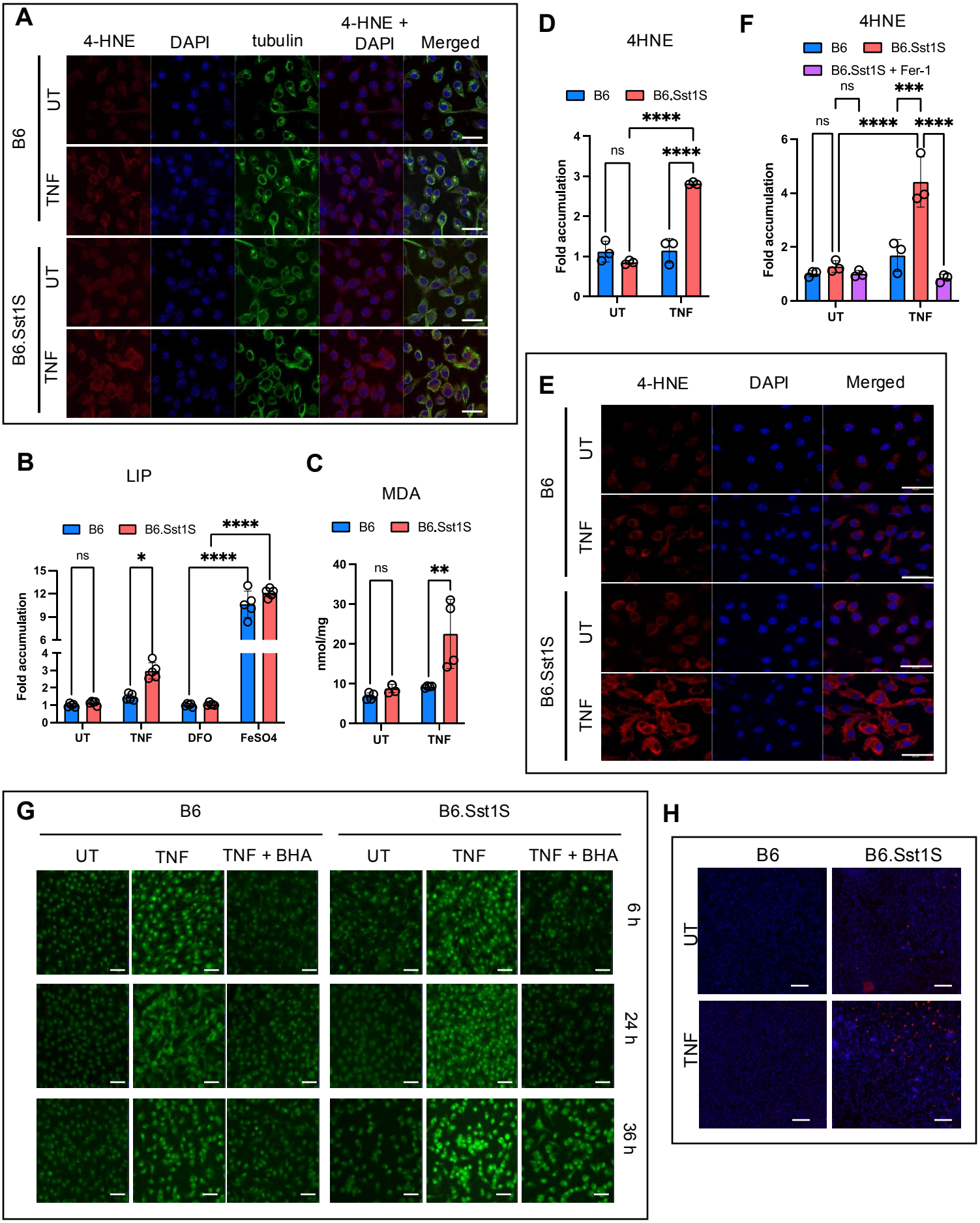

Supplemental Figure 3

Supplemental figure 3: Regulation of TNF-induced ROS, labile iron pool and lipid peroxidation in B6 and B6.Sst1.S BMDMs.

A. B6 and B6 BMDMs were treated with 10 ng/mL TNF of left untreated for 48 h. The cells were stained to observe 4-HNE accumulation and cellular structure using anti-4-HNE and anti-tubulin Ab respectively. The images were acquired using confocal microscopy. Scale bar = 20 m.

B. The labile iron pool (LIP) in B6 and B6.Sst1.S BMDMs treated with 10 ng/mL TNF or left untreated for 48 h. LIP was calculated using Calcein AM method and represented as fold change. DFO was used as negative control and FeSo4 was used as positive control.

C. Production of lipid peroxidation metabolite malondialdehyde (determined by MDA assay) by B6 and B6.Sst1S BMDMs treated with 10 ng/mL TNF for 48 h. UT - untreated control.

D - F. The intracellular 4-HNE accumulation in B6 and B6.Sst1.S BMDMs treated with 10 ng/mL TNF for 30 h (D and E) and 48 h (F). The 4-HNE accumulation was quantified using ImageJ and plotted as a fold accumulation compared to B6 untreated group. Scale bar = 20 m.

G. Reactive oxygen species (ROS) levels were observed using the CellROX assay and imaged by fluorescence microscopy in B6 and B6.Sst1S BMDMs either treated with TNF (10 ng/mL) or left untreated for 6, 24, and 36 h. BHA (100 M) was used as a positive control. Scale bar = 50 m.

H. Cell death in B6 and B6.Sst1S BMDMs stimulated with 50 ng/mL TNF for 48 h. Imaging was performed by automated microscopy using Live-or-DyeTM 594/614 Fixable Viability stain (Biotium) and Hoechst staining. Scale bar = 100 m.

The data represent the means SD of three samples per experiment, representative of three independent experiments.
The statistical significance was performed by two-way ANOVA using Bonferroni's multiple comparison test (Panels B, C, D and F). Significant differences are indicated with asterisks (*, $P < 0.05$; **, $P < 0.01$; ***, $P < 0.001$; ****, $P < 0.0001$).

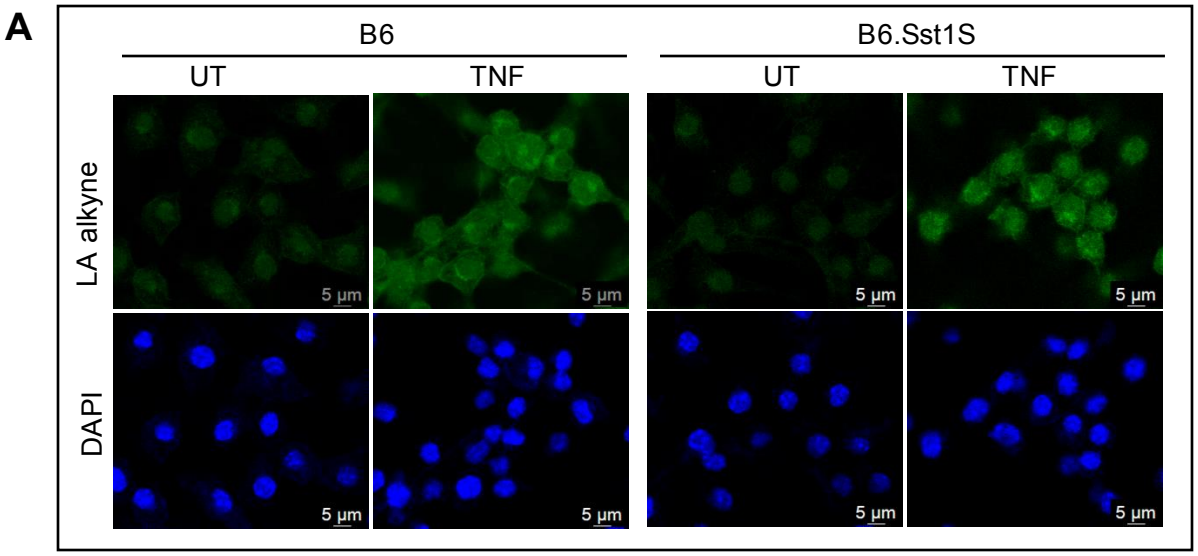

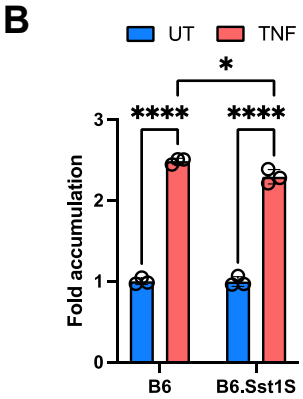

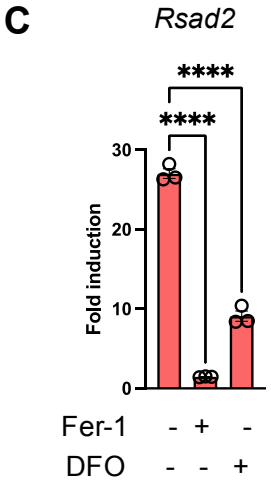

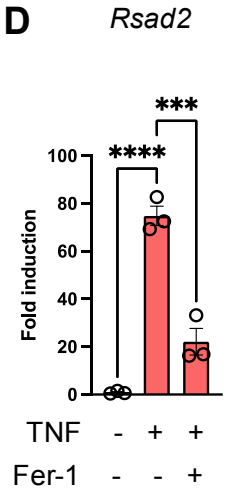

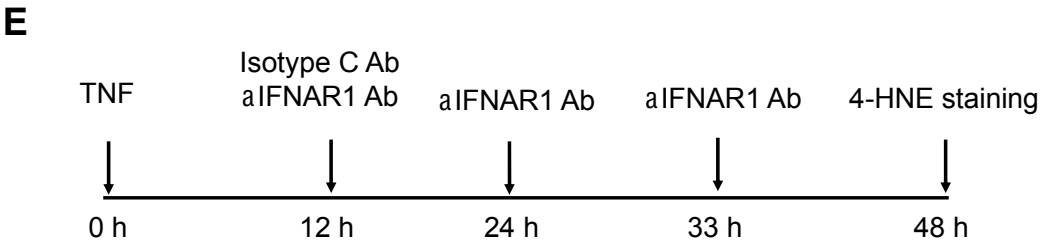

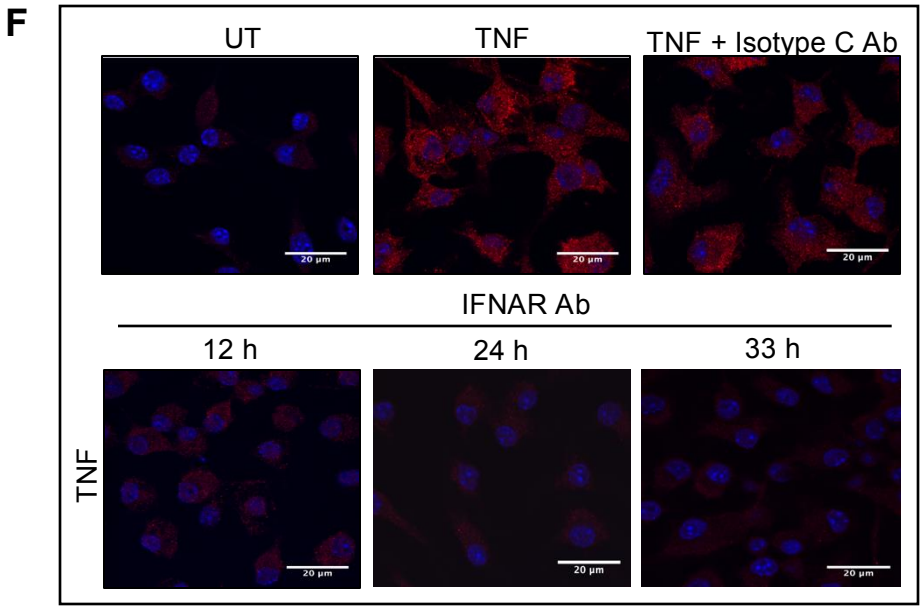

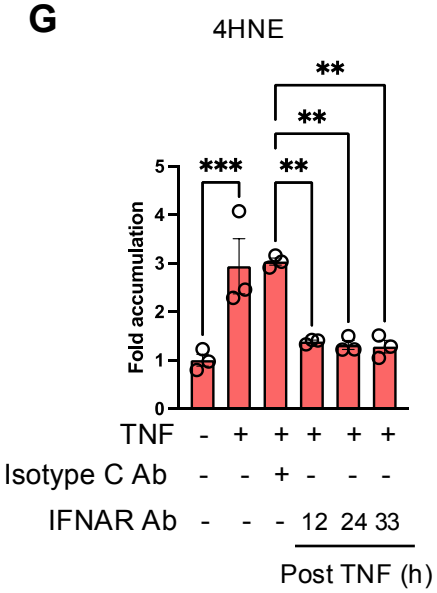

Supplemental Figure 4

Supplemental figure 4: Regulation of lipid peroxide production and type I IFN expression in TNF-stimulated B6 and B6.Sst1.S BMDMs.

A - B. B6 and B6.Sst1S BMDMs were either treated with 10 ng/mL TNF or left untreated for 6 h. The LPO production was observed using Click-iT linoleamide alkyne (LAA) method and imaged using confocal microscopy (A). The quantification of signal per field was performed using ImageJ (B). Scale bar = 5 m.

C. Inhibition of lipid peroxidation prevented the superinduction of *Rsad2* mRNA. B6.Sst1S BMDMs were stimulated with 10 ng/mL TNF for 2h, then the LPO inhibitor (Fer-1) or iron chelator DFO were added for the remaining 14 h. Fold induction was calculated using untreated control as average one-fold by utilizing the Ct method with 18S as the internal control.

D. Inhibition of TNF and lipid peroxidation reversed the *Rsad2* mRNA superinduction after prolonged TNF stimulation. B6.Sst1S BMDMs were stimulated with 10 ng/mL TNF for 18 h, then the LPO inhibitor (Fer-1) was added for the remaining 12 h. Fold induction was calculated using untreated control as average one-fold by utilizing the Ct method with 18S as the internal control.

E. Experimental design for panels F G..

F - G. Inhibition of the 4-HNE accumulation in TNF-stimulated B6.Sst1.S BMDMs by IFNAR1 blocking antibodies. Cells were treated with 10 ng/mL TNF for 48 h in presence of IFNAR1 blocking antibodies. 4HNE was detected using specific antibody staining and confocal microscopy. The isotype C Ab was added 12 h post TNF and anti-IFNAR Ab was added at 12, 24 and 33 h post TNF stimulation. The 4-HNE accumulation was quantified using ImageJ and plotted as fold accumulation compared to untreated group. Isotype C Ab - isotype matched negative control antibodies. Scale bar = 20 m.

The data are presented as means ± standard deviation (SD) from three-five samples per experiment, representative of three independent experiments. The statistical significance was performed by Ordinary one-way ANOVA using Bonferroni's multiple comparison test (B-D) and two-way ANOVA using Tukey's multiple comparison test (Panel E), Significant differences are indicated with asterisks (*, $P < 0.05$; **, $P < 0.01$; ***, $P < 0.001$; ****, $P < 0.0001$).

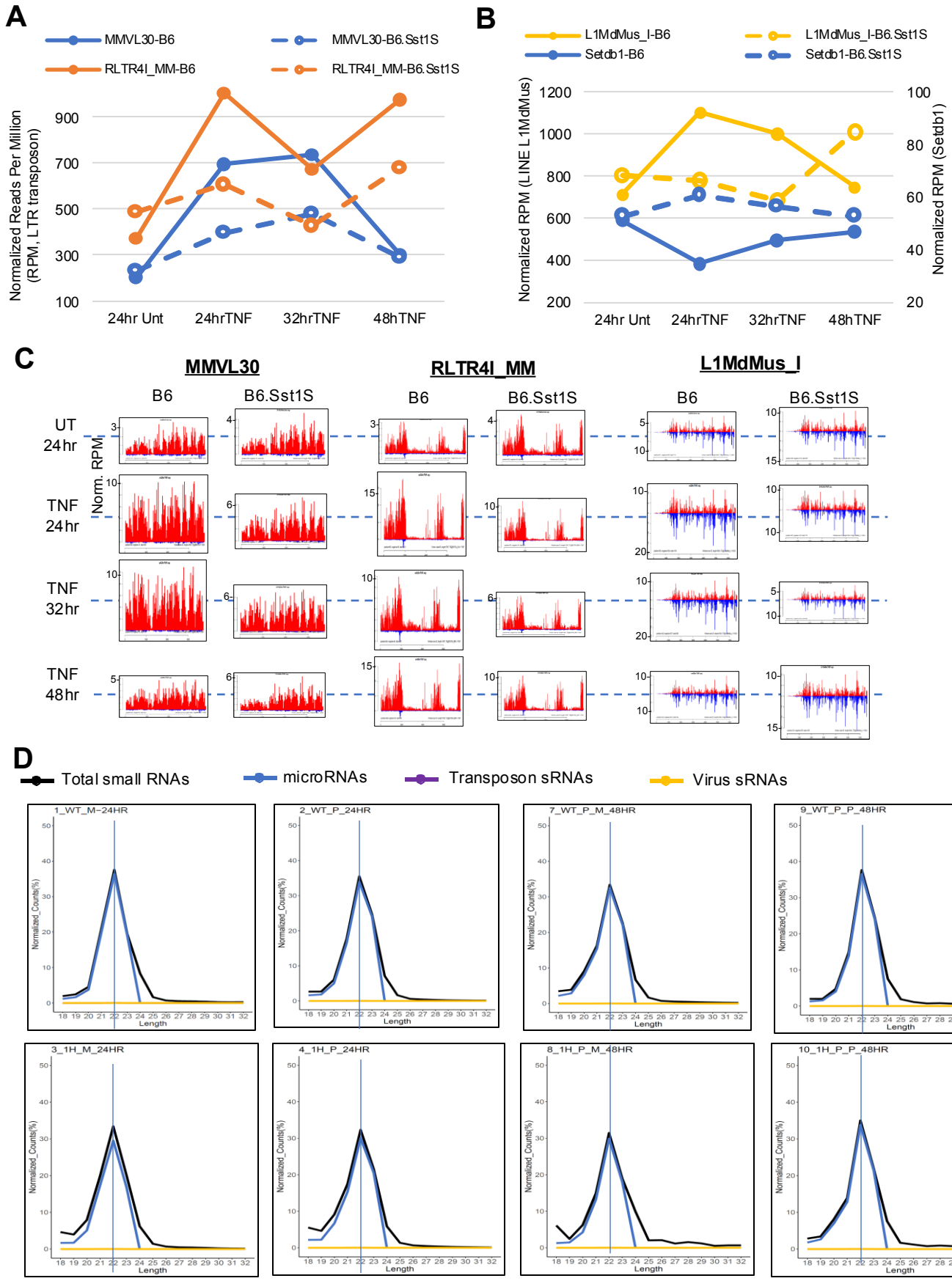

Supplemental Figure 5

Supplementary Figure 5. The transient upregulation of transposon mRNAs in B6 macrophages after TNF treatment is affected in the B6.Sst1S.

A. Line graphs displaying the expression of two mouse LTR transposons, mVL30 and RLTR4i activated in expression by TNF treatment in WT macrophages with the levels less stimulated in the B6.Sst1S.

B. A LINE transposon L1Md expression pattern compared to the distinct expression dynamics of Setdb1 after TNF stimulation between B6 and B6.Sst1S macrophages. Setdb1 protein is implicated as the histone methyltransferase marking H3K9me3 on these two transposons.

C. Reads coverage plots show extensive transcript representation and positive strand bias for LTR transposons, but double-stranded RNA expression from the LINE transposon.

D. Size distribution plots with functional annotations indicate the vast majority of macrophage small RNAs are mainly microRNAs, with little detection of viral and transposon small RNAs that would be indicative of these small interfering RNAs being processed by putative longer double-stranded RNA precursors.

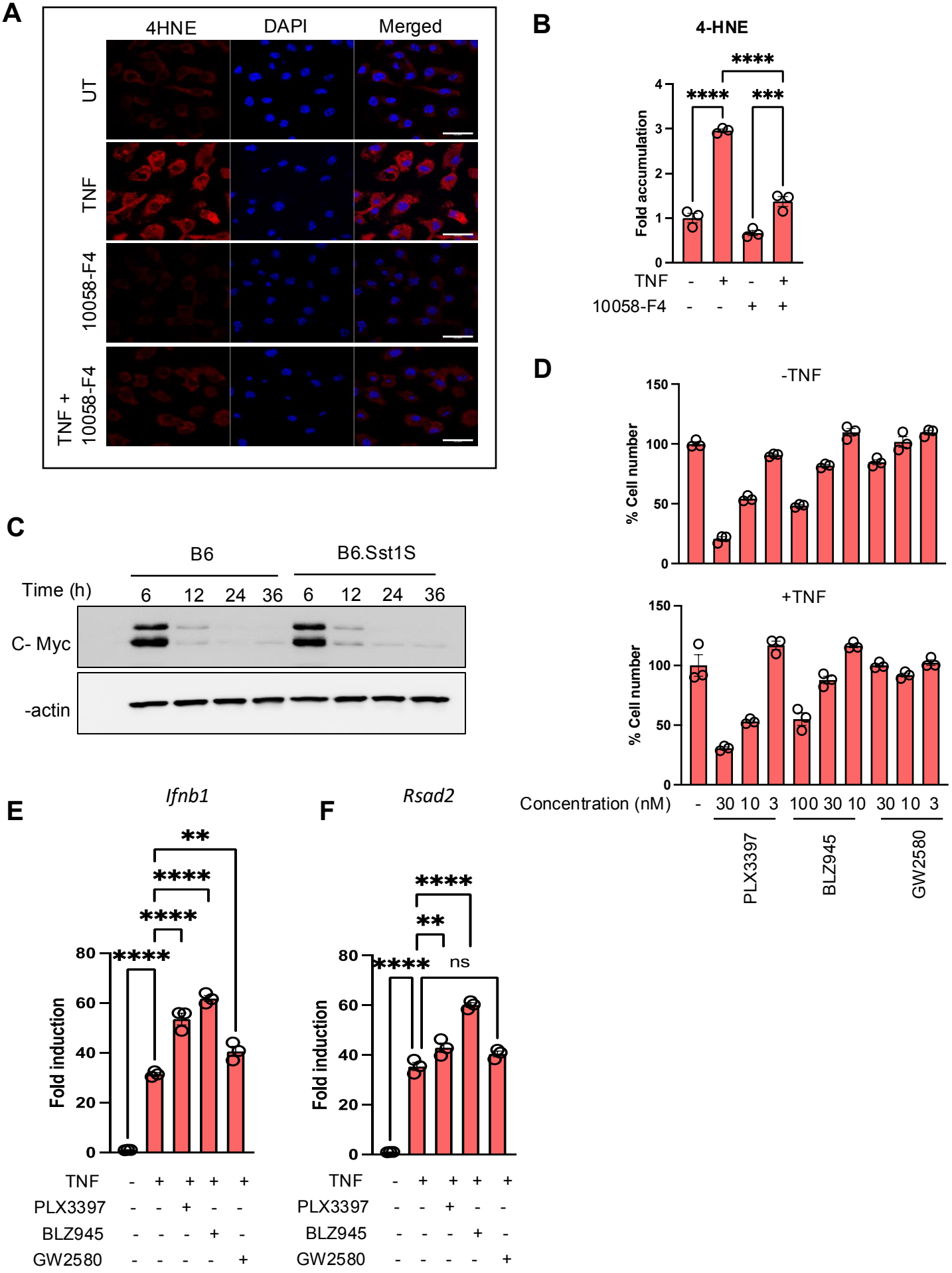

Supplemental Figure 6

Supplemental Figure 6: Effects of Myc and CSF1R inhibition on B6.Sst1S macrophage activation by TNF.

A. Myc inhibitor 10058-F4 (10) prevents the 4-HNE accumulation in TNF-stimulated B6.Sst1S BMDMs. B6.Sst1S BMDMs were treated with 10 ng/mL TNF for 48 h. The inhibitor was added 2 h post TNF stimulation. The accumulation of lipid peroxidation product, 4-HNE was detected by confocal microscopy using 4-HNE-specific antibody. Scale bar = 20 m.

B. Myc inhibition reduced lipid peroxidation in TNF-stimulated B6.Sst1S BMDMs. Cells were treated with 10 ng/mL TNF in presence or absence of 10058-F4 for 48 h. The inhibitor was added 2 h post TNF stimulation. The accumulation of lipid peroxidation product, 4-HNE was detected by confocal microscopy using 4-HNE specific antibody. The 4-HNE accumulation was quantified using ImageJ and plotted as fold accumulation compared to untreated group.

C. Media change induces Myc upregulation and similar downregulation in B6 and B6.Sst1S BMDMs. Myc protein levels were monitored using Western blot.

D. Selection of non-toxic concentration of CSF1R inhibitors. BMDMs from B6.Sst1S were either left untreated or treated with 10 ng/mL TNF. Post 2 h of TNF stimulation the inhibitors of CSF1R were added at different concentrations. PLX3397 (30, 10 and 3 nM), BLZ945 (100, 30 and 10 nM) and GW2580 (30, 10 and 3 nM) for 46 h. Percent of cell number was determined by automated microscopy.

E and **F.** CSF1R inhibitors do not prevent the IFN-I pathway hyperactivity in TNF-stimulated B6.Sst1S macrophages. BMDMs from B6.Sst1S were treated with 10 ng/mL TNF alone or in combination with CSF1R inhibitors, PLX3397 (3 nM), BLZ945 (10 nM) and GW2580 (10 nM) for 20 h. CSF1R inhibitors were added 2 h post TNF stimulation. Expression of *Ifnb1* and *Rsad2* were quantified by the Ct method using qRT-PCR and expressed as a fold induction compared to the untreated group. 18S was used as the internal control.

The data are presented as means ± standard deviation (SD) from three-five samples per experiment, representative of three independent experiments.
The statistical significance was performed by ordinary one-way ANOVA using multiple comparison test (Panel B, E and F). Significant differences are indicated with asterisks (*, $P < 0.05$; **, $P < 0.01$; ***, $P < 0.001$; ****, $P < 0.0001$).

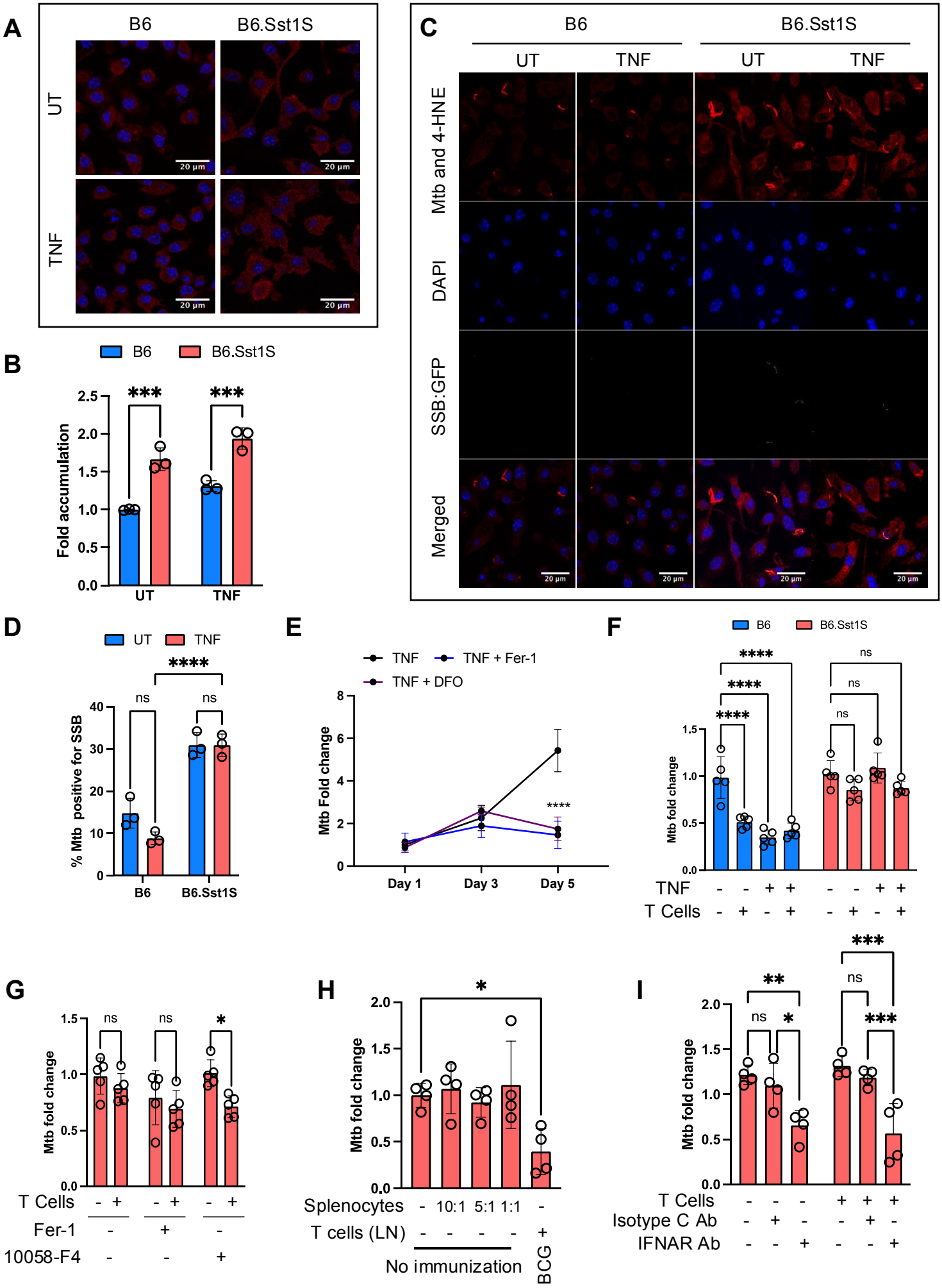

Supplemental Figure 7

Supplemental Figure 7. Inhibition of lipid peroxidation improves Mtb control by B6.Sst1S macrophages.

A-B. Accumulation of 4-HNE in Mtb-infected B6 and B6.Sst1.S macrophage monolayers infected with Mtb. BMDMs were either treated with 10 ng/mL TNF or left untreated (UT), and subsequently infected with Mtb at MOI=1. 4-HNE was detected by confocal microscopy using 4-HNE specific antibody 3 dpi. The 4HNE accumulation was quantified at 3 dpi using ImageJ and plotted as fold accumulation compared to untreated B6 (UT). Scale bar = 20 m.

C-D. Naïve and TNF-stimulated B6 and B6.Sst1S BMDMs were infected with Mtb Erdman reporter strain (Mtb SSB-GFP, smyc ::mCherry) at MOI=1 for 5 days. The 4-HNE accumulation and Mtb SSB were observed using confocal microscopy at day 5 p.i. (C). The percent of replicating Mtb was quantified by calculating number of Mtb (red) and SSB-GFP puncta (green) (D). Scale bar = 20 m.

E. Control of Mtb growth by B6.Sst1.S BMDMs pre-treated with 10 ng/mL TNF alone or in combination with Fer-1 (3 M) or DFO (50 M). Macrophages were pretreated 16 h before Mtb infection and infected with Mtb at MOI=1. Mtb loads were determined on days 1, 3 and 5 post infection using a qPCR-based method.

F. Differential effect of BCG-induced T cells on Mtb control by B6 and B6.Sst1.S macrophages. BMDMs of both backgrounds were treated with 10 ng/mL TNF or left untreated and subsequently infected with Mtb at MOI=1. T lymphocytes purified from lymph nodes of BCG vaccinated B6 mice were added to the infected macrophage monolayers 24 h post infection. The Mtb load was calculated by qPCR-based method after 1 day of co-culture with T lymphocytes (day 2 post infection). The dotted line indicates the Mtb load in untreated cells at day 2 post infection.

G. Inhibition of Myc and lipid peroxidation improves control of Mtb by B6.Sst1S macrophages co-cultured with immune T cells isolated from BCG-vaccinated B6 mice. BMDMs were pretreated with 10 ng/mL TNF alone or in combination with either Ferrostatin 1 (3 M) or 10058-F4 (10 M) for 16 h and subsequently infected with Mtb at MOI 1. At 24 h post infection the lymphocytes from BCG immunized B6 mice were added to the infected macrophage monolayers. The Mtb loads were determined by qPCR-based method after 1 day of co-culture with T cells (2 days post infection).

H. BMDMs from B6 were infected with Mtb at MOI 1. At 24 h post infection the splenocytes from non-immunized mice at 10:1, 5:1 and 1:1 ratio (splenocytes:macrophages) or lymphocytes from BCG immunized B6 mice were added to the infected macrophage monolayers. The Mtb loads were determined by qPCR-based method after 1 day of co-culture with T cells (2 days post infection).

I. Inhibition of type I IFN receptor improves control of Mtb by B6.Sst1S macrophages. BMDMs were pretreated with 10 ng/mL TNF alone or in combination with anti-IFNAR Ab or Isotype C Ab for 16 h and subsequently infected with Mtb at MOI 1. At 24 h post infection the lymphocytes from BCG immunized B6 mice were added to the infected macrophage monolayers. The Mtb loads were determined by qPCR-based method after 1 day of co-culture with T cells (2 days post infection).

The data represent the means SD of three samples per experiment, representative of three independent experiments.
The statistical significance was performed by two-way ANOVA using Bonferroni's multiple comparison test (Panel B, D, F, G and I), and multiple comparison test (Panel E) and One-way ANOVA using Bonferroni's multiple comparison test (Panel H). Significant differences are indicated with asterisks (*, $P < 0.05$; **, $P < 0.01$; ***, $P < 0.001$; ****, $P < 0.0001$).

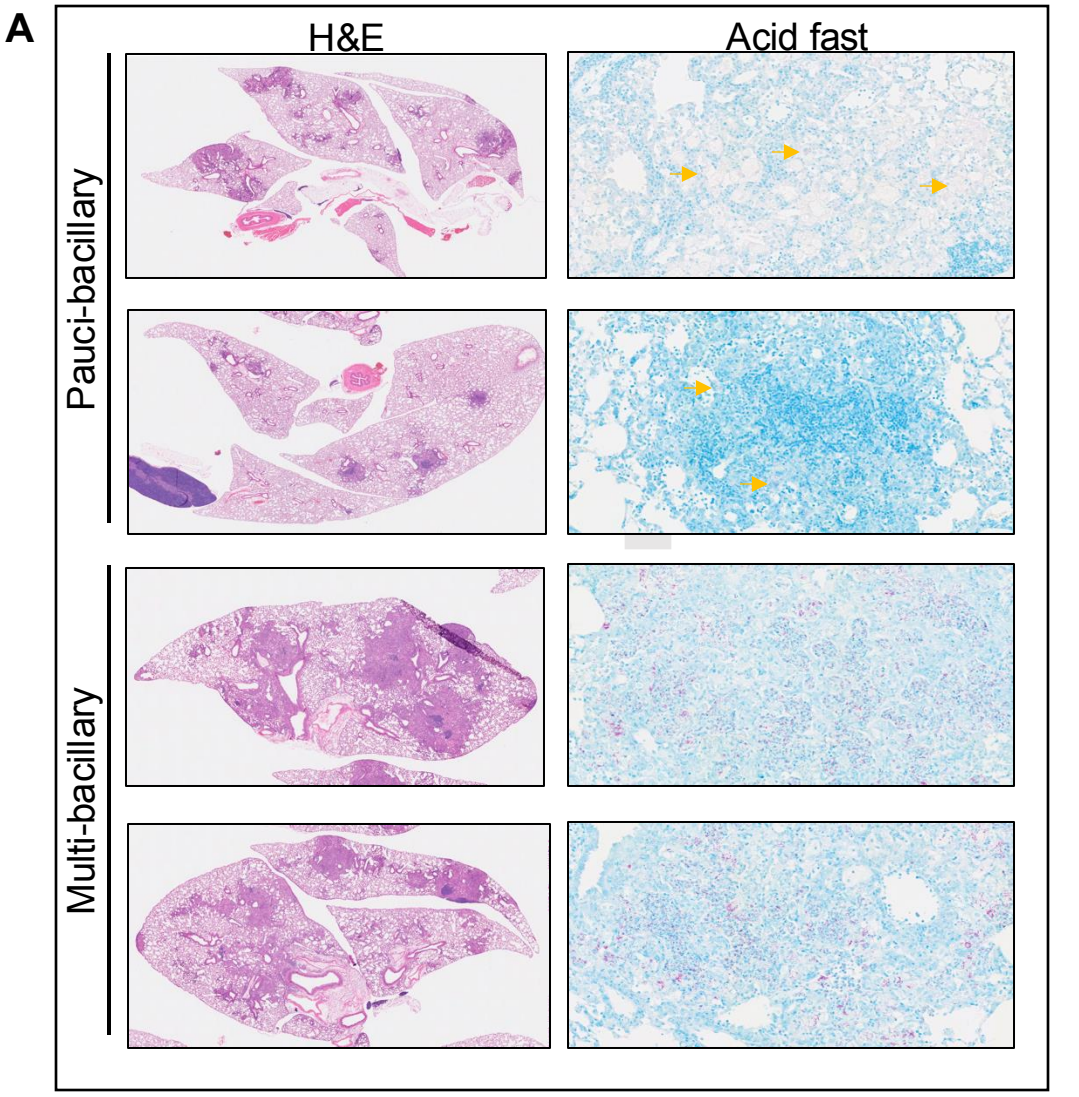

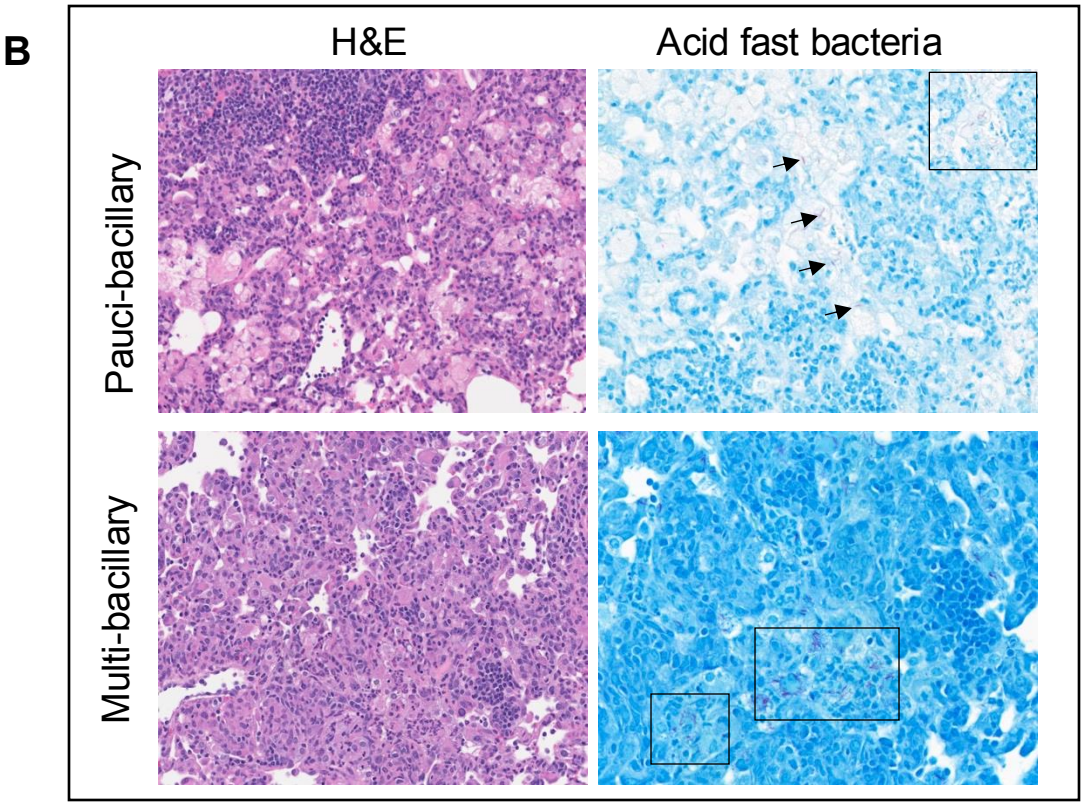

Supplemental Figure 8

Supplemental Figure 8. Pauci- and multi-bacillary pulmonary lesions of Mtb infected B6.Sst1S mice.

A. Representative histopathology and Acid Fast Bacteria (AFB) loads in of B6.Sst1S mouse lungs at 14 weeks after infection with 10^6 CFU of Mtb Erdman. Arrows indicate acid-fast bailli (Mtb).

B. Left- Representative H & E staining and Right - acid fast staining of B6.Sst1S Mtb infected lungs at 200X original magnification. Arrows and boxes indicate acid-fast bailli (Mtb).

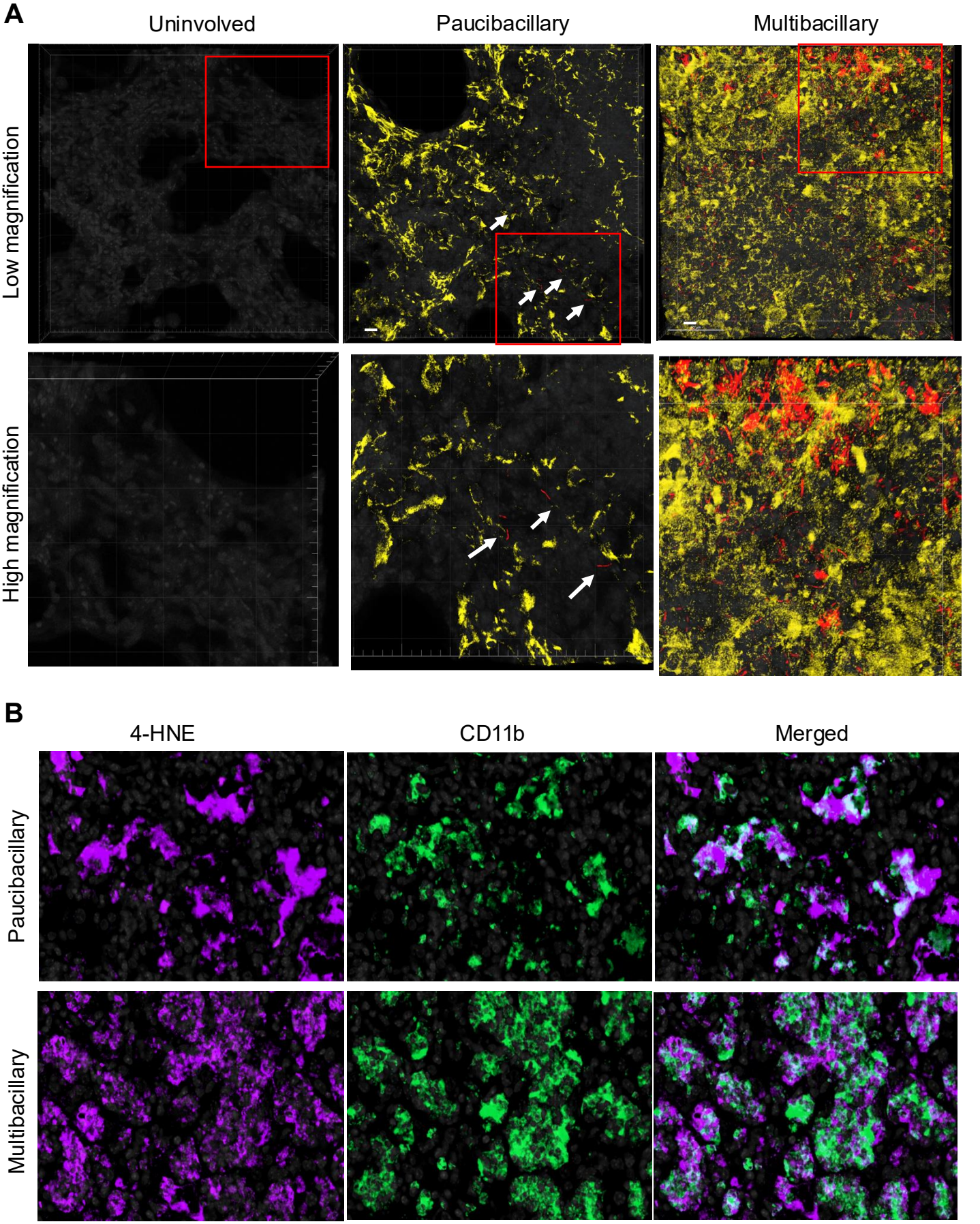

Supplemental Figure 9

Supplemental Figure 9. Accumulation of 4-HNE and Ifnβ producing cells in Mtb-infected B6.Sst1S mouse lung lesions.

A. 3D images of uninvolved lung and pulmonary TB lesions in Mtb-infected B6.Sst1S,*Ifnb1*-YFP mice presented in Fig.7A at low and high magnification. 4HNE+ staining - is yellow, and the reporter Mtb (smyc' :: mCherry) is red. The mice were infected for 20 weeks. Scale bar = 10 µm. Arrows indicate Mtb reporter strain expressing mCherry. Lower panels are magnified area of insets shown in top panels.

B. Representative fluorescent single channel images of pauci- and multibacillary PTB lesions in B6.Sst1S mice and merged images corresponding to Fig.7B. 4-HNE (magenta), CD11b (green) and DAPI (grey).

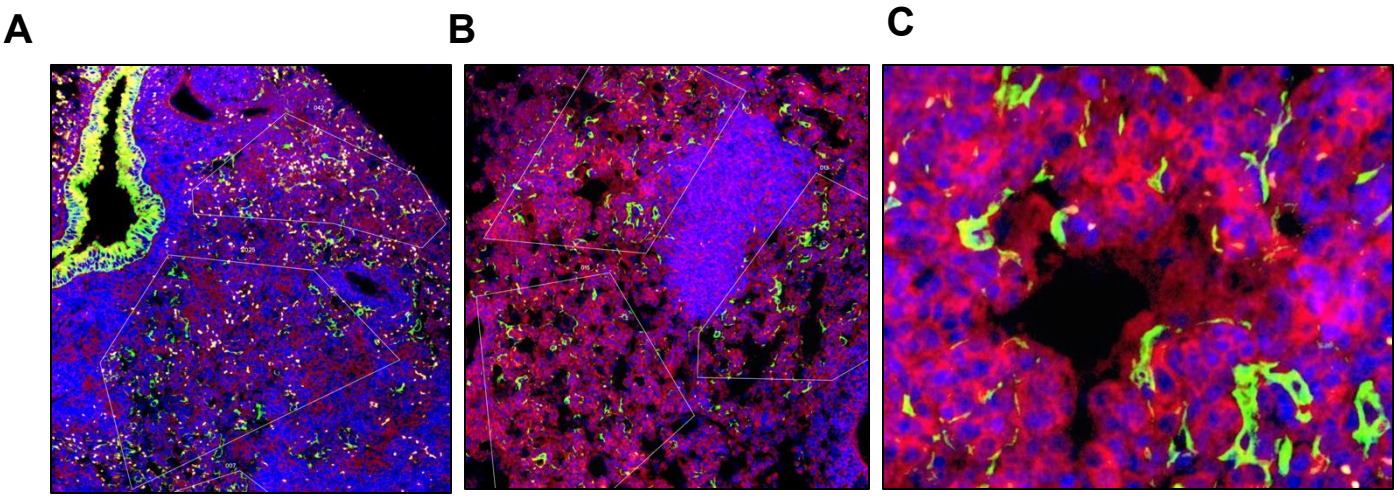

Supplemental Figure 10. Representative Images of GeoMX Region of Interests (ROIs).

Representative Images of GeoMX ROIs (Regions of Interest) with tuberculous lesions labeled with DAPI (nuclear stain, blue), anti-pancytokeratin (epithelial cells, green) and anti-Iba1 (macrophages, red). A&B Low magnification views with two (A) or three (B) ROIs outlined (white) containing abundant macrophages (red) and scattered enlarged alveolar epithelial cells (green), as illustrated in a higher magnification view in (C). (Original magnification, A&B 40X, C 400X).

The profiling used the Mouse Whole Transcriptome Atlas (WTA) panel which targets ~21,000+ transcripts for mouse protein coding genes plus ERCC negative controls, to profile the whole transcriptome, excluding uninformative high expressing targets such as ribosomal subunits. We assembled lungs from two mice with paucibacillary and two mice with multibacillary lesions to prepare a tissue array of paraffin-embedded lung tissues, and used acid fast Mtb staining on serial sections to classify individual TB lesions in the Mtb paucibacillary and multibacillary categories (**Suppl.Fig.8**).

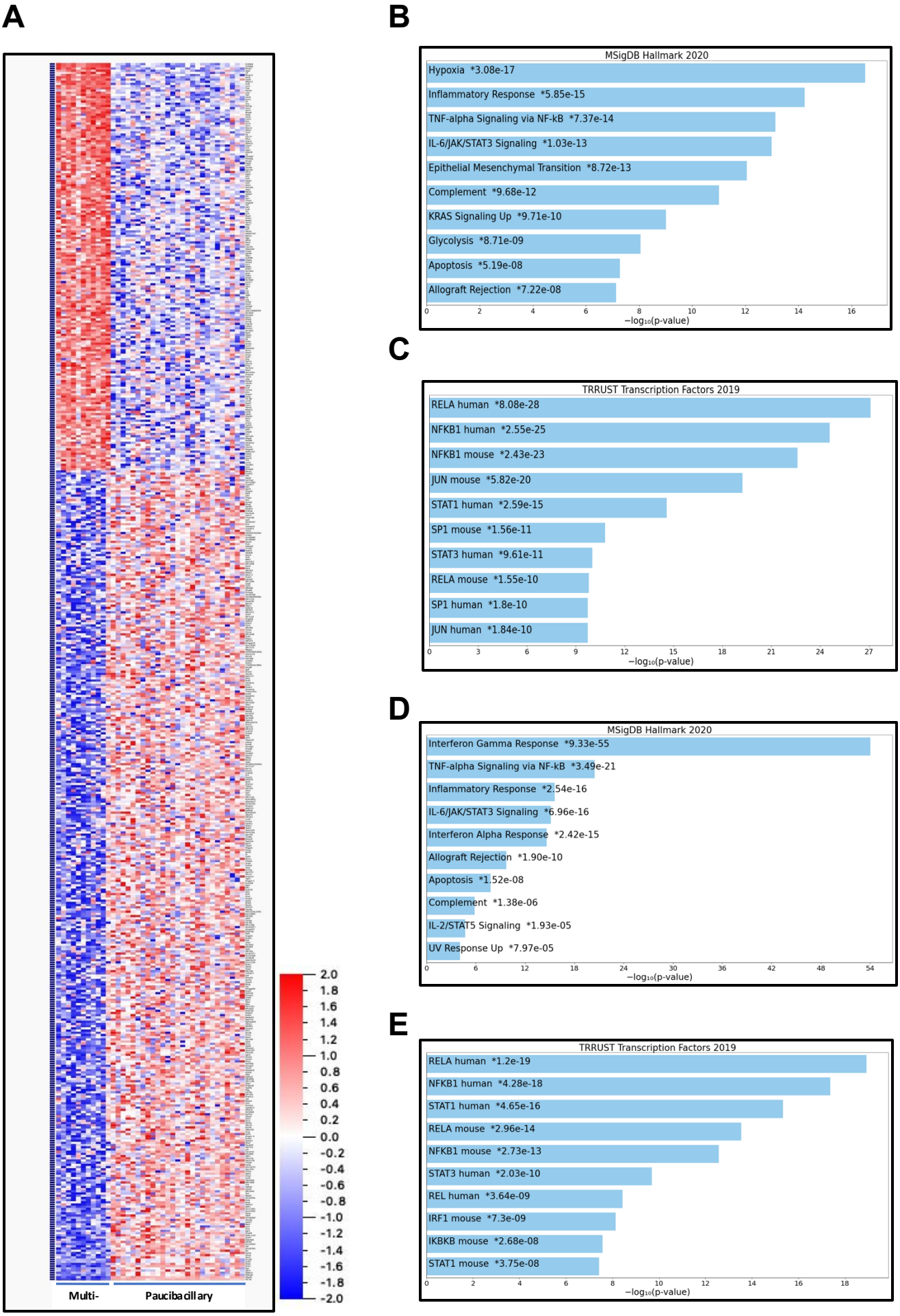

Supplemental Figure 11

Supplemental Figure 11. Analysis of spatial transcriptomics data from Iba1+ cells in pauci- and multi-bacillary lesions in Mtb infected B6.Sst1S mouse lungs.

A. Heatmap of all differentially expressed genes (fold change 2 and above) by Iba1+ cells in Multibacillary vs Paucibacillary TB lesions.

B. Top 10 Hallmark pathways upregulated in Iba1+ cells in multibacillary lesions.

C. Top 10 transcription factors enriched in promoters of genes upregulated in Iba1+ cells in multibacillary lesions.

D. Top 10 Hallmark pathways upregulated in the combined gene set of IFN-inducible genes expressed by Iba1+ cells in multibacillary lesions.

E. Top 10 transcription factors enriched in promoters of genes upregulated in the list of IFN-inducible genes expressed by Iba1+ cells in multibacillary lesions.

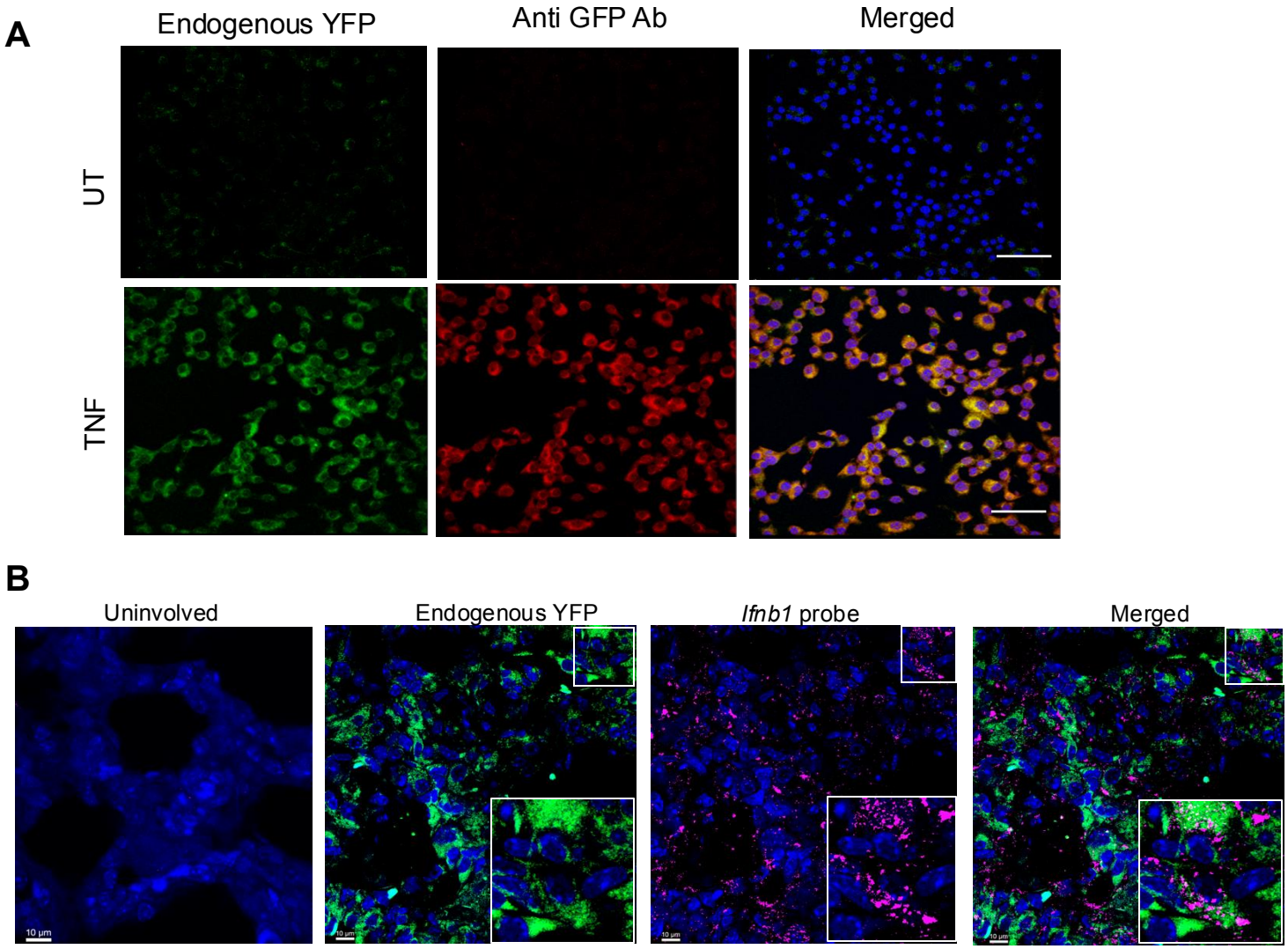

Supplemental Figure 12

Supplemental Figure 12. Accumulation of 4-HNE and Ifn producing cells in Mtb-infected B6.Sst1S mouse lung lesions.

A. Confocal images of BMDMs isolated from B6.Sst1S, *Ifnb1*-YFP mice stimulated with TNF (10 ng/ml) in vitro for 24 h or left untreated. The endogenous YFP signal is shown in green. Staining with anti-YFP antibody was used to demonstrate YFP expression in activated BMDMs, as a control of specificity. Nuclei in blue (DAPI). Scale bar = 50 m.

B. Confirmation of YFP signal from B6.Sst1S,*Ifnb1*-YFP reporter mice using IFnb1 mRNA in situ hybridization. 3D confocal images of florescent in situ hybridization with *Ifnb1* mRNA probes (red) showed overlap with YFP+ cells. Insets at lower right corner is an enlarged image of inset at top right corner which is showing the same cells expressing both signals. The mice were infected for 20 weeks. Scale bar = 10 m.

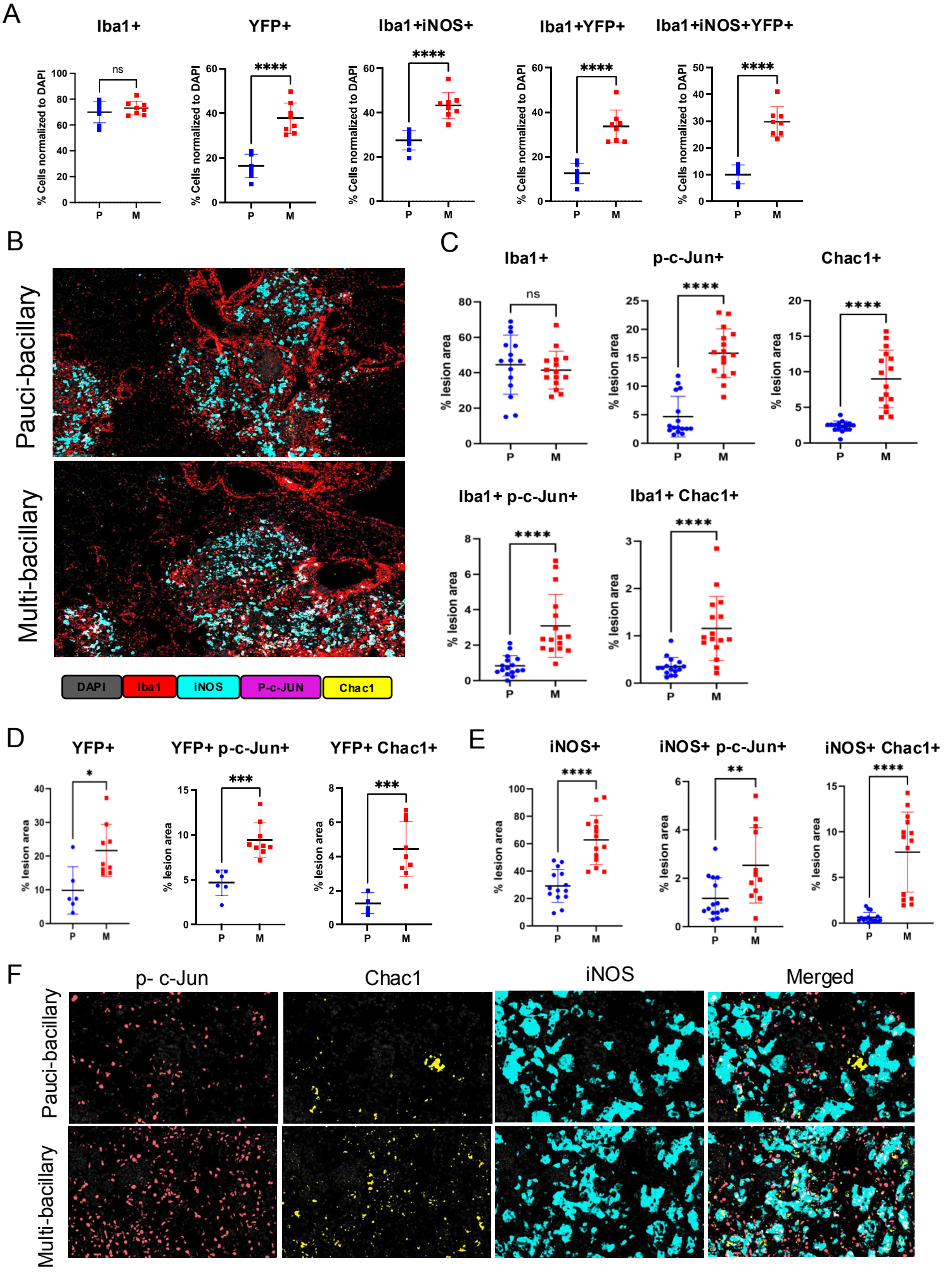

Supplemental Figure 13

Supplemental Figure 13. Fluorescent multiplexed immunohistochemistry (fmIHC) images representing increased expression of stress markers in macrophages within multi-bacillary pulmonary TB lesions of B6.Sst1S mice.

A. Quantification of IFN-I producing (YFP positive) myeloid cells in pauci-bacillary (n=8) and multi-bacillary (n=8) lesion of B6.Sst1S, *Ifnb1*-YFP reporter mice. The quantification was performed by manually counting total and individual group of markers at different lesions at 400X magnification and calculated the percentage cell number as compared to total DAPI. The average total cell number (DAPI) per field was 140.

B - C. fmIHC images and quantification of total macrophages (Iba1 positive) co-expressing stress markers in paucibacillary (n=15) and multibacillary (n=15) PTB lesions. The quantification was performed using Halo automated analysis as percent lesion area. The different markers are shown as p-c-Jun (peach), Chac-1 (yellow) an Iba1 (red) at 200X magnification. The mice were infected for 20 weeks.

D. Quantification of IFN-I producing (YFP positive) cells accumulating stress markers in pauci-bacillary (n=6) and multi-bacillary (n=9) lesion of B6.Sst1S, *Ifnb1*-YFP reporter mice using Halo automated analysis.

E F. quantification and representative fmIHC images of activated (iNOS+) macrophages co-expressing stress markers in paucibacillary (n=14) and multibacillary (n=14) PTB lesions. The quantification was performed using Halo automated analysis and the signals are presented as percent lesion area. The different markers are shown as phospho-c-Jun (peach), Chac-1 (yellow) an iNOS (teal) at 400X magnification. The mice were infected for 20 weeks.

The data represent the means ± SD and the statistical significance was performed by two-tailed unpaired t-test (Panel A, C-E). Significant differences are indicated with asterisks (*, $P < 0.05$; **, $P < 0.01$; ***, $P < 0.001$; ****, $P < 0.0001$).

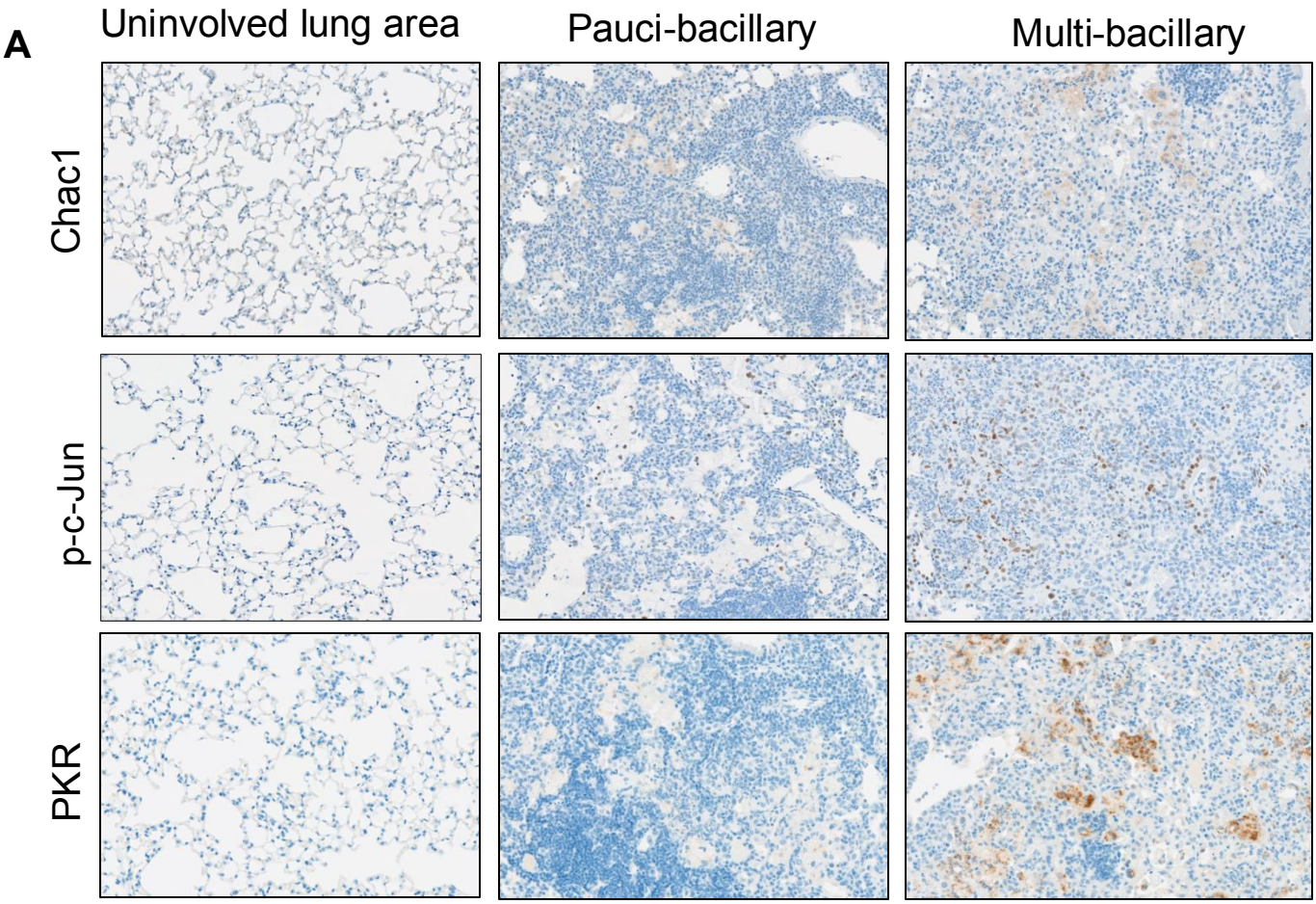

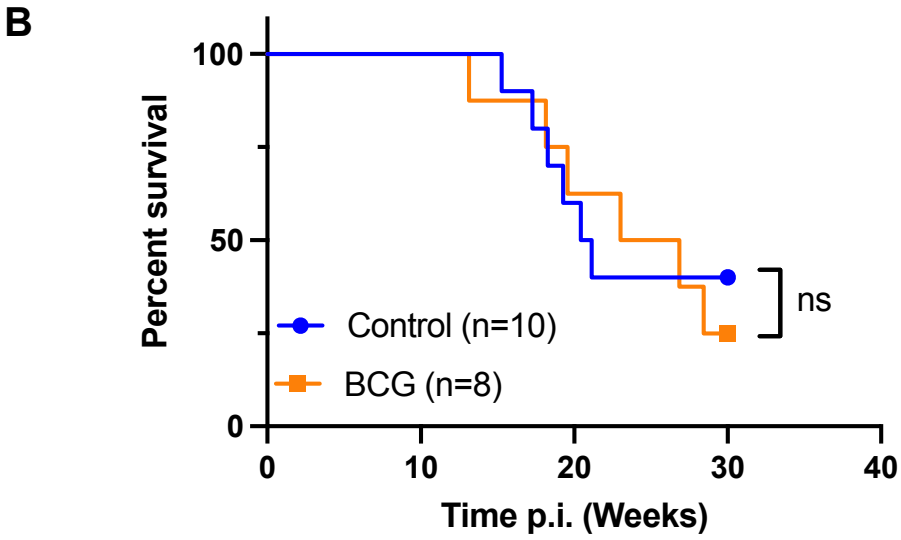

Supplemental Figure 14

Supplemental Figure 14. Expression of stress markers in pauci- and multi-bacillary lesions of Mtb-infected B6.Sst1S mouse lungs.

A. Representative monochromogenic immunohistochemistry staining images of Chac1, p-c-Jun and PKR in uninvolved lung area, paucibacillary and multibacillary pulmonary lesions in Mtb-infected B6.Sst1S mice. were infected for 14 weeks.

B. No effect of post-exposure BCG vaccination on the survival of Mtb-infected B6.Sst1S mice. Mice were infected with Mtb and BCG-vaccinated two months post infection. The survival curves of vaccinated and non-vaccinated mice were compared using the Log-rank (Mantel-Cox). Numbers of mice per group indicated in parentheses. This experiment was performed once. -rank (Mantel-Cox) test was applied to determine statistical significances between the groups for panel B. Significant differences are indicated with asterisks (*, $P < 0.05$; **, $P < 0.01$; ***, $P < 0.001$; ****, $P < 0.0001$).

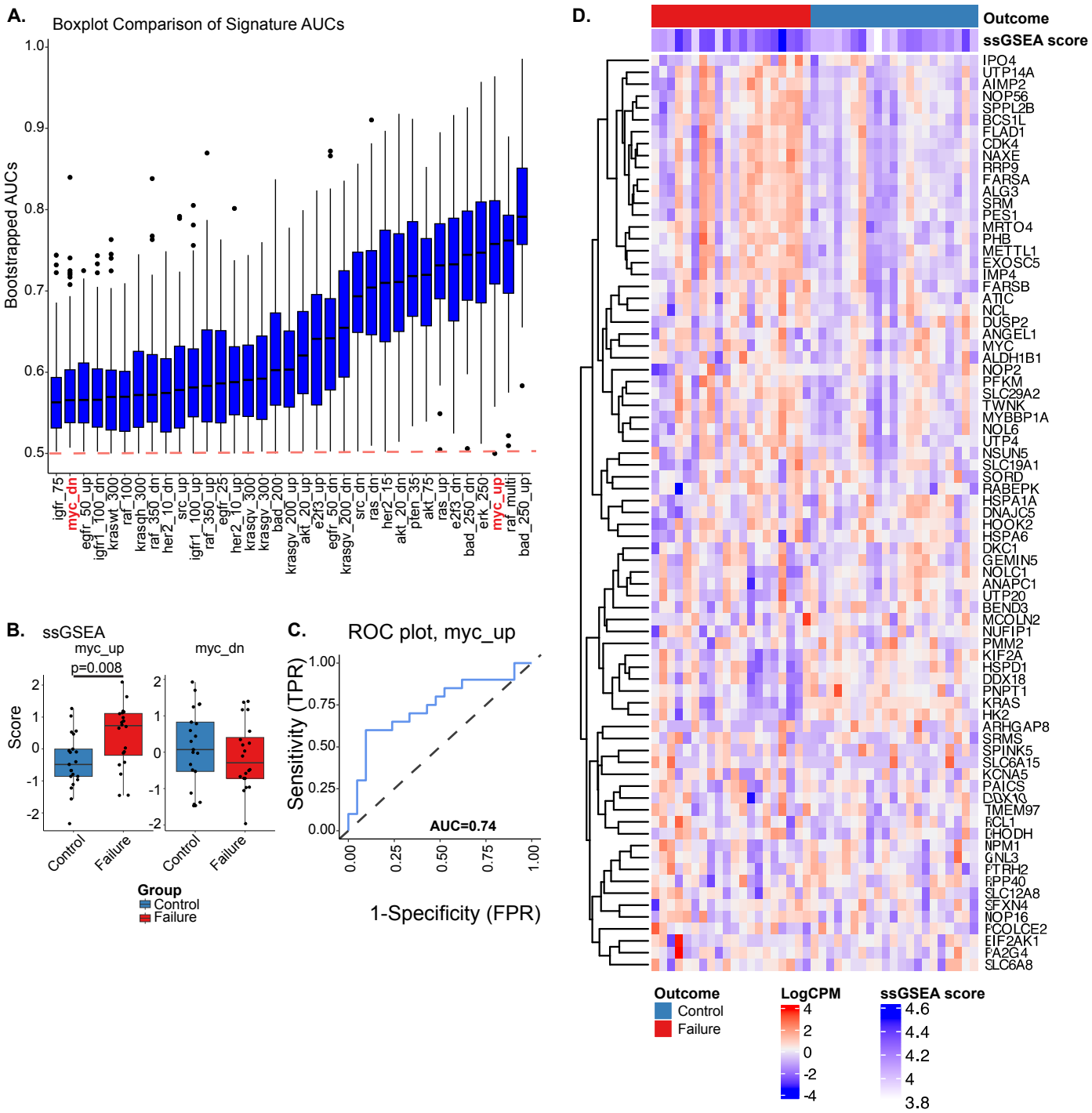

Supplemental Figure 15

Supplemental Figure 15. Myc upregulated gene signature in peripheral blood of TB patients is associated with treatment failures.

A. PBMC gene expression profiling of TB patients prior to TB treatment. Boxplot of bootstrapped ssGSEA enrichment AUC scores from several oncogene signatures ranked from lowest to highest area under curve (AUC) score (Y-axis), with *Myc*_up and *Myc*_dn gene sets (X-axis) are highlighted in red.

B C. Boxplots of myc upregulated (*Myc*_up) and downregulated (*Myc*_dn) gene signatures in successful (control) or failed (failed) TB therapy groups, with the receiver-operating characteristic (ROC) curve of *Myc*_up depicted in C.

D. Heatmap of all genes utilized in ssGSEA enrichment of the myc_up signature are depicted with individual ssGSEA scores for each patient sample. All plots were generated with the TBSignatureProfiler in R and p-values were determined by a t-test.

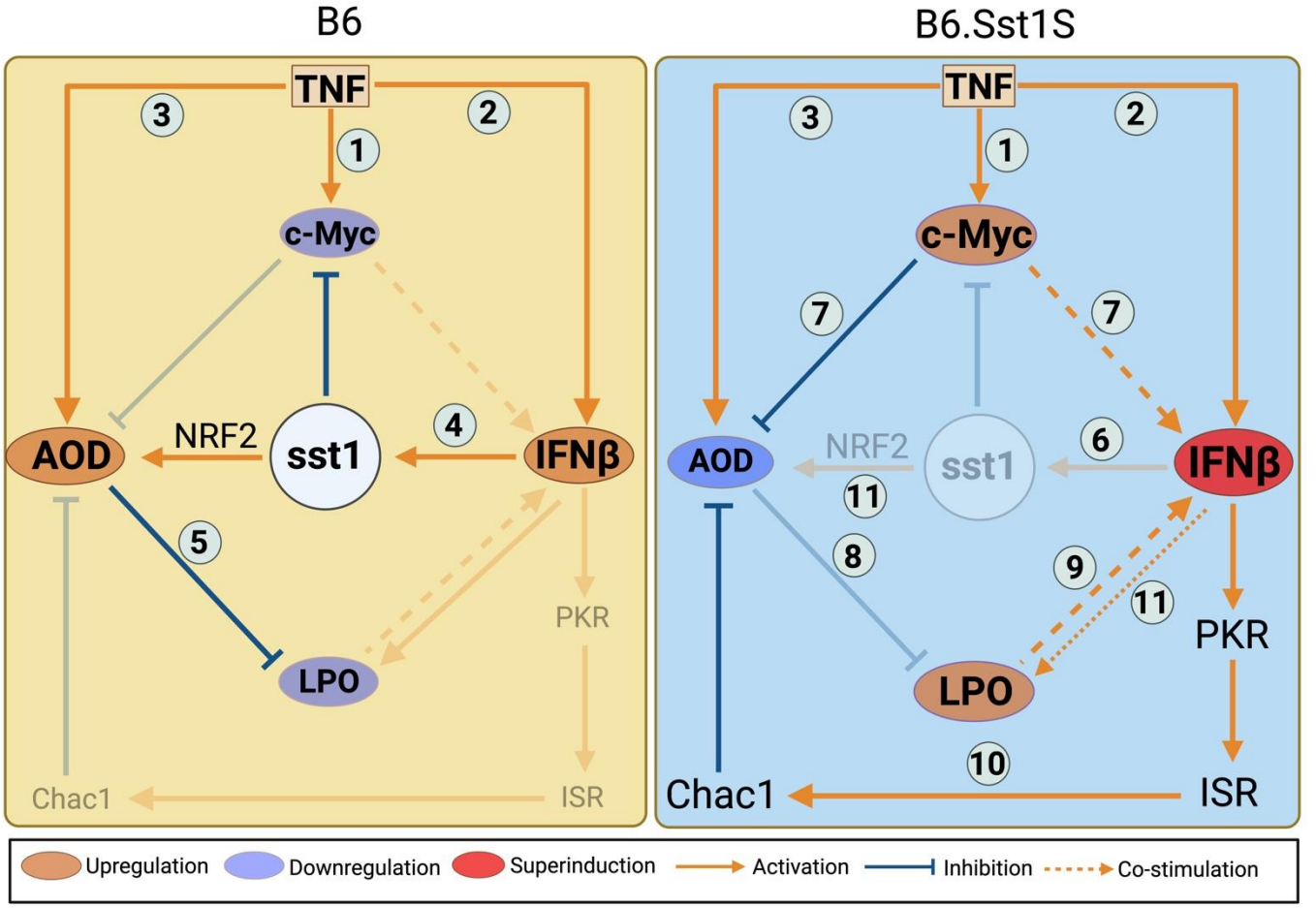

Supplemental Figure 16

Supplemental Figure 16: Schematic representation of B6 and B6.Sst1S macrophage responses to TNF

Common for B6 and B6.Sst1S:
1. TNF activates c-Myc expression.
2. TNF induces moderate *Ifnb1* expression.
3. TNF stimulation upregulates Nrf2.

B6-specific:
4. Ifn induces the sst1-encoded SP110 and SP140 nuclear proteins that co-activate Nrf2 and suppress c-Myc.
5. Nrf2 activates antioxidant defense (AOD) that inhibits lipid peroxidation (LPO)

B6.Sst1S-specific:
6. *Sp110* and *Sp140* are not expressed.
7. Myc is upregulated, inhibits ferritin expression and coactivates *Ifnb1* transcription.
8. Deficient AOD activation coupled with increased labile iron pool promotes accumulation of LPO products.
9. LPO further co-stimulates *Ifnb1* superinduction.
10. IFN-I hyperactivity activates ISR and induces Chac1 that further inhibits the AOD and increases LPO.
11. Alternative mechanisms of IFN-mediated dysregulation of AOD defense and iron homeostasis.

Supplemental Tables

Supplemental Table 1. Cell cycle analysis of B6 and B6.Sst1S BMDMS 24 h after TNF stimulation using scRNA-seq.

Sample	G1	S	G2M	G1/S
R	3257	299	507	10.9
S	3073	437	540	7
RT	1877	638	507	2.9
ST	2049	1107	367	1.9

Supplemental Table 2. Cell cycle analysis of B6 and B6.Sst1S specific BMDM subpopulations 24 h after TNF stimulation using scRNA-seq.

Cluster	G1	S	G2M	G1/S
2	267	573	133	0.5
3	1627	269	41	6
4	943	220	17	4.3
5	718	308	29	2.3

Supplemental Table 3. Gene set enrichment analysis of differentially activated pathways in B6 and B6.Sst1S BMDMs 12 h after TNF stimulation.

Gene set enrichment analysis results for the top enriched gene sets from the KEGG, MSigDB Hallmark, Reactome databases when comparing B6.Sst1S vs B6 BMDMs stimulated with TNF for 12 h. Output includes gene set names and FDR corrected p-values. The analysis was performed using FPKM data and the camera function from the limma R package.

Gene Set Enrichment Analysis

	Gene set	FDR
Overrepresented genesets for comparison B6.Sst1S.TNF vs B6.TNF	SUMOYLATION (Reactome)	0.00271
	SUMOYLATION OF DNA DAMAGE RESPONSE AND REPAIR PROTEINS (Reactome)	0.00277
	TNFA SIGNALING VIA NFKB (MSigDB Hallmark)	0.00293
	SPLICEOSOME (KEGG)	0.00816
	DNA DOUBLE-STRAND BREAK REPAIR (Reactome)	0.01653
	DNA REPAIR (Reactome)	0.03494
	HOMOLOGOUS RECOMBINATION (KEGG)	0.03746
	E2F TARGETS (MSigDB Hallmark)	0.05488
Underrepresented genesets for comparison B6.Sst1S.TNF vs B6.TNF	LYSOSOME (KEGG)	8.26E-09
	OXIDATIVE PHOSPHORYLATION (KEGG)	1.36E-05
	OXIDATIVE PHOSPHORYLATION (MSigDB Hallmark)	6.82E-05
	NONSENSE MEDIATED DECAY (NMD) INDEPENDENT OF THE EXON JUNCTION COMPLEX (EJC) (Reactome)	0.00027
	FATTY ACID METABOLISM (MSigDB Hallmark)	0.00206
	RESPONSE TO ELEVATED PLATELET CYTOSOLIC CA2+ (Reactome)	0.00212
	DETOXIFICATION OF REACTIVE OXYGEN SPECIES (Reactome)	0.00225
	FATTY ACID METABOLISM (KEGG)	0.00290
	FERROPTOSIS (KEGG)	0.00452
	MTORC1 SIGNALING (MSigDB Hallmark)	0.00642
	REACTIVE OXYGEN SPECIES PATHWAY (MSigDB Hallmark)	0.00806
	PEROXISOME (MSigDB Hallmark)	0.01475
	CHOLESTEROL_HOMEOSTASIS (MSigDB Hallmark)	0.03076

Supplemental Table 4. Transcription factor binding sites analysis of differentially expressed genes in B6 and B6.Sst1S BMDMs 12 h after TNF stimulation.

The functional profiling and transcription factor binding sites analysis (TFBs) was performed for two sets of genes which represent B6.Sst1S and B6 BMDMs responses to TNF.

Functional pathway profiling

	Enriched pathways	Adjusted p.value	genes
Sst1.S response	TNF signaling pathway (KEGG)	0.0002965	Map3K5, Casp3, Jun, Nfkb1, Mapk8, Edn1, Ripk1, Il6
	Cellular Senescence (Reactome)	0.0040589	Map3K5, Jun, Cbx8, Mapk8, Mapk7, Mdm2, Ets1, Kdm6B
	MyD88-independent TLR4 cascade (Reactome)	0.0065647	Jun, Nfkb1, Mapk8, Tlr4, Ripk1, Mapk7
	Toll Like Receptor 4 (TLR4) Cascade (Reactome)	0.0129301	Jun, Nfkb1, Mapk8, Tlr4, Ripk1, Mapk7
	Oxidative Stress Induced Senescence (Reactome)	0.0247333	Map3K5, Jun, Cbx8, Mapk8, Mdm2, Kdm6B
B6 response	Detoxification of Reactive Oxygen Species (Reactome)	1.48E-15	Gpx1, Txn2, Prdx1, Gpx3, Cat, Txnrd1, Prdx2, Sod2, Sod1, Prdx3, Prdx5, Gsr
	TP53 Regulates Metabolic Genes (Reactome)	3.4733E-05	Akt1, Prdx1, G6Pdx, Txnrd1, Prdx2, Prdx5, Gsr
	Ferroptosis (KEGG)	9.9415E-05	Slc11A2, Gpx4, Slc7A11, Atg7, Prnp, Gclm
	HIF-1 signaling pathway (KEGG)	0.003628	Akt1, Mapk3, Ldha, Egln1, Pdk1, Mapk1, Camk2G
	Peroxisome (KEGG)	0.0054955	Cat, Mpv17, Idh1, Sod2, Sod1, Prdx5

Supplemental Table 5. The list of identified transcription factors associated with differences between activated genes in response to TNF stimulation in B6 and B6.Sst1S BMDMs.

Transcription factor binding sites analysis

B6.sst1S response

Motif ID	Possible TF	NES
transfac_M04823	E2f4	4.46
transfac_M04797	Egr1	4.33
transfac_M04683	Nfya	4.09
taipale_TEAD4	Tead4,Cebpd	4.05
transfac_M07390	Nfe2l1	3.96
transfac_M02743	E2f3	3.94
cisbp_M2272	E2f4	3.91
factorbook_NFY	Nfyb,Nfya	3.90
cisbp_M4473	Pbx3	3.87
cisbp_M4504	Egr1	3.75

B6.WT response

Motif ID	Possible TF	NES
cisbp_M6156	Bach1	5.72
cisbp_M1966	Nfe2l2	5.48
factorbook_NFE2	Nfe2	5.46
jaspar_MA0150.2	Nfe2l2	5.43
hocomoco_BACH1	Bach1	5.23
taipale_ELK1	Elk1	4.52
jaspar_MA0501.1	Nfe2	4.48
transfac_M02022	Mafk	4.32
cisbp_4629	Nfe2	4.28
transfac_M07374	Bach1	4.12

Supplemental Table 6. Master regulator analysis of the transcription factors associated with differences between activated genes in response to TNF stimulation in B6 and B6.Sst1S BMDMs.

Master regulator analysis was performed using Virtual Inference of Protein Activity by Enriched Regulon Analysis (VIPER) algorithm, the mice macrophage gene regulatory network and log2 transformed FPKM values of genes from gene ontology category GO: 0006979. The table shows the identified list of transcription factors associated with differences between activated genes in response to TNF stimulation in B6.Sst1S vs B6 BMDMs.

Master regulator analysis

TFs	t	p.value
Nfe2l1	12.34	0.000248
Atf5	9.49	0.000688
E2f3	4.82	0.00855
E2f6	-10.51	0.000463
Zfp523	-10.76	0.000423
Zfp623	-12.46	0.000239
Zkscan8	-13.39	0.00018
Zfp568	-16.23	8.44E-05
Zfp251	-58.59	5.08E-07